Development of Novel Radiotracer for Imaging High Affinity Choline Transporter and Vesicular Acetyl Choline Transporter

AZIM MOHAMMAD ANWAR-UL

July 2014

Doctoral Dissertation

Development of Novel Radiotracer for Imaging High Affinity Choline Transporter and Vesicular Acetyl Choline Transporter

Graduate School of
Natural Science and Technology
Kanazawa University

Major Subject: Division of Life Sciences
Course: Molecular Effects

School Registration No.: 1123032330
Name: Azim Mohammad Anwar-Ul
Chief Advisor: Professor Kazuhiro Shiba, Ph.D
Division of Tracer Kinetics,
Advanced Science Research Center,
Kanazawa University

Index

Page

Page

Abstract

Introduction: Alzheimer's disease (AD) is the most common form of irreversible dementia and characterized clinically by progressive deterioration of intellectual abilities, including cognitive and behavioral dysfunctions. Pathologically, AD is characterized by the extracellular deposits of amyloid-β peptides and aggregation of intraneuronal neurofibrillary tanglets. The degeneration of cholinergic neurons in the basal forebrain and the associated loss of the cholinergic neurotransmission in the cerebral cortex and other area contributed significantly to the deterioration in cognitive function in AD. Deficiency in high affinity choline uptake (HACU) and the loss of vesicular acetylcholine transporter (VAChT), are two characteristic neurochemical changes in AD. In cholinergic neurons, HACU by the high affinity choline transporter (HAChT) is a rate-limiting and regulatory step for the synthesis of Ach and VAChT mediates the loading of presynaptic vesicles with newly synthesized acetylcholine. Thus, both the HAChT and VAChT appear to be two relatively specific presynaptic marker for cholinergic neurons in AD brain.

Objectives: This PhD thesis can be divided into two parts. The objective of PART A includes the syntheses and *in vitro* evaluation of MKC-231, tacirine and its corresponding 2-oxo-1-pyrrolidineacetyl derivative as high affinity choline transporter imaging agent. The objective of PART B is to develop radiobromine labeled *o*-bromo-*trans*-decalinvesamicol (OBDV) as a potent and new PET radiotracer for VAChT imaging in AD brain through *in vivo* evaluation and *ex vivo* autoradiography.

Methods: In PART A, the inhibition activities of tacirine, the 2,3-dimethylfuran derivative of tacirine (DMTA) and their corresponding 2-oxo-1-pyrrolidineacetyl derivatives, namely PTAA and MKC-231 were measured by displacement of a typical HAChT antagonist [^{3}H]HC-3 (Dissociation constant: K_d = 19.1 nM) in rats cerebral membrane. The percent inhibition against the binding of [^{3}H]HC-3 to HAChT were calculated using GraphPad Prism v4 software. In Part B, *in vivo* evaluation of [^{77}Br]OBDV was performed instead of 2[^{76}Br]OBDV, because of the longer half-life of ^{77}Br ($t_{1/2}$ = 57.0 h). [^{77}Br]OBDV was radiosynthesized by the tin-bromine exchange reaction from trimethylstannyl precursor, *o*-trimethylstannyl-*trans*-decalinvesamicol (OTDV). *In vivo* biodistribution study of [^{77}Br]OBDV in blood, brain regions and major organs of rats was performed at 2,30 and 60

min post-injection. *In vivo* blocking study was performed to check the binding selectivity of [^{77}Br]OBDV for VAChT. *In vivo* metabolism of [^{77}Br]OBDV in the blood and brain of SD rats at 60 min post-injection was examined using TLC. Ex vivo autoradiography was performed to reveal the regional brain distribution of [^{77}Br]OBDV at 30 min post-injection.

Results: In PART A, only HC-3 showed affinity for HAChT (IC_{50} = 20 nM) in the *in vitro* binding assay. A very insignificant inhibition activity (IC_{50} = 1000 nM) of Tacrine was revealed. The newly synthesized tacirine derivatives, DMTA and PTAA did not show any affinity for HAChT. Although MKC-231 was reported to enhance cholinergic activity at synaptic terminals, it also did not show any affinity for the HAChT in [^{3}H]HC-3 binding assay. Other inhibitors like choline chloride (ChCl), Acetylcholine chloride (AChCl), Carbamylcholine Chloride (CaChCl) showed no binding affinity for HAChT. In part B, [^{77}Br]OBDV was radiosynthesized with radiochemical purity of greater than 99%, and the radiochemical yield was 52.3 ~ 65.8%. The specific activity (SA) of [^{77}Br]OBDV was found to be 322 ~ 406 GBq/μmol. At 2 min post-injection time, the uptake of [^{77}Br]OBDV in blood and brain regions was found 0.14 ± 0.01%ID/g and 0.62 ± 0.7 %ID/g respectively, which confirmed blood-brain barrier penetration of [^{77}Br]OBDV. In *in vivo* biodistribution studies, at 30 min post-injection, the accumulation of [^{77}Br]OBDV in cerebral cortex, striatum and cerebellum of the rat brain was 0.52 ± 0.11 %ID/g, 0.59 ± 0.05 %ID/g and 0.56 ± 0.04 %ID/g respectively. In *in vivo* blocking studies, (+/-)-vesamicol blocked regional brain uptake of [^{77}Br]OBDV by 41%. In contrast, no blocking effects were observed by both the (+)-3-PPP (σ_1, σ_2 receptor ligand) and (+)-pentazocine (σ_1 receptor ligand). In *ex vivo* autoradiography, accumulation of [^{77}Br]OBDV was observed in VAChT rich brain regions, such as the cerebral cortex, diagonal band, hippocampus, posterolateral cortical amygdaloidal nucleus.

Conclusion: In Part A, *in vitro* [^{3}H]HC-3 binding assay revealed no affinity of MKC-231, tacirine and its corresponding 2-oxo-1-pyrrolidineacetate derivative towards HAChT. So, it is worthy to develop radiolabeled HC-3 derivatives with high affinity for HAChT, which can diffuse the BBB, to enable the *in vivo* investigation of HACU system. In Part B, *In vivo* results showed that [^{77}Br]OBDV selectively bound to VAChT with high affinity in rat brain in vivo. Hence, OBDV radiolabeled with ^{76}Br was suggested to be a potent VAChT imaging probe for PET.

Acknowledgements

All praises are for the One above all of us, the omnipresent God, for giving me the strength and courage and all the opportunities to finish my PhD successfully.

This dissertation would not have been possible without the guidance and the help of several individuals who extended their valuable support in the preparation and completion of this study.

First and foremost, I would like to express deepest sense of gratitude to my respected supervisor Professor Dr. Kazuhiro Shiba, Division of Tracer Kinetics, Advanced Science Research Center, Kanazawa University, Japan for the frequent advice, motivation and valuable support over the last 3 years of my PhD study. Moreover, I wish to express my sincere appreciation to him for his enthusiasm and intense knowledge in molecular neuroimaging, radiopharmaceutical chemistry, *in vitro*, *in vivo* and *ex vivo* autoradiographic techniques, neuroscience, neurodegenerative disease mechanism and other research related topics for the development of SPECT/PET neuroimaging probe. His valued supervision and ideas helped me a lot in the preparation of this dissertation and other sub-theses.

I take this opportunity also to express my gratitude to Dr. Yoji Kitamura, Associate professor, Division of Tracer Kinetics, Advanced Science Research Center, Kanazawa University, Japan not only for his interest in my research but also for providing constructive support and insightful suggestions during my PhD research.

I accord my heartily respect and indebtedness to Dr. Takashi Kozaka, Assistant Professor, Division of Tracer Kinetics, Advanced Science Research Center, Kanazawa University, Japan for his whole-hearted co-operation, encouragement and enthusiastic suggestion throughout my research work and also enlightening me some important parts of my research. Besides my supervisor, acknowledgements must go to him because of his constructive criticism, solemn instructions during the various experiments and invaluable support through some of the toughest times in my PhD research tenure in Japan.

I cherish the desire to thank Professor Dr. Yasushi Kiyono, from Molecular imaging division of Biomedical Imaging Research Center, University of Fukui, Japan for providing [^{77}Br]Br^{-}. Without [^{77}Br]Br^{-}, it would have not been possible to develop the PET neuroimaging probe presented in this thesis

I take this opportunity to express my gratitude to Dr. Kazuma Ogawa, Associate professor, Institute of Medical, Pharmaceutical and Health Sciences, Kanazawa University, Japan for his interest in my research and assistance to bring [^{77}Br]Br^{-} form Fukui University.

I would like to express my gratitude to all the respected reviewers of my dissertation committee for their continuous support, insightful comments and encouragements.

I would also like to thank all the lab members, especially Mr. Daisuke Miwa and Ms. Izumi Uno, for their sincere and cordial co-operation during my studies, and for all the fun we have had in the last three years. I will always remember our time in the lab with care. Appreciation and thanks are also extended to Ms. Miyuki Nakashima for her assistance with the *in vitro* and *in vivo* experiments.

I also wish to thank all the support staffs of Kanazawa University for their sympathetic help in secretarial works during my staying in Japan. Especial thanks go to the office staffs of Central Institute of Radioisotope Science, Advanced Science Research center, Kanazawa University, namely, Ms. Yoko Nagai, Ms. Keiko Matsunaga and Mr. Masao Misaki, for their enormous support from secretarial and technical assistance to more personal help when needed.

I am also grateful to the Japanese Government (Monbukagakusho) for the financial supporting through MEXT scholarship. Especial Thanks are extended to the National Institute of Nuclear Medicine and Allied Sciences (NINMAS), Bangladesh Atomic Energy Commission (BAEC) for sanctioning study leave for 3 years in my favor to come to Kanazawa University, Japan.

At last but not least my warmest thanks go to my family members, especially to my parents, brother and sisters, who have supported me throughout my life and always believed in my ability to succeed. I am especially indebted to my wife, Syeda Shayma Arzumand, for her tireless help and heartiest co-operation to keep me focused to the objective. The existence and activities of our two boys, Azim Mohammad Fiaz and Azim Mohammad Wasif, were always the inspiration of all the works that I have done and am doing.

List of related Publications

A list of the accomplished research reports (published, accepted or presented) under the supervision of Professor Dr. Kazuhiro Shiba during my doctoral course tenure (October, 2011–September, 2014) in the Kanazawa University, Japan is compiled in this section.

Journal Articles

[1] **Mohammad Anwar-ul Azim,** Takashi Kozaka, Izumi Uno, Daisuke Miwa, Yoji Kitamura, Kazuma Ogawa, Akira Makino, Yasushi Kiyono, Kazuhiro Shiba; The Potential of *o*-Bromo-trans-decalinvesamicol as a New PET Ligand for Vesicular Acetylcholine Transporter Imaging. *Synapse 2014; 68(10): 445-453.*

[2] Takashi Kozaka, Izumi Uno, Yoji Kitamura, Daisuke Miwa, **Mohammad Anwar-ul Azim,** Kazuma Ogawa, Kazuhiro Shiba. 2014. Regional brain imaging of vesicular acetylcholine transporter (VAChT) using *o*-[^{125}I]iodo-*trans*-decalinvesamicol as a new potential imaging probe. *Synapse 68(3): 107-113.*

Conference Papers

[1] **Mohammad Anwar-ul Azim,** Takashi Kozaka, Izumi Uno, Daisuke Miwa, Yoji Kitamura, Kazuma Ogawa, Keiichi Kawai, Yasushi Kiyono, Kazuhiro Shiba, Introduction of radiobromine labeled decalinvesamicol analogue as a new and promising PET vesicular acetylcholine transporter (VAChT) imaging probe, J Nucl Med. Vol. 55, Supplement 1, May 2014 (Abstract No. 115), In: *Proceedings of the Society of Nuclear Medicine and Molecular Imaging (SNMMI) 2014 Annual Meeting,* (June 7-11, St. Louis, Missouri, USA), 2014.

[2] **Mohammad Anwar-ul Azim,** Takashi Kozaka, Izumi Uno, Daisuke Miwa,Yoji Kitamura, Kazuma Ogawa, Keiichi Kawai, Yasushi Kiyono, Kazuhiro Shiba, The Potential of The Vesicular Acetylcholine Transporter (VAChT) Imaging Using Radiolabeled *o*-Bromo-*trans*-decalinvesamicol (OBDV) as a New PET Ligand, In: *Proceedings of the 5th International Workshop on Molecular Functional Imaging for Brain and Gynecologic Oncology*, (March 3-4, 2014, Fukui, Japan), 2014 (Organized by Biomedical Imaging research Center & Faculty of Medical science, the university of Fukui).

[3] **Mohammad Anwar-ul Azim,** Takashi Kozaka, Izumi Uno, Daisuke Miwa,Yoji Kitamura, Kazuma Ogawa, Keiichi Kawai, Yasushi Kiyono, Kazuhiro Shiba, A new and promising VAChT imagiung probe for PET: Radiobromine labeled analogue of decalinvesamicol, In: *Proceedings of the 134th annual meeting of the Pharmaceutical Society of Japan,* March 27-30, Kumamoto, Japan), 2014.

[4] **Mohammad Anwar-ul Azim,** Takashi Kozaka, Izumi Uno, Daisuke Miwa, Yoji Kitamura, Kazuma Ogawa, Keiichi Kawai, Yasushi Kiyono, Kazuhiro Shiba, *In vivo* evaluation of radiobromine labeled *o*-bromo-decalinvesamicol (OBDV) as a potent VAChT imaging prob,. In: proceedings of the *13th Seminar on radiopharmaceutical diagnostic imaging agent,* (December 14, Kyoto, Japan.), 2013.

[5] Izumi Uno, Yoji Kitamura, Takashi Kozaka, Daisuke Miwa, **Mohammad Anwar-ul Azim,** Kazuma Ogawa, Keiichi Kawai, Junichi Taki, Seigo Kinuya, K. Shiba, In vivo evaluation of radioiodinated *o*-iodo-*trans*-decalinvesamicol as a vesicular acetylcholine transporter (VAChT) imaging agent, Journal of Nuclear Medicine, Vol. 54, Supplement 2, P 234, May 2013, **In:** *Proceedings of the Society of Nuclear Medicine and Molecular Imaging (SNMMI) 2013 Annual Meeting,* (June 8-12, Vancouver, Canada), 2013.

[6] Takashi Kozaka, Daisuke Miwa, Izumi Uno, Yoji Kitamura, **Mohammad Anwar-ul Azim,** Kazuma Ogawa, Seigo Kinuya, Keiichi Kawai, Kazuhiro Shiba, The development of a potential vesicular acetylcholine transporter (VAChT) PET imaging probe, Journal of Nuclear Medicine, Vol. 54, Supplement 2, P 232, May 2013, **In:** *Proceedings of the Society of Nuclear Medicine and Molecular Imaging (SNMMI) 2013 Annual Meeting,* (June 8-12, Vancouver, Canada), 2013.

[7] **Mohammad Anwar-ul Azim,** Takashi Kozaka, Izumi Uno, Daisuke Miwa, Yoji Kitamura, Kazuma Ogawa, Keiichi Kawai, Seigo Kinuya, Kaiichi Kawai, Kazuhiro Shiba, Synthesis and *in vitro* evaluation of OBBV as a potential σ-1 receptor imaging probe, Japanese Society for Molecular Imaging, Vol 6 (2), May 2013, P-115, **In:** *Proceedings of the 8th Annual meeting of the Japanese Society for Molecular Imaging,* (May 30-31, Yokohama, Japan), 2013.

[8] Izumi Uno, Takashi Kozaka, Daisuke Miwa, Yoji Kitamura, **Mohammad Anwar-ul Azim,** Kazuma Ogawa, Kaiichi Kawai, Kazuhiro Shiba, Separation and evaluation of diastereomeric OIDV as a selective VAChT imaging agent, In: *Proceedings of the 133rd annual meeting of the Pharmaceutical Society of Japan,* (March 27-30, Yokohama,, Japan), 2013.

[9] Yoji Kitamura, Kazuma Ogawa, Takashi Kozaka, **Mohammad Anwar-ul Azim,** Izumi Uno, Daisuke Miwa, Yutaka Saito, Kazuhiro Shiba, *S*tudy of the Application of ATR for the Measurement of Infrared Absorption Spectrum of Identical Tests, In: *Proceedings of the 133rd annual meeting of the Pharmaceutical Society of Japan,* (March 27-30, Yokohama,, Japan), 2013.

[10] Takashi Kozaka, Daisuke Miwa, Izumi Uno, Yoji Kitamura, **Mohammad Anwar-ul Azim,** Kazuma Ogawa, Kaiichi Kawai, Kazuhiro Shiba, The synthesis and in vivo evaluation of [^{11}C]OMV as a VAChT imaging probe for early diagnosis of Alzheimer's disease, In: *Proceedings of the 133rd annual meeting of the Pharmaceutical Society of Japan,* (March 27-30, Yokohama, Japan), 2013.

List of Tables

List of Figures

Page

Page

Abbreviations

A-4	4,4'-bis-[1-hydroxy-2-(4-methylpiperidin-1-yl)ethyl]biphenyl
Aβ	Amyloid-beta
AcCoA	Acetyl coenzyme
ACh	Acetylcholine
AChE	Acetylcholinesterase
AD	Alzheimer's disease
AF64A	Ethylcholine mustard aziridinium
ANOVA	Analysis of variance
APP	Amyloid precursor protein
BBB	Blood-brain barrier
ChAT	Choline acetyltransferase
ChT	Choline transporter
Cdk5	Cyclin-dependent kinase 5
(-)-[^{11}C]-OMV	(-)-[^{11}C]- *ortho*-methylvesamicol
^{11}C–pipzA-4	4-[1-hydroxy-2-(4-^{11}C-methylpiperazin-1-yl)ethyl]-4'-[1-hydroxy-2-(4-methylpiperidin-1-yl)ethyl]-biphenyl
CNS	Central Nervous System
DV	Decalinvesamicol
DMTA	2,3-dimethyl-5,6,7,8-tetrahydrofuro[2,3-b]quinolin-4-amine
DTG	1,3-di-(2-tolyl)guanidine
SDTA	Senile Dementia of Alzheimer Type
[^{18}F]NEFA	[^{18}F] 2-fluoro-N-(2-(2-nitro-1H-imidazol-1-yl)ethyl)acetamide
[^{18}F]FEOBV	[^{18}F]fluoroethoxybenzovesamicol
[^{18}F]FBT	p-[^{18}F]fluorobenzyltrozamicol
^{18}F-FA-4	4-[1-hydroxy-2-(4-^{18}F-fluoromethylpiperidin-1-yl)ethyl]-4'-[1-hydroxy-2-(4-methylpiperidin-1-yl)ethyl]-biphenyl
GABA	Gamma-aminobutyric acid
Glu	Glutamate.
GSK-3β	Glycogen synthase kinase 3β

HACU	High Affinity Choline Uptake
HAChT	High-affinity choline transporter
HC-3	Hemicholinium-3
H_3-HRs	H_3 histamine receptors
HPLC	High Performance Liquid Chromatography
5-HT	5-hydroxytryptamine
IC_{50}	The half maximal inhibitory concentration
%ID/g	Percent of injected dose per gram of tissue
[^{125}I]IBVM	[^{125}I]iodobenzovesamicol
(-)-[^{125}I]-oIV	(-)-[^{125}I]-*ortho*-iodovesamicol
[$^{123/125}$I]MIBT	m-[^{125}/^{123}I]iodobenzyl)trozamicol
IHC	Immunohistochemistry
ISHC	In *situ* hybridization histochemistry
K_d	The dissociation constant of the corresponding radioligand
MAP	Microtubule-associated Protein.
MKC-231	2-(2-Oxo-pyrrolidine-1-yl)-N-(2,3-dimethyl-5,6,7,8-tetrahydro furo [2, 3-b]quinolin-4-yl) acetoamide
MOA	Mode of Action
mAChR	ACh muscarinic receptor
mRNA	Messenger-Ribonucleic acid
nAChR	ACh nicotinic receptor
NFTs	Neurofibrillary tangles
OBDV	*ortho*-Bromo-*trans*-decalinvesamicol
O.C.T	Optimum cutting temperature
OIDV	*ortho*-Iodo-*trans*-decalinvesamicol
OTDV	*ortho*-trimethylstannyl-*trans*-decalinvesamicol
PDH	Pyruvate dehydrogenase
PET	Positron Emission Tomography
P-gp	P-glycoprotein
PHFs	Paired helical filaments

PP-1	Protein phosphatase 1
PP-2A	Protein phosphatase 2
PS	Phosphatidylserine
PTAA	2-(2-Oxo-pyrrolidin-1-yl)-N-(1,2,3,4-tetrahydro-acridin-9-yl) -acetamide
(+)-3PPP	3-(3-hydroxyphenyl)-N-n-propylpiperidine
Pyr	Pyruvate
RRC	Relative radioactivity concentration
SFs	Straight filaments
SD rat	Sprague Dawley rat
SPECT	Single Photon Emission Computed Tomography
THA	9-amino-1,2,3,4-tetrahydroacrydine (Tacirine)
TLC	Thin Layer Chromatography
VAChT	Vesicular Acetylcholine Transporter
VAChT-IR	Vesicular Acetylcholine Transporter -immunoreactive axon

Chapter I:
General Introduction

1.1 Alzheimer's disease:

Alzheimer's disease (AD), also called as Senile Dementia of Alzheimer type (SDAT), is a progressive neurologic disease of the brain leading to the irreversible loss of neurons and the loss of intellectual abilities, including memory and thinking, which become severe enough to hamper social or occupational functioning. This neurodegenerative disease is named after the German psychiatrist Alois Alzheimer, who first described it in 1906. It is a disorder of the gray matter of the cerebral cortex and generally diagnosed in people over 65 years (Brookmeyer R et al., 1998) of age, but the less-prevalent early-onset Alzheimer's can also occur much earlier. Clinically, the disease is characterized by progressive dementia and pathologically by the extracellular deposition of senile plaques and intraneuronal neurofibrillary tangles. AD starts in the entorhinal cortex and then progresses to the hippocampus, basal nuclei, and then to the neocortex. It spares primary motor and sensory cortices, preferentially attacking association areas in the frontal, parietal, and temporal lobes. Affected regions are associated with the neurochemical deficits of acetylcholine, glutamate, and serotonin and the degree of dementia correlates with the decline of these neurotransmitters, revealed in biopsy or autopsy tissue. Dementia is a clinical syndrome, which include memory disorder plus at least one other cognitive sign: language, motor or procedural memory (praxis), spatial function, and executive function (decision making, planning, and control of behavior) (Stephen S Flitman 2011).

The disease course can be sub-divided into four stages (National institute of Aging 2007, Rizzo S 2009). Although the symptoms of AD in each individual patients are distinctive, there are some common symptoms with the progressive pattern of cognitive and functional deficiency (National institute of aging 2007, Rizzo S 2009).

1.1.1 Predementia

The most noticeable impairment is memory loss, which was expressed as difficulty in remembering the most recent events or facts and inability to gain new informations. Problems associated with the executive functions, such as attentiveness, scheduling, flexibility, and immaterial thinking, or impairments in sematic memory (memory of meaning, and concept of relationships), can also be symptoms at the early stage of AD.

1.1.2 Early dementia

The progressive impairment of learning and memory are two important clinical symptoms in AD. In a small proportion of AD patients, difficulties with language, executive functions, agnosia, or apraxia are more prominent than the impairment of learning and memory. In this stage, the person with AD is usually adequately capable of communicating basic ideas. While difficulties may be present in performing fine motor tasks, such as writing, drawing or dressing, coordination in certain movement, planning and ultimately the patient is appeared clumsy.

1.1.3 Moderate dementia

In this stage, speech difficulties become evident, which leads to paraphasias. Reading and writing skills are also progressively lost. As time passes, complex motor sequences become less coordinated and the ability to perform most normal daily living activities is reduced. In this phase, memory problems are worsen and the patients may not able to recognize close relatives. Long-term memory, which was previously intact, become impaired, and behavioral changes become more prominent.

1.1.4 Advanced dementia

Language is reduced to simple phrases or even single word, ultimately leading to the complete loss of speech. Despite the loss of verbal language ability, patients can

often understand and return emotional signals. Ultimately, patients will not be able to perform even the simplest tasks without the assistance from others. Finally comes death, usually caused directly by external factors such as pressure, ulcers, and pneumonia, not by the AD itself.

1.1.5 Pathological hallmarks

Although the origin of AD is still unknown, pathological hallmarks include neurofibrillary tangles (NFTs), amyloid-β plaques, neuropil threads, Hirano's bodies, granulovacuolar bodies, cerebral amyloid angiopathy (Cvetkovic-dozic D et al., 2001) and synaptic loss. At autopsy, the AD brain is characterized by a number of important pathological changes, including a marked loss of neurons and synapses in many areas of the CNS, which include hippocampus, parahippocampus, and amygdala (Cvetkovic-dozic D et al., 2001). In addition, there is a reduction of neurotransmitters level, noradrenaline, dopamine, glutamate, substance P and acetylcholine (ACh) was also observed in AD. Among the neurotransmitters, ACh is the most important cause of the clinical manifestations of AD.

1.1.6 Epidemiology of Alzheimer's disease

Two main measures are used in epidemiological studies: incidence and prevalence. Incidence is the number of new cases per thousand person–years, while prevalence is the total number of cases of the disease in the population at a given time.

1.1.6.1 Prevalence of Alzheimer's disease

The pooled data of population-based studies in Europe suggests that the age-standardized prevalence in people over 65 years old is 6.4% for dementia and 4.4% for AD (Lobo A et al., 2000). In the US, the study of a national representative sample of people aged over 70 years yielded prevalence for AD of 9.7% (Plassman BL et al., 2007). Worldwide, the global prevalence of dementia was estimated to be 3.9% in

people aged over 60 years, with the regional prevalence being 1.6% in Africa, 4.0% in China and Western Pacific regions, 4.6% in Latin America, 5.4% in Western Europe, and 6.4% in North America (Cleusa P Ferri et al., 2005). More than 25 million people in the world are currently affected by dementia, most suffering from AD, with around 5 million new cases occurring every year (Cleusa P Ferri et al., 2005, Wimo A et al., 2003, Brookmeyer R et al., 2007). Among developed nations, approximately 1 in 10 older people (over 65 years) is affected by some degree of dementia, whereas more than one third of very old people (over 85 years) may have dementia-related symptoms and signs (Von Strauss E et al., 1999; Corrada MM et al., 2008).

1.1.6.2 Incidence of Alzheimer's disease

The pooled incidence rate of AD among people over 65 years of age in Europe was 19.4 per 1000 person-years (Fratiglioni L et al., 2000). The pooled data from two large-scale community-based studies of people aged over 65 years in the US Seattle and Baltimore areas yielded an incidence rate for AD of 15.0 (male, 13.0; female, 16.9) per 1000 person-years (Kawas C et al., 2000; Kukull WA et al., 2002). The incidence rate of AD increases almost exponentially with increasing age until 85 years of age (Fratiglioni L et al., 2000; Kukull WA et al., 2002; Jorm AF et al., 1998; The Canadian Study of Health and Aging Working Group. 2000). Studies have confirmed that AD incidence in developing countries is generally lower than in North America and Europe. For example, the incidence rate of AD among people aged over 65 years was 7.7 per 1000 person-years in Brazil and 3.2 per 1000 person-years in India (Kalaria RN et al., 2008; Chandra V et al., 2001).

1.1.7 Impact of Alzheimer's disease at individual and societal levels

At the individual level, AD is one of the principal causes of physical disability, institutionalization, and decreased quality of life. It is estimated that among individuals

over 60 years of age dementia contributes 11.2% of the years lived with disability, compared with 9.5% for stroke, 8.9% for musculoskeletal disorders, and 5.0% for cardiovascular disease (Mathers C et al., 2000). Moreover, AD is associated with a two to five fold increased risk of death (Helzner EP et al., 2008; Mehta KM et al., 2008). The recent study indicated that in 2006 the world wide total number of patients with AD was 26.6 million, and by 2050 the number will quadruple (Brookmeyer R et al., 2007). It was estimated that about 43% of AD patients require a high level of care such as nursing home and institutions. The worldwide overall societal costs of dementia were estimated to be more than US$315 billion in 2005, including one third for informal care; (Wimo A et al., 2007). Approximately three fourths of the global costs for dementia occurred in middle income countries where about 46% of dementia patients reside (Kalaria RN et al., 2008). Thus, AD will place heavy economic burden on the family and society due to the needs of persistent care and therapy.

1.2 Etiopathologies of Alzheimer's disease:

A considerable research had been undergoing over the past two decades to discover the cause of Alzheimer's disease with the ultimate hope of developing safe and effective pharmacological treatments. There are several competing hypotheses trying to explain the cause of the disease.

1.2.1 Cholinergic hypothesis

In the late 1960s and early 1970s, the biochemical investigation of the brains of AD patients began with the hope to detect neurochemical abnormality and to provide the basis for the development of rational therapeutic interventions analogous to levodopa treatment of Parkinson's disease. Outcome of the research came in the mid-1970s with reports of substantial neocortical deficits in the enzyme, choline acetyltransferase (ChAT), responsible for the synthesis of acetylcholine (ACh) (Bowen

DM et al., 1976; Davies P et al., 1976; Perry EK et al., 1977). Successive findings of reduced choline uptake (Rylett RJ et al., 1983), ACh release (Nilsson L et al., 1986) and loss of cholinergic perikarya from the nucleus basalis of Meynert (Whitehouse PJ et al., 1982) confirmed a substantial presynaptic cholinergic deficit in AD. These studies, together with the emerging role of ACh in learning and memory (Drachman DA et al. 1974), led to the "cholinergic hypothesis of Alzheimers disease" **[**Figure 1(a) and 1(b)] **(**Francis PT et al., 1999**)**. Thus it was proposed that degeneration of cholinergic neurons in the basal forebrain and the associated loss of the cholinergic neurotransmission in the cerebral cortex and other areas contributed significantly to the deterioration in cognitive function seen in patients with Alzheimer's disease (Bartus RT et al., 1982).

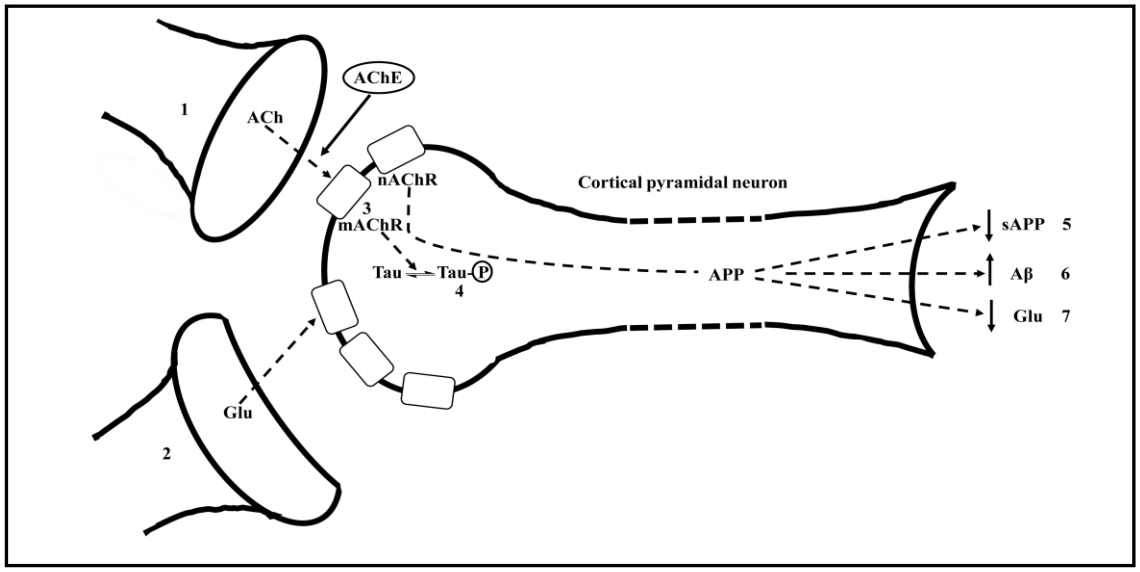

Figure 1(a): Propose neurochemical changes in Alzheimer's disease (Francis PT et al., 1999). *Key to figure 1(a):* ***1.*** *reduced cortical cholinergic innervation;* ***2****. reduced corticocortical glutamatergic neurotransmission due to neuron or synapse loss;* ***3.*** *reduced coupling of muscarinic M_1 receptors to second messenger system;* ***4.*** *shift of tau to the hyperphosphoryalted state—precursor of neurofibrillary tangles;* ***5.*** *reduced secretion of soluble APP;* ***6.*** *increased production of β-amyloid protein;* ***7.*** *decreased glutamate production.*

It is hypothesized that these changes give rise to the clinical symptoms of Alzheimer's disease and contribute to the spread of pathology (Francis PT et al., 1993; Nitsch RM. 1996; Palmer AM et al., 1990).

The cholinergic hypothesis of Alzheimer's disease is based on the presynaptic deficits found in the brains of patients with Alzheimer's disease and studies of the role of ACh in animal and human behavior **(**Francis PT et al., 1999**).**

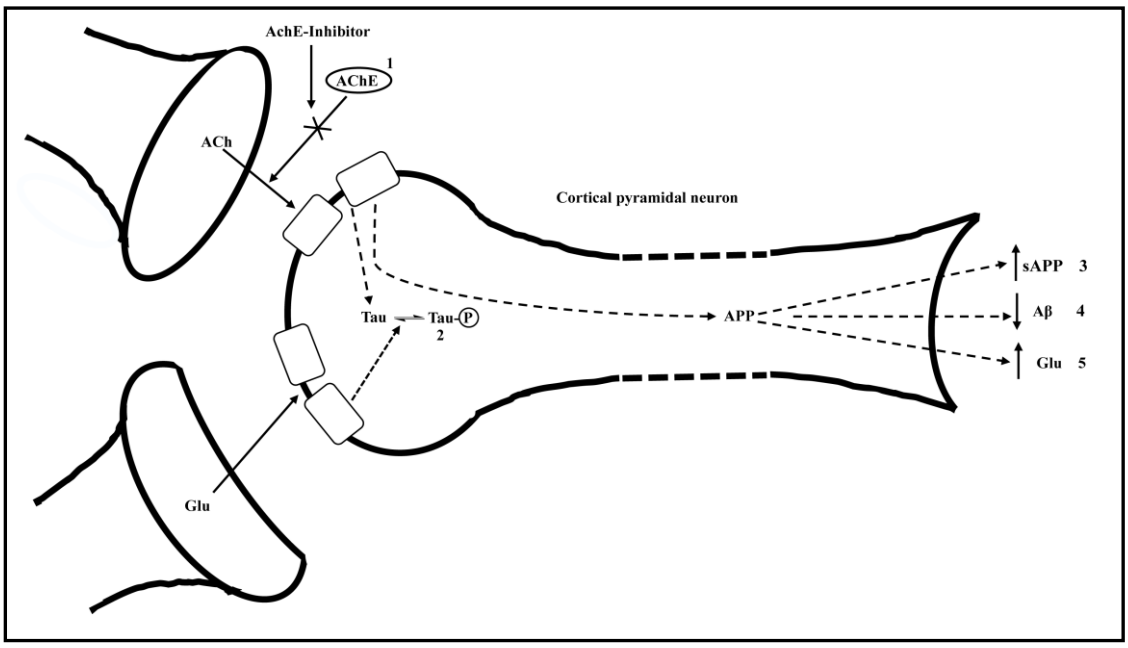

Figure 1(b): Rectification of neurotransmission with cholinesterase inhibitors (Francis PT et al., 1999). *Key to figure 1(b):* ***1.*** *AChE inhibitors reduce the breakdown of endogenously released ACh, resulting in greater activation of postsynaptic ACh receptors; hypothesized consequences:* ***2.*** *reduced phosphorylation of tau;* ***3.*** *secretion of sAPP returned towards normal;* ***4.*** *reduced β-amyloid production;* ***5.*** *glutamatergic neurotransmission returns towards normal, possibly due to activation of muscarinic and nicotinic receptors.*

The treatment for AD has mainly been focused in the cholinergic hypothesis **(**Paul T Francis et al., 1999**)**. It includes:

1.2.1.1 Acetylcholinesterase inhibitors:

The enhancement of the central cholinergic function has been regarded as one of the most promising approaches for the treatment of AD by means of AChE inhibitors. Tacrine, which is an acridine derivatives, was found to be a potent acetyl cholinesterase inhibitor. It is an orally active amine and readily enters CNS and increases the release of ACh from cholinergic nerve endings. It is useful in improving memory performance in AD patients. Unfortunately, Tacrine has shown side effects such as hepatotoxicity, abdominal cramps, nausea, and vomiting. Physostigmine, has shown some efficacy in improving cognitive function in Alzheimer's disease (Arockia BM et al., 2005). Heptyl physostigmine, a more lipophilic analogue is reported to be less toxic than physostigmine while retaining its *in vitro* AChE inhibiting potency. Donepzil and rivastigmine have been marked recently for the treatment of the cognitive symptoms of AD (Chen YL et al., 1992; Brayson HM et al., 1997).

1.2.1.2 Acetylcholine release modulators:

Acetylcholine release modulator, linopiridine enhances the potassium evoked ACh release from rat cortex, hippocampus and caudate nucleus *in vitro* (Fulton B et al., 1996). Another mechanism of the stimulation of the ACh is via antagonists H_3 histamine receptors (H_3-HRS). Two drugs namely Clobenpropit (H_3-HR antagonist) and thioperamide (H_3-HR agonist) have been reported for the treatment of AD (Schnee ME et al., 1998; Stark H et al., 19969). Stimulation of ACh release via the increase of the presynaptic uptake of endogenous choline, found due to the AChE catalyzed enzymatic degradation of ACh, is considered to be an alternative to the receptor regulated ACh release (Miyazaki S et al., 1997).

1.2.2 Tau hypothesis and neurofibrillary tangles

Neurofibrillary tangles (NFTs) are an additional neuropathological hallmark of AD. These are particularly found in cell bodies, apical dendrites as NFT, in distal dendrites as neuropil threads and in the abnormal neurites that are associated with some neuritic plaques. The main components of these neuritic plaques are abnormal filaments such as straight filaments (SFs) or paired helical filaments (PHFs). The basic component of these filaments is the microtubule-associated protein tau (Akaike A. et al., 1998) which is widely expressed in the mammalian nervous system. Tau, a normal axonal protein which binds to microtubules through its microtubulebinding domains thus promotes microtubule assembly and stability. Six tau isoforms are produced in the adult human brain and are found in neurofibrillary lesions of AD patients (M. Goedert et al, 1988). Tau phosphorylation is controlled by the delicate balance between multiple kinases (eg, GSK- 3β and CDK5) and phosphatases (eg, PP-1 and PP-2A) (Goedert M et al., 1992). Tau hyperphosphorylation in AD begins intracellularly and leads to sequestration of normal tau and other microtubule associated proteins. Hyperphosphoryalted tau becomes prone to the aggregation into insoluble PHFs and larger aggregates in tangles. Both the loss of microtubule stabilization and the tangle formation compromise neuronal and synaptic function (Blennow K et al., 2006) (Figure 2). Tau in tangles becomes ubiquitinated for non-lysosomal degradation, but this process is inefficient, and tangles may finally choke affected neurons to death (Goedert M et al., 1997).

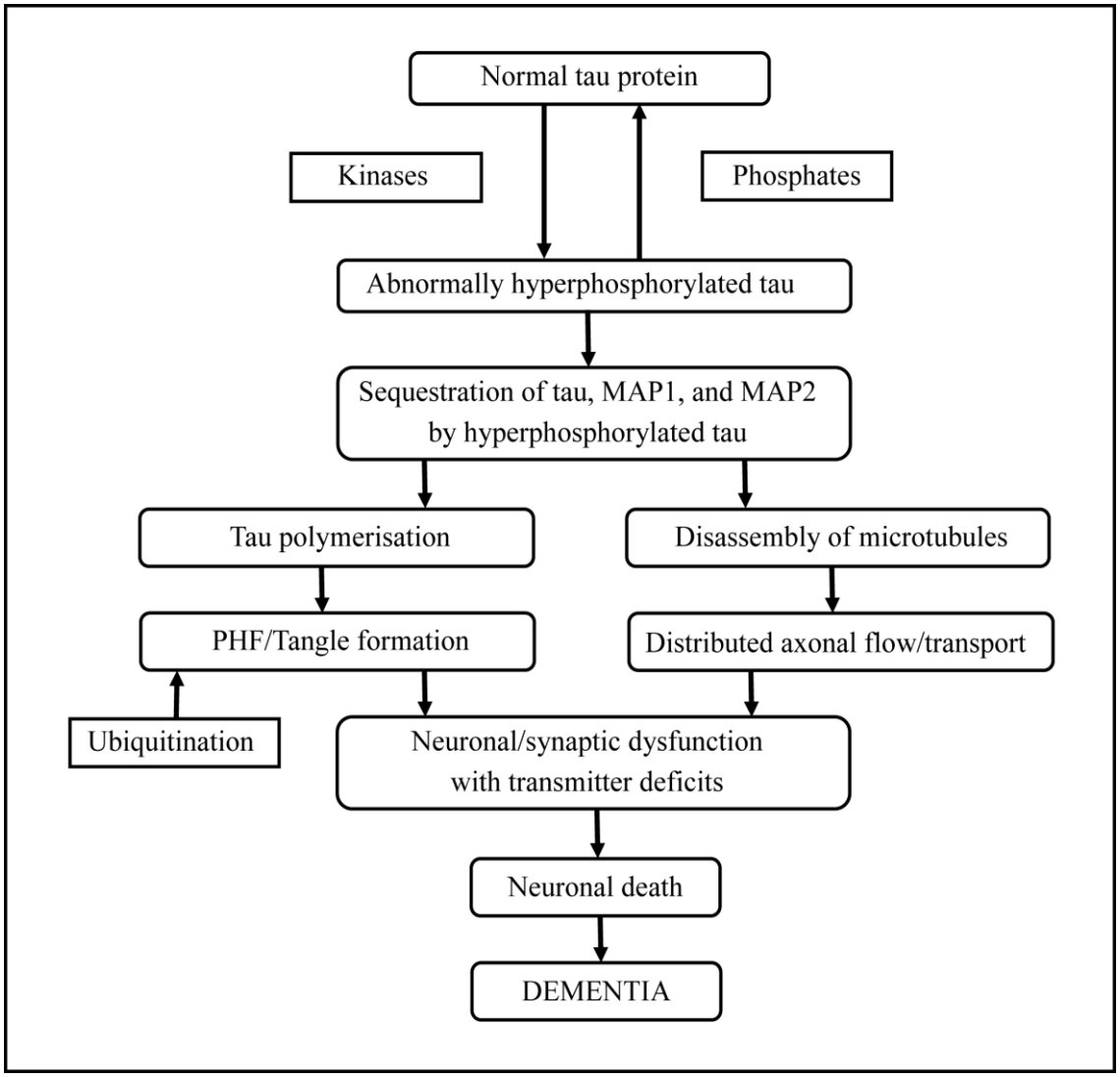

Figure 2: Flow chart of tau hyperphosphorylation and tangle formation.

1.2.3 Amyloid Cascade Hypothesis

It is the most preferred model used to explain the pathogenic events causing AD. According to this hypothesis, the central event in the disease pathogenesis is an imbalance between Aβ production and clearance, with increased Aβ production in familial disease and decreased Aβ clearance in sporadic disease. Aβ oligomers could directly inhibit hippocampal long-term potentiation and impair synaptic function, in addition to the inflammatory and oxidative stress caused by aggregated and deposited Aβ. These processes impair neuronal and synaptic function with resulting neurotransmitter deficits and cognitive symptoms (K. Blennow et al., 2006) (Figure 3). The hypothesis is supported by several evidences and observations (Hardy J et al., 2002).

1. Persons with the Dawn syndrome have an additional copy of the APP gene and thus produce more Aβ.
2 Mutations causing hereditary AD in the APP or PS genes increase the production of the longer and more amyloidogenic $A\beta_{42}$ form of the Aβ peptide.
3 The Aβ is neurotoxic to several cell lines.
4 Transgenic mice that are knocked out for β-secretase show rescue of memory impairments found in the parental strain with an intactβ-secretase gene. This indicates that the overexpression of APP does not cause memory deficits and that the production of Aβand or APP C-terminal fragments are required for the demonstration of reduced memory function in the mice (Ohno M et al., 2004).
5 The levels of the deposited Aβ associated with cognitive decline and severity of the disease in AD patients and in transgenic animals (Näslund J et al., 2000).

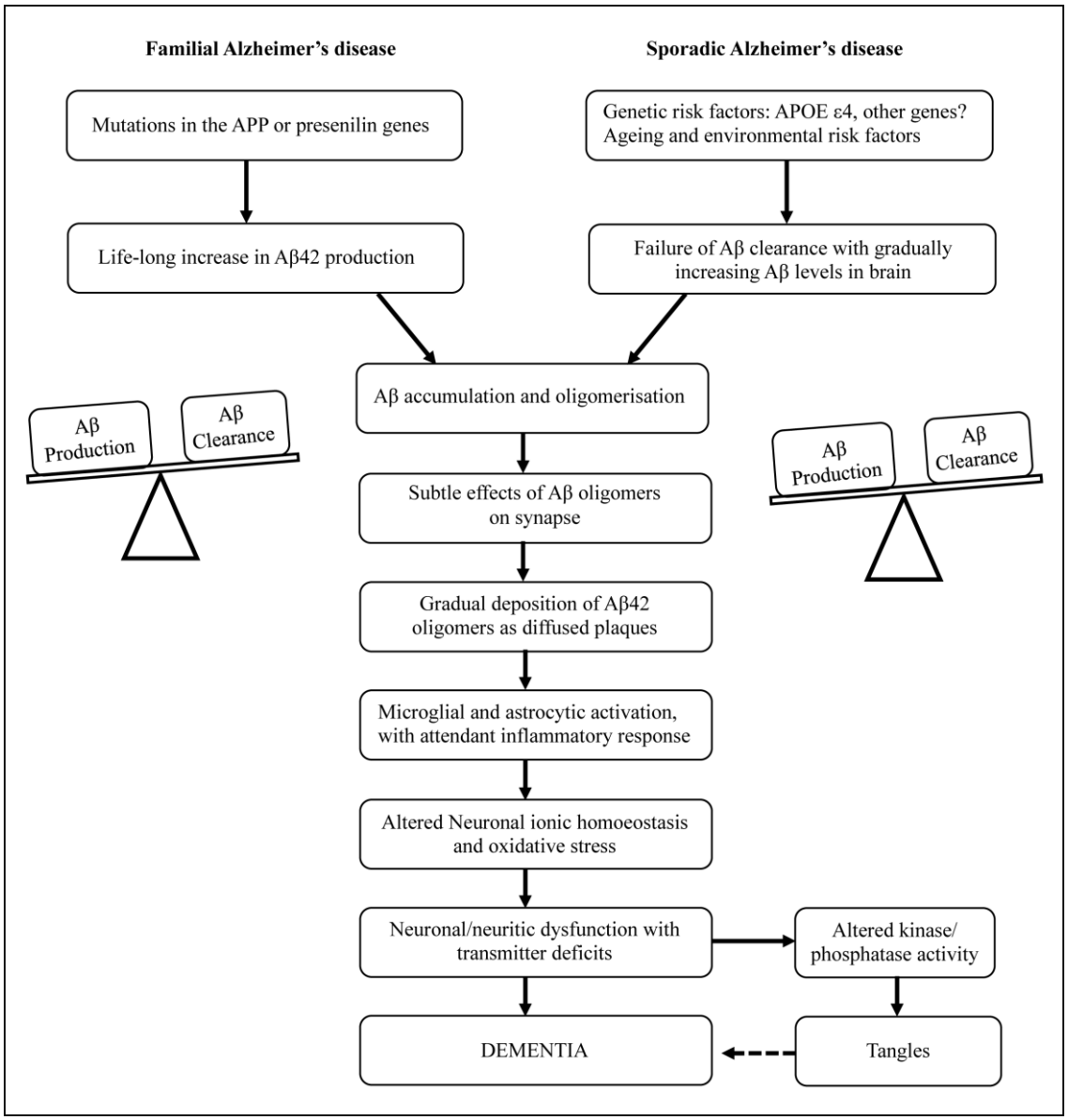

Figure 3: Schematic representation of amyloid cascade hypothesis.

Chapter II:
Cholinergic Markers and Neurotransmission

2.1 Cholinergic neurotransmission and it's components:

Cholinergic neurotransmission requires the synthesis of acetylcholine in the cytoplasm, accumulation of acetylcholine in synaptic vesicles, and release of acetylcholine from the terminal of the cholinergic neuron. ACh is synthesized from choline and acetyl coenzyme A (AcCoA) by the enzyme choline acetyltransferase (ChAT). Choline gains access to the nerve terminal by active transport from the extracellular fluid via the high-affinity choline transporter (HAChT). AcCoA is synthesized in mitochondria from pyruvate (Pyr) by the enzyme pyruvate dehydrogenase (PDH). AcCoA is transported out of the mitochondria for the synthesis of ACh. ACh is transported into synaptic vesicles by a vesicular ACh transporter. The arrival of an action potential at the nerve terminal causes the synaptic vesicles to fuse with the nerve membrane, followed by the exocytotic release of ACh. Upon release, ACh can activate postjunctional muscarinic (M) or nicotinic (N) receptors as well as presynaptic muscarinic receptors (M); stimulation of the latter inhibits the release of ACh. The actions of ACh are rapidly terminated by acetylcholinesterase (AChE), which hydrolyzes ACh into choline and acetate. The choline can be transported back into the nerve terminal for the synthesis of new Acetylcholine (ACh).

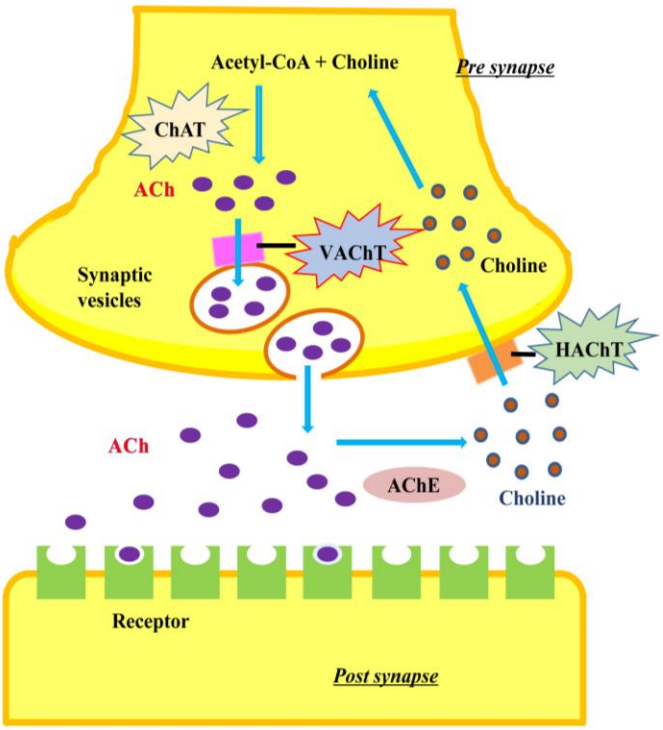

Figure 4: Schematic representation of cholinergic neurotransmission

According to the cholinergic hypothesis, extensive loss of cholinergic neurons found in brains of AD patients postulates a connection between of the cognitive impairments of this disorder-especially the loss of memory and a disturbance in cholinergic neurotransmission. There are some components which are involved in the regulation of presynaptic cholinergic neurotransmission (Table 1) (Sarter M et al., 2005).

Table 1: Important components in the regulation of presynaptic cholinergic neurotransmission.

Components of Cholinergic neurotransmission	Role of the components in the presynaptic Cholinergic neurotransmission
Acetyl-coenzyme A (AcCo-A)	A precursor for the synthesis of ACh by a reaction, catalyzed by AChE.
Acetylcholine (ACh)	The neurotransmitter that is the primary signaling molecule of cholinergic neurons.
Acetylcholinesterase (AChE)	The enzyme that hydrolyses ACh to Ch and acetate. AChE inhibitor increases the extracellular ACh levels and are widely used as drugs to treat the cognitive symptoms of AD disease, such as donepezil, rivastigmine or galantamine.
Choline (Ch)	An amine that is a precursor for the synthesis of ACh. Choline is required nutrient and has many biological functions (Blusztajn J.K et al., 1998).
Choline acetyltransferase (ChAT)	The enzyme that catalyzes the synthesis of ACh from Ch and AcCoA in the presynaptic terminal of cholinergic neurons.
High-affinity choline transporter (HAChT)	Sodium- and chloride –dependent transporter protein with a high affinity for Choline. The uptake of Choline by this transporter is the rate-limiting step for the synthesis of ACh.
Muscarinic autoreceptors	In the cortex, ACh binds to presynaptic terminals mainly through M2 receptors. Stimulation of these G-protein-coupled receptors with ACh or muscarinic receptor agonist attenuates ACh release; conversely, blockade of these receptors, by drugs such as atropine or scopolamine, increases ACh release.
Vesicular Acetylcholine Transporter (VAChT)	Neurotransmitter transporter protein that transports newly synthesized ACh into synaptic vesicles. This process can be blocked by the drug vesamicol.

Choline acetyltransferase (ChAT), vesicular acetyl choline transporter (VAChT), and high-affinity choline transporter (HAChT) are considered as the three most important specific markers for cholinergic neurons (Hoover DB et al., 2004).

2.1.1 Choline acetyltransferase (ChAT)

Choline acetyltransferase (CHAT), responsible for the synthesis of acetylcholine, is presently the most specific indicator for monitoring the functional state of cholinergic neurones in the central and peripheral nervous systems.

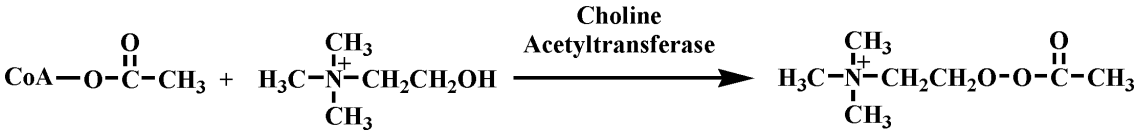

Figure 5: Synthesis of Acetyl choline (Ach)

It is a single-strand globular protein, synthesized in the perikaryon of cholinergic neurons and transported by both slow and rapid axoplasmic flows to the nerve terminals. In cholinergic nerve terminals, ChAT exists in (a) soluble, and (b) non-ionically membrane-bound forms. Multiple mRNA species of ChAT (R-, N-and M-types) are produced by different splicing in the mouse, rat, and human and transcribed from different promoter regions. All transcripts encode the same ChAT protein in rodents, while in case of human M-type mRNA has the capability to generate both the large and small forms of ChAT proteins and R-and N-types ChAT mRNA generate a small form, which corresponds to the rodent ChAT (Oda Y., 1999). The genomic structure of ChAT is unique compared to the other enzymes for neurotransmitters. The first intron of the ChAT gene includes the open reading frame encoding another protein VAChT, which mediates the storage of the newly synthesized acetylcholine from the cytoplasm into the synaptic vesicles. The expression of ChAT and VAChT appear to be regulated by the several regulatory elements in cholinergic

neurons. Immunohistochemical and *in situ* hybridization studies have revealed that in the central nervous system, the medial septal nucleus, the nucleus of the diagonal band of Broca, the basal nucleus of Meynert, the caudate nucleus, the laterodorsal tegmental nucleus, the medial habenular nucleus, the parabigeminal nucleus, some cranial nerve nuclei, and the anterior horn of the spinal cord, are the regions of localization of cholinergic neurons. The complicated cholinergic network, constructed by the fibers projection of focally distributed cholinergic neurons to many areas in the central nervous system, play an important role in neuropsychic activities, such as learning, memory, sleep and movement (Oda Y., 1999). Dysfunction of the central cholinergic neurons are involved in several neurodegenerative diseases such as Alzheimer's disease and amyotrophic lateral sclerosis, in which disturbance of the central cholinergic system does not appear to be closely related to the etiology, but rather to the development of clinical symptoms. In addition, recently abnormalities of ChAT have been demonstrated in the case of schizophrenia and sudden infant death syndrome (Oda Y., 1999).

2.1.2 High affinity choline uptake transporter (HAChT)

The high-affinity choline uptake system located in peripheral and central cholinergic nerve terminals plays a regulating and rate-limiting role in the intraneuronal synthesis of acetylcholine (ACh) (Smart LA et al., 1983; Gilissen C et al., 2003). Choline is transferred into the cell by the high-affinity choline transporter where it reacts with acetyl CoA in the presence of the enzyme choline acetyltransferase (ChAT) to form acetylcholine. Brain synaptosome studies demonstrate two carrier-mediated transport systems for choline uptake (Haga T et al., 1971; Yamamura HI et al., 1972; Haga T et al., 1973; Kuhar MJ et al., 1978; Kuhar MJ et al., 1973). At high concentrations, choline transported primarily by a low-affinity and Na^+-independent

system that at is inhibited by hemicholinium-3 (HC-3) (Happe HK et al., 1993) with a high K_i of approximately 50 μM. This system thought to be ubiquitously present in cells and to be required for phosphatidylcholine synthesis. At low concentrations choline is transported by a high-affinity, Na^+-dependent system that is inhibited by HC-3 with a low K_i of 10–100 nM. The high-affinity system is supposed to be present specifically in cholinergic neurons, because a substantial proportion of choline is converted to acetylcholine only when taken up through the high-affinity system (Haga T et al., 1971; Haga T et al., 1973; Kuhar MJ et al., 1978). The proposal that the high-affinity choline transport system is unique to cholinergic neurons is supported by the selective loss of the high-affinity choline uptake following depletion of cholinergic terminals in a variety of denervation studies (Kuhar MJ et al., 1978; Kuhar MJ et al., 1973). Choline uptake is generally believed to be the rate-limiting step in acetylcholine synthesis (Haga T et al., 1971; Yamamura HI et al., 1972; Haga T et al., 1973; Kuhar MJ et al., 1978; Kuhar MJ et al., 1973; Tucek R. 1985). In addition, the high-affinity choline uptake is regulated by neuronal activity (Simon JR et al., 1975; Murrin LC et al., 1976), suggesting that neuronal activity also regulates acetylcholine synthesis. In Alzheimer's disease, cholinergic neurons selectively degenerate. Consistent with the above hypothesis, the high-affinity choline transporter is reduced in Alzheimer's disease (Pascual J et al., 1991).

2.1.3 Vesicular acetylcholine transporter (VAChT)

In cholinergic neurotransmission, acetylcholine (ACh) is the primary signaling molecule of cholinergic neurons. The transportation of newly synthesized ACh from the cytosol to the cholinergic synaptic vesicles is mediated by VAChT (Arvidsson U et al., 1997; Bravo DT et al., 2004; Usdin TB et al., 1995). It was reported that, in both the peripheral and central nervous systems, there is a strong relationship between the levels

of VAChT expression and ACh release (Prado VF et al., 2006). A marked diminution of VAChT expression was necessary to interrupt neurotransmission at the neuromuscular junction. Even a modest deficiency of VAChT is sufficient to interfere with release of ACh in the brain and to affect cognitive behavior in object and social recognition and memory function (Prado VF et al., 2006). In the rat brain, staining for both VAChT protein & mRNA and ChAT protein & mRNA have explicitly revealed that the VAChT is localized in synaptic vesicles within cholinergic terminals (Gilmor ML et al., 1996; Ichikawa T et al., 1997; Schafer MK et al., 1995; Schafer MK et al., 1994; Weihe E et al., 1996). With the *in situ* hybridization histochemistry (ISHH) and immunohistochemistry (IHC), it was revealed that VAChT-rich presynaptic cholinergic nerve terminals are widely distributed in various brain regions, including the cerebral cortex, striatum, diagonal band, hippocampus, thalamus, amygdaloidal nucleus, cerebellum, and nuclei of cranial nerves. VAChT is now decisively recognized as a reliable cholinergic marker, and the development of radiolabeled VAChT imaging probe might be a tool for the early detection of AD by using Positron Emission Tomography (PET) or Single Photon Emission Computed Tomography (SPECT).

From the above discussions, it can be concluded that both the HAChT and VAChT can be considered as reliable biomarker for studying the cholinergic function in AD brain. Radioligands which bind specifically to the HAChT or VAChT, are assumed to be used as a neuroimaging probe to investigate the cholinergic neurodegenerative process using PET or SPECT.

Chapter III:

Previous research on HAChT and VAChT imaging probes

3.1 Research on HAChT imaging probes:

High affinity choline uptake transporter can be served as a useful marker of the functional status of the cholinergic presynaptic terminals and associated with a variety of diseases, such as Parkinson's disease, Alzheimer's disease, coronary heart diseases, tumor cancers (Hara T et al., 2006; Mulholland GK et al., 1998; Gao M et al., 2007). Thus, choline transporter systems provide attractive targets for the development of PET biomarkers to probe brain, heart, and cancer diseases. HC-3 is a gold standard for studying the high-affinity choline transport *in vitro* (Gilissen C et al., 2003). Carbon-11 and fluorine-18 labeled HC-3 analogues, [^{11}C]hemicholinium-3 ([^{11}C]HC-3) and [^{18}F]hemicholinium-3 ([^{18}F]HC-3), may serve as in vivo PET agents for the choline transporter (Zheng QH et al., 2007). Several ^{11}C & ^{18}F labeled derivatives of hemicholinium-3, such as [^{11}C] pipzA-4 (Gilissen C et al., 2003) & [^{18}F]FA-4 (Gilissen C et al., 2003) were also synthesized and evaluated for the visualization of HACU system.

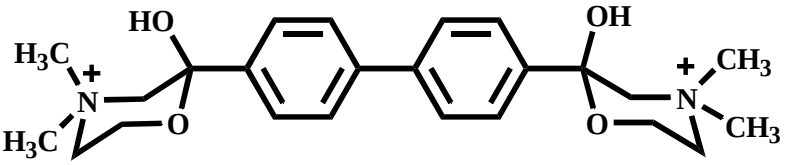

Hem-3

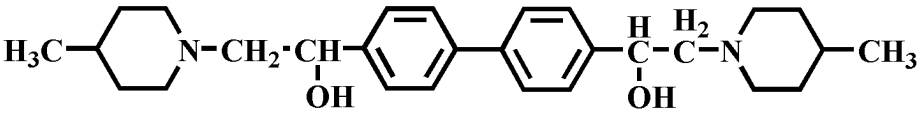

A-4

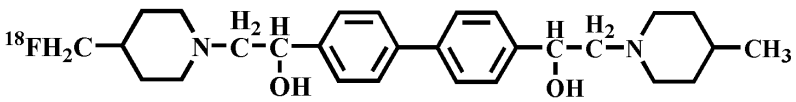

^{18}F-FA-4

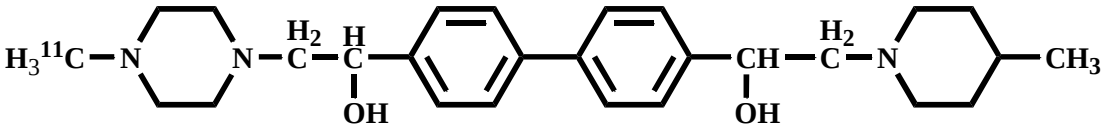

^{11}C-pipzA-4

Figure 6: Structure of Hemicholinium-3 and its analogues as PET HAChT imaging probe

3.2 Research on VAChT imaging probe:

Vesamicol [2-(4-phenylpiperinyl) cyclohexanol] (Figure 7) binds with the vesamicol binding site on VAChT protein with moderate affinity which lead to blockade of vesicular ACh storage and subsequent inhibition of release of this neurotransmitter (Parsons S M et al., 1993; Prior C et al., 1992). Thus, (-)-[^{3}H] vesamicol acts as an indirect antagonist of cholinergic transmission (Altar CA et al., 1988). However, additional moderate to high affinity for sigma (σ) receptors (Efange SM et al., 1994) and it's marginal selectivity for VAChT versus σ_1 & σ_2 receptors, makes vesamicol less useful as a selective radiotracer for VAChT imaging. Therefore, numerous efforts have been undertaken to improve the selectivity of vesamicol through structural modifications. Examples include vesamicol e.g. (–)-[^{125}I]oIV (Shiba K et al., 2002; Shiba K et al., 2003), (–)-[^{11}C]OMV (Shiba K et al., 2006; Kawamura K et al., 2006), benzovesamicol e.g. [^{18}F]NEFA (Rogers GA et al., 1994), [^{18}F] FEOBV (DeGrado TR et al., 1994; Mulholland G K et al., 1998) or [^{125}I]IBVM (Jung YW et al., 1990; Sorger D et al., 2000) and trozamicol e.g. [^{18}F]FBT (Mach RH et al., 1997; Efange SM et al., 1994; Gage HD et al., 2000; Voytko ML et al., 2001) [$^{123/125}$I]MIBT (Efange SM et al., 1993; Staley JK et al., 1997) (Figure 7).

Only [^{123}I] IBVM and [^{18}F] NEFA were used for human studies (Kuhl DE et al., 1994; Widen L et al., 1993) and rest of them were described as potential radiotracers because of their *in vivo* evaluation in rats, rodents or nonhuman primates. But none of these ligands is really accepted for clinical application due to undesired side effects. For

instance, (+)-[^{18}F] FBT resulted excessively high nonspecific binding in human subjects due to its relatively higher affinity for σ receptors (Zhude T et al., 2009) and in the human temporal cortex post-mortem, *in vitro* [$^{123/125}$I] MIBT binding was reduced by 45% relative to age-matched controls. [^{18}F]FEOBV invariably exhibits highest binding within the striatum and relatively lower accumulation in the VAChT – rich cerebral cortex (Giboureau N et al., 2007; Parent M et al., 2012). Currently, (−)-5-[^{123}I]-iodobenzovesamicol ([^{123}I]IBVM) is the only radiotracer used for imaging VAChT levels in living human brain using single-photon emission computed tomography (SPECT). But a significant decrease in [^{123}I]IBVM binding (47−62%) in cingulate cortex and parahippocampal amygdaloid in AD subjects compared to control patients has been observed (Barret O et al., 2008). However, the slow binding kinetics of [^{123}I]IBVM requires scanning for approximately 6 h post-injection, which can be stressful for patients (Junfeng Li et al., 2013). Positron emission tomography (PET) imaging will be able to carry out scans with higher sensitivity and spatial resolution (3−5 mm) compared to SPECT (10 mm) (Rahmim A et al., 2008; Jansen FP et al., 2007).

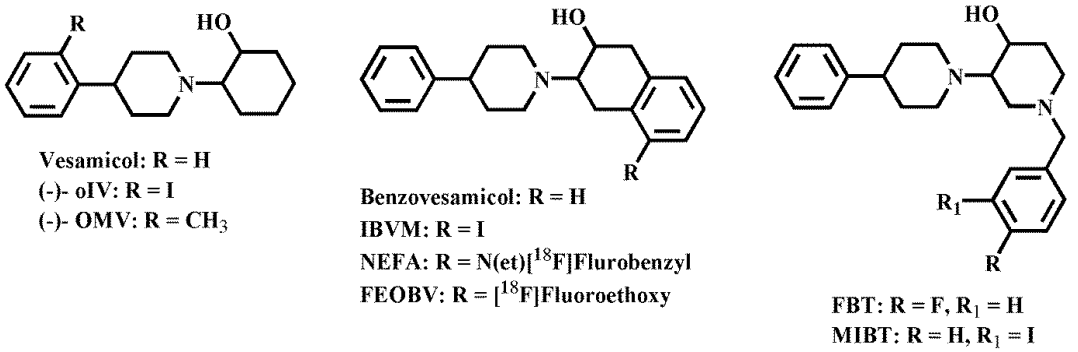

Figure 7: Analogues of vesamicol as VAChT imaging probe.

Zhude Tu and his colleagues have recently reported the synthesis of a new class of VAChT ligands (Figure 8) containing a carbonyl group to the 4-position of the piperidine ring of vesamicol. *In vitro* and *in vivo* evaluation of these compounds have revealed that the modification of the vesamicol structure by introducing a carbonyl group in between the two rings of the 4-phenylpiperidinyl fragment in the vesamicol structure yields benzovesamicol analogues with not only an increased affinity for VAChT but also high selectivity for VAChT versus σ receptors (Zhude Tu et al., 2009, Zhude Tu et al., 2012, Efange SM et al., 2010, Junfeng L et al., 2013).

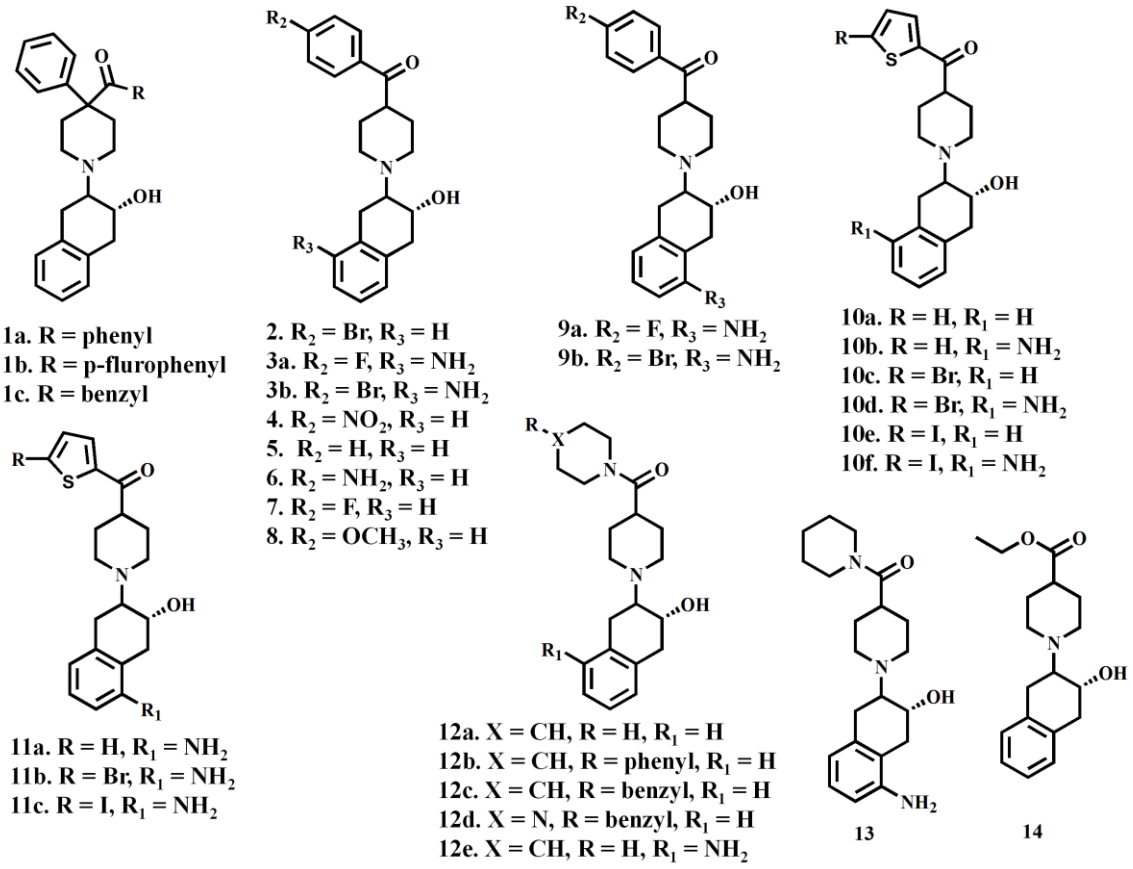

Figure 8: Analogues of vesamicol as VAChT imaging probe containing a carbonyl group to the 4-position of the piperidine ring of vesamicol

Kozaka T et al. in 2014, developed [^{125}I]OIDV (Figure 9), a new decalinvesamicol (DV) analogue, as a potent SPECT VAChT imaging probe through *in vivo* biodistribution experiment (Table 2), *in vivo* blocking experiment (Figure 10), *in vivo* metabolite study and *ex vivo* autoradiography (Figure 11).

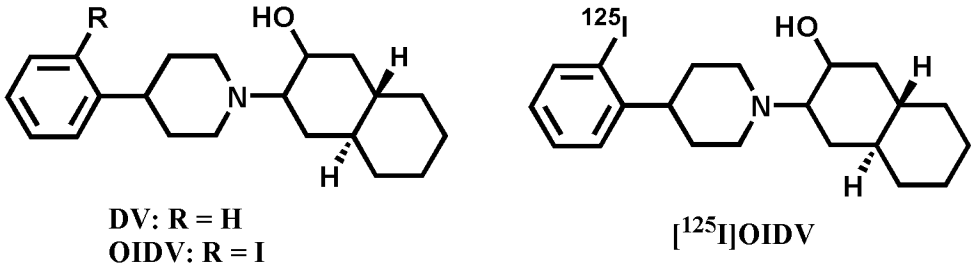

Figure 9: Structure of DV, OIDV and [^{125}IOIDV

Table 2: Biodistribution in rats after an injection of [^{125}I]OIDV (Kozaka T et., 2014).

Organs	Radioactivities [% ID/g]			
	Time post-injection			
	10 min	30 min	60 min	120 min
Blood	0.07 ± 0.02	0.05 ± 0.00	0.04 ± 0.01	0.04 ± 0.00
Heart	0.69 ± 0.11	0.34 ± 0.05	0.23 ± 0.04	0.13 ± 0.01
Lung	3.44 ± 1.21	1.82 ± 0.39	0.96 ± 0.13	0.70 ± 0.10
Liver	2.48 ± 1.48	2.09 ± 0.53	1.97 ± 0.26	1.51 ± 0.16
Spleen	1.38 ± 0.53	1.47 ± 0.32	1.45 ± 0.45	0.87 ± 0.10
Pancreas	2.08 ± 0.97	3.00 ± 0.46	3.10 ± 0.85	2.89 ± 0.37
Stomach	1.18 ± 0.36	0.54 ± 0.08	0.75 ± 0.21	0.40 ± 0.18
Small intestine	1.01 ± 0.55	1.03 ± 0.21	1.98 ± 0.51	1.86 ± 0.62
Kidney	2.18 ± 0.92	2.06 ± 0.42	1.57 ± 0.35	1.23 ± 0.09
Thigh muscle	0.19 ± 0.06	0.17 ± 0.02	0.12 ± 0.01	0.07 ± 0.05
Cerebral cortex	0.45 ± 0.07	0.42 ± 0.08	0.40 ± 0.06	0.26 ± 0.05
Striatum	0.44 ± 0.18	0.36 ± 0.07	0.37 ± 0.04	0.25 ± 0.07
Cerebellum	0.43 ± 0.06	0.36 ± 0.07	0.38 ± 0.05	0.25 ± 0.03
Rest brain	0.45 ± 0.00	0.37 ± 0.06	0.38 ± 0.07	0.27 ± 0.04

Values are the mean percent injected dose per gram ± standard deviation.

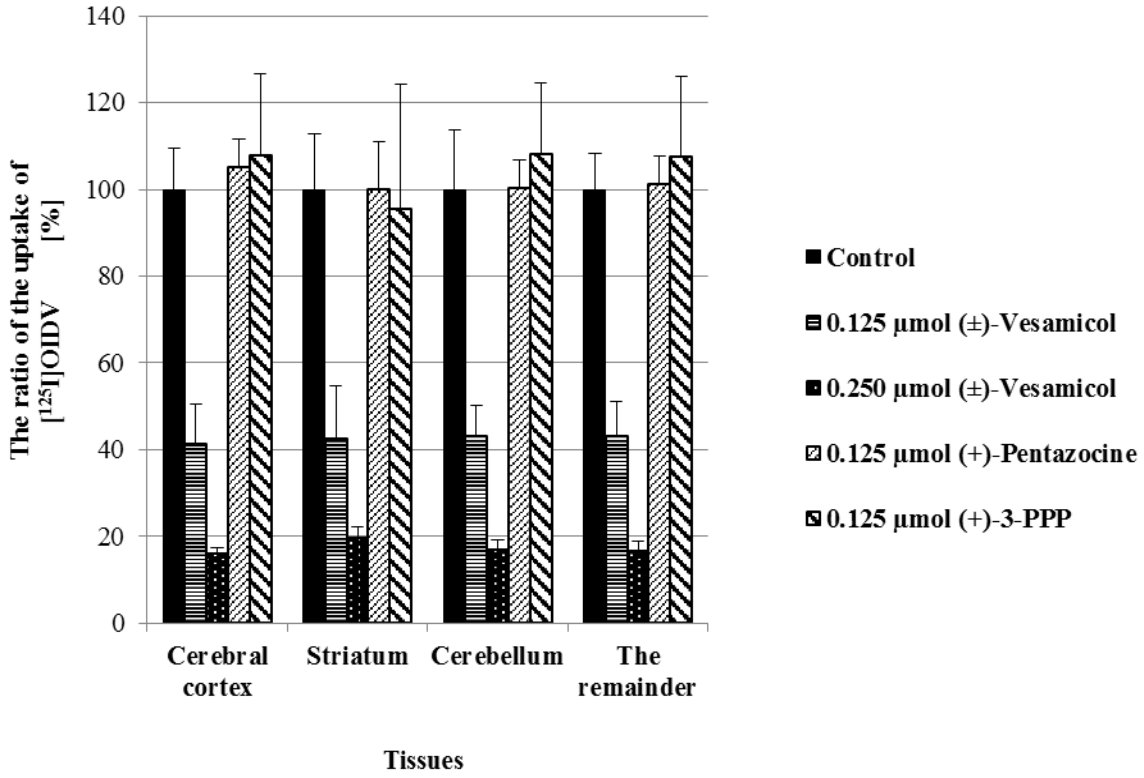

Figure 10: The effect of inhibitors on the uptake of [^{125}I]OIDV. The vertical axis shows the mean radioactivity ratio in the brain regions (cerebral cortex, striatum, cerebellum, and the remainder) of each group co-injected with (+/-)-vesamicol (0.125 and 0.250 mmol), (+)-pentazocine (0.125 mmol), and (+)-3-PPP (0.125 mmol), estimating the control ([^{125}I]OIDV only) as 100% (Kozaka T et., 2014).

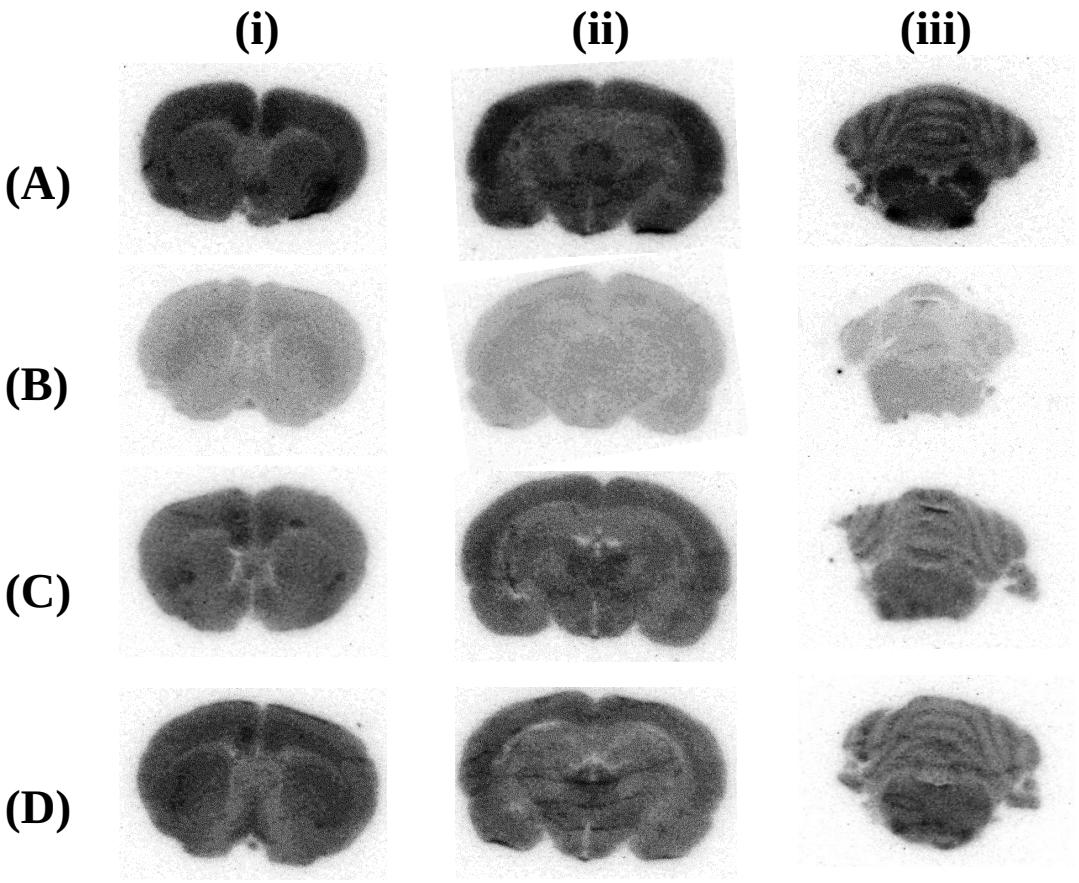

Figure 11: *Ex vivo* autoradiography of [^{125}I]OIDV in rat brain at 60 min after intravenous injection: (A) control; (B) with (+/-)-vesamicol (0.125 μmol) as an inhibitor; (C) with (+)-pentazocine (0.125 μmol) as an inhibitor; and (D) with (+)-3-PPP (0.125 μmol) as an inhibitor. Each column of images shows (i) cerebral cortex and striatum; (ii) hippocampus; and (iii) cerebellum (Kozaka T et al., 2014).

Despite promising *in vitro*, *ex vivo*, and initial *in vivo* studies, most of the radioligand ligands, so far developed, are unsuitable for clinical use due to poor selectivity over σ receptors in brain, low extraction from the blood, slow brain kinetics, or fast metabolism. The demand to provide higher accuracy in clinical imaging of VAChT levels in humans makes the identification of a PET tracer for VAChT very important.

Chapter IV:

Objectives and outline of the PhD thesis

4.1 Objectives of the Thesis:

Pathogenesis background of AD is highly complex. Researchers, around the glove, have proposed several hypotheses for explaining the mechanism of AD development. Among the hypotheses, cholinergic hypothesis has been widely approved and the most characteristic abnormality associated with AD is the decline of cholinergic neurotransmission. Deficiency in high affinity choline uptake (HACU) and the loss of vesicular acetylcholine transporter (VAChT), are two characteristic neurochemical changes in AD. In cholinergic neurons, HACU by the high affinity choline transporter (HAChT) is a rate-limiting and regulatory step for the synthesis of Ach and VAChT mediates the loading of presynaptic vesicles with newly synthesized acetylcholine. Thus, both the HAChT and VAChT appear to be two relatively specific presynaptic marker for cholinergic neurons in AD brain. Our research group at the tracer kinetics division of Advanced Science Research Center of Kanazawa University has been involved for several years in the synthesis and development of vesamicol derivatives as VAChT and sigma receptors SPECT/PET imaging probe for the early diagnosis of AD (Shiba K et al., 1995, Shiba K et al., 1996, Shiba K et al., 2002, Shiba K et al., 2005, Shiba K et al., 2006, Kozaka T et al., 2012, Kozaka T et al., 2014).

This PhD thesis can be divided into two parts. The objective of PART A includes the synthesis and *in vitro* evaluation of MKC-231, tacirine and its corresponding 2-oxo-1-pyrrolidineacetyl derivative as high affinity choline transporter imaging agent. The objective of PART B is to develop radiobromine labeled *Ortho*-bromo-*trans*-decalinvesamicol (OBDV) as a potent and new PET radiotracer for VAChT imaging in AD brain through *in vivo* evaluation and *ex vivo* autoradiography.

PART A

9-amino-1,2,3,4-tetrahydroacrydine (THA, Tacrine; commercial name: Cognix) is well known AchE inhibitors, which produce clinically significant improvement in some cognitive deficits observed in AD patients by increasing the synaptic availability of Ach by inhibiting the AChE-mediated degradation of ACh to choline and acetate. But efficacies of this drug are limited and commonly associated with gastrointestinal side effects during long treatment period (Terry A V Jr et al., 2003). Besides this, there is a deficiency of choline uptake in AD patients. Hence, activation of the presynaptic cholinergic function by improving the reduced HACU is another better approach for the treatment of AD.

Although, THA has no effect as HACU enhancer, THA contained 4-aminopyridine (4- AP) as a partial structure which is already known to increase HACU and 1-nitrogen atom of 4-AP also corresponds to the quaternary amine of ACh. In 1995, Chaki, H., et al showed acylation of THA lead to the synthesis of novel choline uptake enhancers which improve the reduced HACU and some of the structural features of N-acyl derivatives of THA resembles acetylcholine. But due to this structural modification THA loose its activity as AChE inhibitors ([I]Chaki H., et al., 1995; [II]Chaki H., et al., 1995).

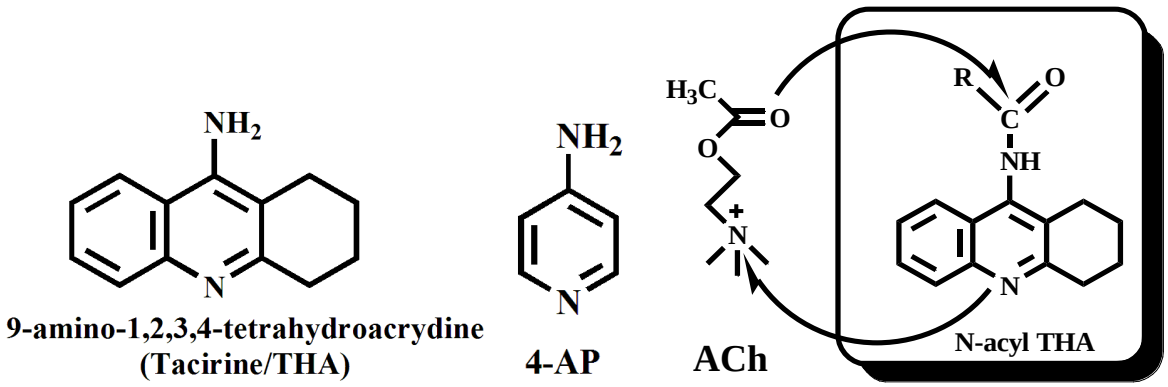

Figure 12: Chemical Structures of THA, 4-AP, Ach and N-acyl THA

Taking the consideration of this special characteristic feature of N-acyl derivatives of THA as HACU enhancer and the role of HAChT to enhance HACU, we have synthesized tacirine, the 2,3-dimethylfuran derivative of tacirine (DMTA) and their corresponding 2-oxo-1-pyrrolidineacetyl derivatives, namely PTAA and MKC-231 and evaluated these compounds through *in vitro* [^{3}H]-Hem-3 binding assay. The objectives of the evaluation of these THA derivatives are as follows:

- To check the affinity of MKC-231, tacirine and the newly synthesized THA derivatives (DMTA, PTAA) for HAChT.
- To find out the possible explanation of mode of action (MOA) of HACU enhancer, and
- To make a possible of clarification of the fact that whether the hemicholinium-3 (ChT inhibitor) and HACU enhancer molecules share the same binding sites or not.

■ **<u>The proposed scheme for the synthesis of THA derivatives:</u>**

1. Synthesis of tacirine (THA) and 2-oxo-1-pyrrolidineacetyl derivative of tacirine, namely PTAA.

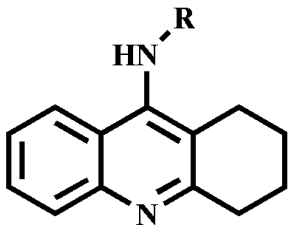

Compounds	R
Tacirine (THA)	H
PTAA	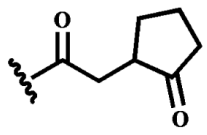

Figure 13: Chemical structures of THA and 2-oxo-1-pyrrolidineacetyl derivative of THA.

2. Replacement of the phenyl ring on the left part of the tricyclic structure of tacirine with a furan ring and synthesis of it's 2-oxo-1-pyrrolidineacetyl derivative (Figure 14).

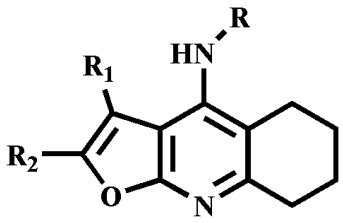

Compounds	R_1	R_2	R
DMTA	Me	Me	H
MKC-231	Me	Me	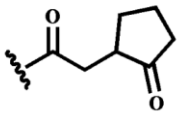

Figure 14: Chemical structures of DMTA and MKC-231

PART B

In 1989, Rogers et al synthesized eighty-four analogues and derivatives of the acetylcholine-storage –blocking drug vesamicol and their potentialities were evaluated with the acetylcholine active-transport assay utilizing purified synaptic vesicles from *Torpedo* electric organ (Rogers GA et al., 1989). The evaluation revealed that(+/-)-*trans*-decalinvesamicol possessed the highest affinity for VAChT and it is 6 times more potent than the (+/-)-*cis*-decalinvesamicol. On the basis of this observations of DV and (–)-oIV (Shiba K et al., 2002, Shiba K et al., 2003), Kozaka T et al. in 2012, have synthesized two new decalinvesamicol (DV) analogues, *o*-bromo-*trans*-decalinvesamicol (OBDV) and *o*-iodo-*trans*-decalinvesamicol (OIDV) with a halogen (-Br, -I) atom at the *ortho*-position of the 4-phenylpiperidine moiety.

Table 3. *In vitro* binding assay of vesamicol analogues (Kozaka T et al., 2012).

Entry	Compounds	K_i (nM)		
		VAChT	σ-1	σ-2
1	OIDV	20.5 ± 5.6	241.8 ± 98.9	118.8 ± 57.0
2	OBDV	13.8 ± 1.2	150.7 ± 62.9	137.5 ± 97.4
3	DV	13.6 ± 8.8	74.1 ± 39.9	68.3 ± 25.5
4	vesamicol	33.9 ± 18.1	22.1 ± 3.6	86.7 ± 35.7
5	DTG	-	131.1 ± 39.2	31.7 ± 3.6
6	pentazocine	-	12.1 ± 5.0	1,880.8 ± 953.9
7	haloperidol	-	3.5 ± 0.8	51.6 ± 14.6

The *in vitro* binding assay of OIDV and OBDV revealed that the OBDV has almost 2.5 times higher affinity than the (+/-)-vesamicol, whereas OIDV was found to possess 1.6 times higher affinity than the (+/-)-vesamicol. So, OBDV was found to possess higher affinity than OIDV towards VAChT and also higher selectivity over sigma receptors. Therefore, there is an opportunity to develop radiolabeled OBDV as a new and promising VAChT PET radiotracer.

A PET tracer provide a useful tool for assessing the severity of cognitive dysfunction and monitoring the efficacy of cholinergic therapies for dementia in neurodegenerative disorders. However, the large potentiality of these cyclotron produced isotopes was not fully explored in clinical nuclear medicine until recently because of their short half-lives ($t_{1/2}$). Oxygen's two minute half-life means that it needs to be pumped directly from a cyclotron to the scan room. Nitrogen's ten-minute half-life and carbon's twenty-minute half-life are a bit easier to work with, but these half-lives mean that there is little time for radiopharmaceutical preparation and delivery to the imaging suite. Fluorine-18 with an approximately two-hour half-life allows more time for synthesis and for imaging somewhat longer physiologic processes. Even with

an on-site cyclotron, these short half-lives limit the biochemical and physiological processes that can be imaged.

Carbon-11, nitrogen-13, and oxygen-15 can only be used to study processes that have rapid uptake. For this reason, our research work was aimed to introduce a novel VAChT imaging probe, radiolabelled with long-lived positron emitters. Because it will allow to radiosynthesize ligand with a good yield and high radiochemical purity and to do biodistribution study even after a long period of post-injection. Besides this, due to the longer half-life, there is a strong possibility of shipping of the PET radiotracer to the research facilities and hospitals for doing research and clinical studies, which don't have any in-house isotope production facility.

Considering the benefits of using long-lived PET radioisotopes as imaging probe for patient diagnosis and research activities and also considering the *ortho* position of –Br substituent in OBDV, the another objective of the PhD thesis is to introduce a radiobromine labelled *o*-bromo-*trans*-decalinvesamicol (OBDV) as a PET radioligand and evaluation of its potentiality as a VAChT imaging probe by various *in vivo* experiments and *ex vivo* autoradiography using rat's brain.

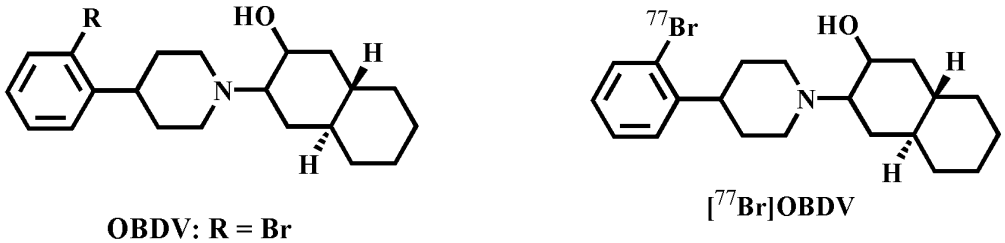

OBDV: R = Br
OTDV: R = $SnMe_3$

[^{77}Br]OBDV

Figure 15: Structure of OTDV, OBDV and [^{77}Br]OBDV

The evaluation of the potentiality of radiobrominated OBDV as a PET VAChT imaging probe was performed the following experiments:

- Radiolabeling of OBDV with ^{77}Br ($t_{1/2}$ = 57.0 h), instead of ^{76}Br ($t_{1/2}$ = 16.0 h) because of the longer half-life. *Ortho*-trimethylstannyl-*trans*-decalinvesamicol (OTDV) was used as a precursor for the radiosynthesis.
- Determination of partition co-efficient of [^{77}Br]OBDV .
- *In vivo* regional biodistribution study of [^{77}Br]OBDV using rats.
- *In vivo* metabolic analysis of [^{77}Br]OBDV.
- *In vivo* blocking study by using rats to investigate the effect of inhibitors on the uptake of [^{77}Br]OBDV.
- *Ex vivo* autoradiography of [^{77}Br]OBDV in rat brain.

4.2 Thesis outline:

The PhD thesis consists of seven different chapters.

Chapter I starts with brief introduction about Alzheimer's disease, several stages of dementia, possible hallmarks of AD, Epidemiology and social impacts of AD disease. Etiopathologies of AD on the basis of amyloid cascade hypothesis, Tau hypothesis and cholinergic hypothesis are also described in this chapter.

Chapter II includes the brief explanation of cholinergic neurotransmission. This chapter also includes short description of three specific cholinergic markers of cholinergic neurotransmission, namely choline acetyltransferase (ChAT), high affinity choline transporter (HAChT) and vesicular acetylcholine transporter (VAChT). This PhD thesis mainly concentrates on the development and evaluation of HAChT and VAChT imaging agent.

Chapter III of the thesis focuses the continuous research works around the world and also research works of the group of Professor Kazuhiro Shiba at Advanced

Science Research Center, Kanazawa University for the development of SPECT/PET HAChT and VAChT imaging probe for the early diagnosis of AD.

Chapter IV describes the main objectives of the PhD thesis in continuation with the previous investigations and reported results. This chapter also includes the brief outline of each chapter of this thesis.

Chapter V describes the evaluations of MKC-21, tacirine (THA) and it's corresponding 2-oxo-1-pyrrolidineacetyl derivative as the HAChT imaging agent which includes the syntheses of tacirine, the 2,3-dimethylfuran derivative of tacirine (DMTA) and their corresponding 2-oxo-1-pyrrolidineacetyl derivatives, namely PTAA and MKC-231 and the *in vitro* evaluation of these compounds through [^{3}H]-Hem-3 binding assay. A brief discussion on the results of the *in vitro* binding assay is also incorporated in this chapter.

Chapter VI focuses on the *in vivo* evaluation of radiobromine labelled OBDV as a new and potent PET VAChT imaging probe, which includes the syntheses of OBDV & OTDV, radiosynthesis of [^{77}Br]OBDV, and several in vivo studies & *ex vivo* autoradiography of rat's brain with [^{77}Br]BDV. Detailed discussion on the basis of the results of *in vivo* studies and *ex vivo* autoradiography is also incorporated in this chapter.

The dissertation ends with the ***Chapter VII*** that gives some concluding remarks on the findings of *in vitro* evaluation of THA derivatives as HAChT imaging agent and *in vivo* evaluations of radiobromine labelled decalinvesamicol analogue and PET VAChT imaging probe. This chapter also includes some direction for future research in the development of SPECT/PET HAChT and VAChT imaging probe for the early diagnosis of AD.

Chapter V:

Evaluation of tacirine derivatives as HAChT imaging probes

5.1 Results

5.1.1 Chemistry:

The cyclization of 2-Amino benzonitrile (**1**) and 2-Amino-4, 5-dimethyl-3-furancarbonitrile (**2**) with cyclohexanone by means of $ZnCl_2$ in toluene, furnished tacirine (**3**) and DMTA (4), respectively (Figure 16).

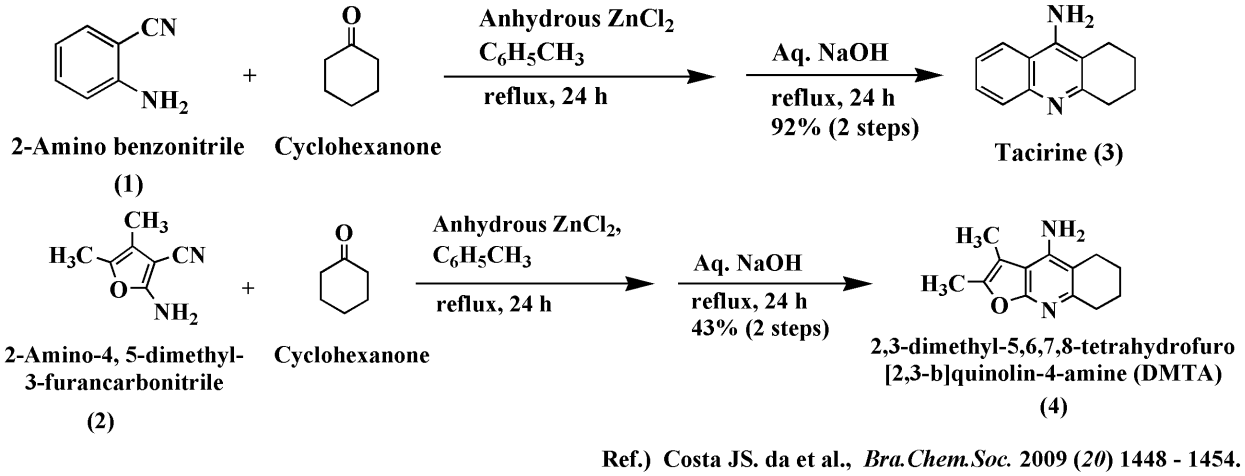

Figure 16: Scheme for the syntheses of tacirine and DMTA.

The acylation of Tacirine (**3**) and DMTA (**4**) with methyl 2-oxo-1-pyrrolidineacetate furnished PTAA (**5**) and MKC-231 (**6**) with the yield of 79% and 65% respectively (Figure 17).

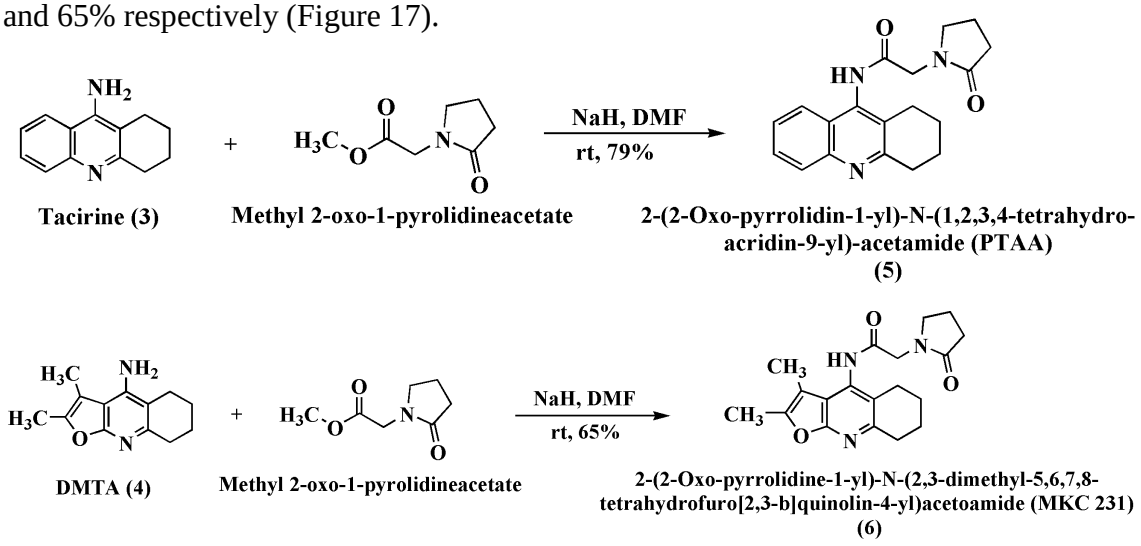

Figure 17: Scheme for the syntheses of PTAA and MKC-231.

5.1.2 *In vitro* HAChT [^{3}H]Hemicholinium-3 ([^{3}H]HC-3) binding assay:

The inhibition activities of tacirine (THA), MKC-231 and the two newly synthesized tacirine derivatives, namely DMTA and PTAA were measured by displacement of a typical HAChT antagonist [^{3}H]HC-3 (Dissociation constant: K_d = 19.1 nM) (Quirion R., 1987, 293-303) in rats cerebral membrane. The percent inhibition against the binding of [^{3}H]HC-3 to HAChT were calculated using GraphPad Prism v4 software (Figure 18). HC-3 showed the highest affinity for HAChT (IC_{50} = 20 nM). Tacrine (THA) showed very insignificant inhibition activity (IC_{50} = 1000 nM). Both the 2,3-dimethylfuran derivative of tacirine, DMTA and 2-oxo-1-pyrrolidineacetyl derivative of tacirine, PTAA showed no affinity for HAChT. MKC-231 also did not show any affinity for the HAChT in [^{3}H]Hemicholinium-3 binding assay.

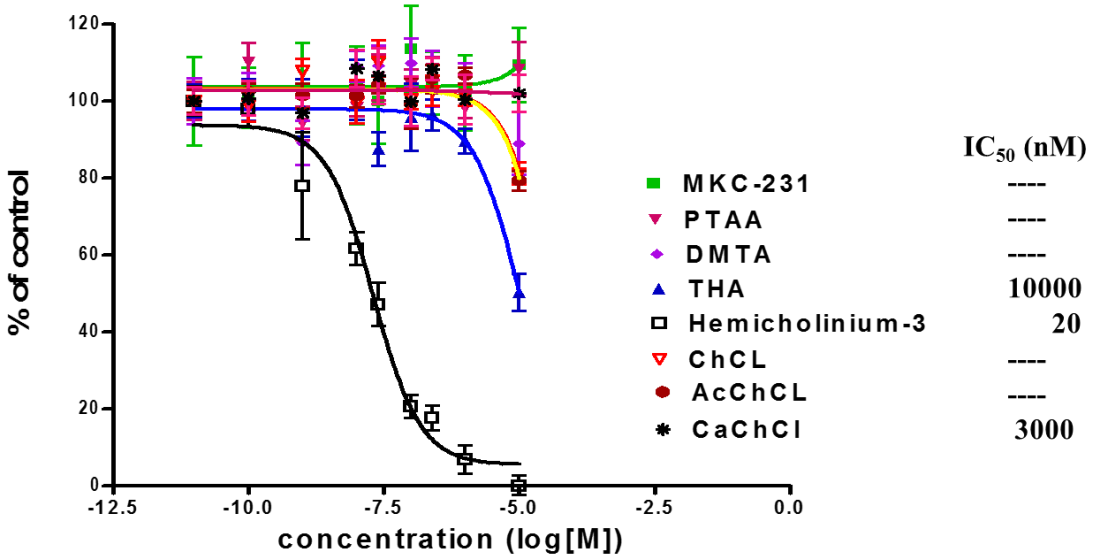

Figure 18: *In vitro* HAChT [^{3}H]Hemicholinium-3 binding assay

5.2 Discussions:

High affinity choline uptake (HACU) system is located especially in presynaptic cholinergic nerve terminals. HACU by the HAChT is found to be a regulating and rate limiting step in the synthesis of ACh. Hence, a ligand with a high affinity for HAChT would be an ideal marker for the study of the state of cholinergic

presynaptic terminals. Hemicholinium-3 is an indirect acetylcholine antagonist, because it decreases the synthesis of acetylcholine by inhibiting the reuptake of choline by the high-affinity choline transporter (ChT). As HC-3 is a quaternary ammonium salt, it cannot cross BBB and radiolabeled quaternary ammonium HC-3 derivatives cannot be used for in vivo visualization of the HACU transporter.

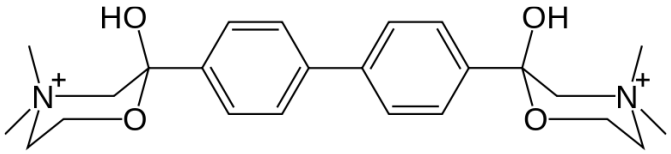

Figure 19: Chemical structure of Hemicholinium-3 (HC-3)

MKC-231, 2-(2-Oxo-pyrrolidine-1-yl)-*N*-(2,3-dimethyl-5,6,7,8-tetrahydrofuro [2, 3-b]quinolin-4-yl) acetoamide, has been reported to enhance HACU in hippocampal synaptosomes in *in vitro* treatment and ameliorates learning deficits in AF64A-treated rats with a single oral administration (Bessho et al., 1996). Although MKC-231 potentially enhances cholinergic activity at synaptic terminals and improves learning impairment observed in AF64A-treated rats and mice, no precise HACU enhancement mechanism has been elucidated.

Acylation of THA, an AchE inhibitor, led to the synthesis of novel choline uptake enhancers which improve the reduced HACU and loose its activity as AChE inhibitors ([I]Chaki H., et al., 1995; [II]Chaki H., et al., 1995).

In the effort of developing HAChT imaging probe we have evaluated tacirine, the 2,3-dimethylfuran derivative of tacirine (DMTA) and their corresponding 2-oxo-1-pyrrolidineacetyl derivatives, namely PTAA and MKC-231 through *in vitro* [^{3}H]Hemicholinium-3 ([^{3}H]HC-3) binding assay to investigate their affinity for HAChT. From the the *in vitro* binding assay, it was revealed that only hemicholinium-3 expressed high affinity for HAChT (IC_{50} = 20 nM). Tacrine (THA) showed some

degree of inhibition activity (IC_{50} = 1000 nM), but it is very insignificant compared to the inhibition activity of hemicholinium - 3 (IC_{50} = 20 nM). Both the 2,3-dimethylfuran derivative of tacirine, DMTA and 2-oxo-1-pyrrolidineacetyl derivative of tacirine, PTAA showed no affinity for HAChT. Although, MKC-231, is known to enhance HACU and increase the synthesis and release of ACh in *in vitro* and *in vivo* studies (Takashina K et al. 2008), it did not show any affinity for the HAChT in [^{3}H]Hemicholinium-3 binding assay. Other inhibitors like choline chloride (ChCl), Acetylcholine chloride (AChCl), Carbamylcholine Chloride (CaChCl) showed no binding affinity for high affinities choline transporter (ChT).

As no inhibitors (except Hem-3), MKC-231, THA and the synthesized THA derivatives did not exhibit any inhibition towards HAChT, so it is worthy to search for the new molecules having high affinity for choline transporter (HAChT) for the extensive study of HACU.

5.3 Experimental:

5.3.1 Syntheses:

5.3.1.1 Synthesis of 1,2,3,4-Tetrahydro-acridin-9-yl amine (THA) (3)

To a mixture of 2-Aminobenzonitrile (**1**) (2 g; 16.93 mmol) and cyclohexanone (14 mL; 135.44 mmol) in toluene (60 mL) placed in a round bottom flask connected to a Dean-Stark water separator, $ZnCl_2$ (6.93 g; 50.79 mmol) was added. The mixture was refluxed for 06 hours. After that, the reaction mixture was cooled at room temperature and the remaining solids were treated with NaOH (2M, 70 mL). This mixture was then again refluxed for about another 06 hours with stirring. On cooling to room temperature, the reaction mixture were extracted with $CHCl_3$. The organic layers were combined, dried over anhydrous $MgSO_4$ and concentrated to dryness under reduced pressure. Purification of the residue by column chromatography on silica-gel by using ethyl

acetate with trace ET_3N afforded the target compound (**3**) (3.10 g, 92.26 %) as a yellow solid; ^1H NMR δ 7.90-7.87 (d, 1H), 7.70-7.67 (d, 1H), 7.58-7.54 (t, 1H), 7.38-7.34 (t, 1H), 4.63 (s, 2H), 3.05-3.01 (t, 2H), 2.64-2.60 (t, 2H), 1.98-1.90 (m, 4H); ^{13}C NMR δ 158.60, 146.58, 146.24, 128.92, 128.40, 123.85, 119.50, 117.13, 110.44, 34.14, 23.75,22.86, 22.78. EI MS *m/z* 199 (M^+, 86.2).

5.3.1.2 Synthesis of 2,3-dimethyl-5,6,7,8-tetrahydrofuro[2,3-b]quinolin-4-amine (DMTA)(4):

To a mixture of 2-Amino-4,5-dimethyl-3-furancarbonitrile (**2**) (2.00 g; 14.69 mmol) and cyclohexanone (12 mL; 117 mmol) in toluene (60 mL) placed in a round bottom flask connected to a Dean-Stark water separator, $ZnCl_2$ (6 g; 44.00 mmol) was added. The mixture was refluxed for 06 hours. After that, the reaction mixture was cooled at room temperature and the remaining solids were treated with NaOH (2M, 70 mL). This mixture was then again refluxed for about another 06 hours with stirring. On cooling to room temperature, the reaction mixture were extracted with $CHCl_3$. The organic layers were combined, dried over anhydrous $MgSO_4$ and concentrated to dryness under reduced pressure. Purification of the residue by column chromatography on silica-gel by using hexane: ethyl acetate (1:1) with trace ET_3N afforded the target compound (**4**) (1.37 g, 43.08 %) as a yellow solid; ^1H NMR δ 4.35-4.30 (s, 2H), 2.89-2.85 (t, 2H), 2.47-2.45 (t, 2H), 2.30 (s, 6H), 1.91-1.81 (m, 4H); ^{13}C NMR δ 160.42, 151.34, 146.10, 145.67, 110.24, 107.28, 105.22, 33.04, 29.00, 22.94, 22.89, 11.28, 10.27. EI MS *m/z* 217 (M^+, 86.9).

5.3.1.3 Synthesis of 2-(2-Oxo-pyrrolidin-1-yl)-*N*-(1,2,3,4-tetrahydro-acridin-9-yl)-acetamide (PTAA) (5).

To a mixture of 1,2,3,4-tetrahydro-acridin-9-yl amine (**3**) (1 g; 5.04 mmol) and DMF (50.4 mL), NaH (4.032 g; 100.08 mmol) was added at room temperature maintaining Argon environment. After 01 hour of stirring, methyl

2-oxo-1-pyrolidineacetate (2.03 mL; 15.12 mmol) was added to the reaction mixture maintaining the argon environment at room temperature. The reaction was kept in stirring for another one hour at room temperature. After a total of 2 hour, the reaction mixture were extracted with ethyl acetate. The organic layers were combined, dried over anhydrous $MgSO_4$ and concentrated to dryness under reduced pressure. Purification of the residue by column chromatography on silica-gel by using ethyl acetate: ethanol (50:1) with trace ET_3N afforded the target compound (**5**) (1.3 g, 79.75 %); ^{1}H NMR δ 8.57-8.56 (s, 1H), 7.99-7.96 (d, 1H), 7.76-7.72 (d, 1H), 7.64-7.59 (t, 1H), 7.48-7.43 (t, 1H), 4.22 (s, 2H), 3.68-3.63 8 (t, 2H), 3.15-3.10 (t, 2H), 2.80-2.75 8t, 2H), 2.50-2.44 (t, 2h), 2.17-2.10 (m, 2H), 1.98-1.93 (m, 2H), 1.88-1.82 (m, 2H); ^{13}C NMR δ 176.76, 166.99, 159.85, 146.90, 137.75, 128.83, 127.22, 126.06, 123.55, 121.95,49.01, 48.24, 33.99, 30.38, 25.54, 22.67, 22.45, 18.25. EI MS *m/z* 324 (M^+, 78.6).

5.3.1.4 Synthesis of 2-(2-Oxo-pyrrolidine-1-yl)-*N*-(2,3-dimethyl-5,6,7,8-tetrahydro furo [2, 3-b] quinolin-4-yl) acetoamide (MKC-231) (6).

To a mixture of 2,3-dimethyl-5,6,7,8-tetrahydrofuro[2,3-b]quinolin-4-amine (0.338 g; 1.56 mmol) (**4**) and DMF (15.6 mL), NaH (1. 248 g; 31.2 mmol) was added at room temperature maintaining Argon environment. After 01 hour of stirring methyl 2-oxo-1-pyrolidineacetate (0.63 mL; 4.63 mmol) was added to the reaction mixture maintaining the argon environment at room temperature. The reaction was kept in stirring for another one hour at room temperature. After a total of 2 hour, the reaction mixture were extracted with ethyl acetate. The organic layers were combined, dried over anhydrous $MgSO_4$ and concentrated to dryness under reduced pressure. Purification of the residue by column chromatography on silica-gel by using ethyl acetate with trace ET_3N afforded the target compound (**6**) (0.350 g, 65%); ^{1}H NMR δ 8.45 (s, 1H), 4.14 (s, 2H), 3.64-3.59 (t, 2H), 2.96-2.91(t, 2H), 2.64-2,59 (t, 2H), 2.47-43

8t, 2H), 2.32-2.09 (m, 8H), 1.88-1.76 (m, 4H); ^{13}C NMR δ 176.48, 167.67, 159.95, 151.65, 150.14, 134.91, 123.50, 116.37, 108.19, 48.84, 47.71, 32.74, 30.29, 24.25, 22.69, 22.60, 18.12, 11.58, 8.92. EI MS *m/z* 342 (M^+, 81.4).

5.3.2 Preparation of homogenate from rat's cerebral tissues:

Animal experiments were performed in compliance with the Guidelines for the Care and Use of Laboratory Animals at the Takara-machi Campus of Kanazawa University. Brain Homogenate of rats were prepared with the slight modification of previously described protocol of Sandberg K et al (Sandberg et al., 1985). Sprague-Dawley rats (8 weeks, male, 250–300 g) cerebrum or livers were homogenized in ice-cold 0.32 M sucrose with a Teflon-glass homogenizer. The homogenate was centrifuged at 1000g at 4 ^{o}C for 10 min. The resulting precipitate was removed and the supernatant was centrifuged at 20,000 g at 4 ^{o}C for 20 min. This crude mitochondrial pellet was resuspended in 20 vols. of ice-cold distilled water and dispersed with the Teflon homogenizer with 1000 rpm and the homogenate centrifuged at 8000 g run for 20 min. The supernatant and buffy coat were collected and pelleted at 48,000 g for 20 min. The pellet was washed 4 times in 20 vols. of 50 mM Glycylglycine buffer (pH 7.8) containing 200 mM NaCl by resuspending via Teflon homogenizer. Then the homogenate was centrifuged at 55,000 g for about 15 min and the resulting pellet was again resuspended in 50 mM Glycylglycine buffer (pH 7.8) containing 200 mM NaCl with a Teflon homogenizer (Figure 20).

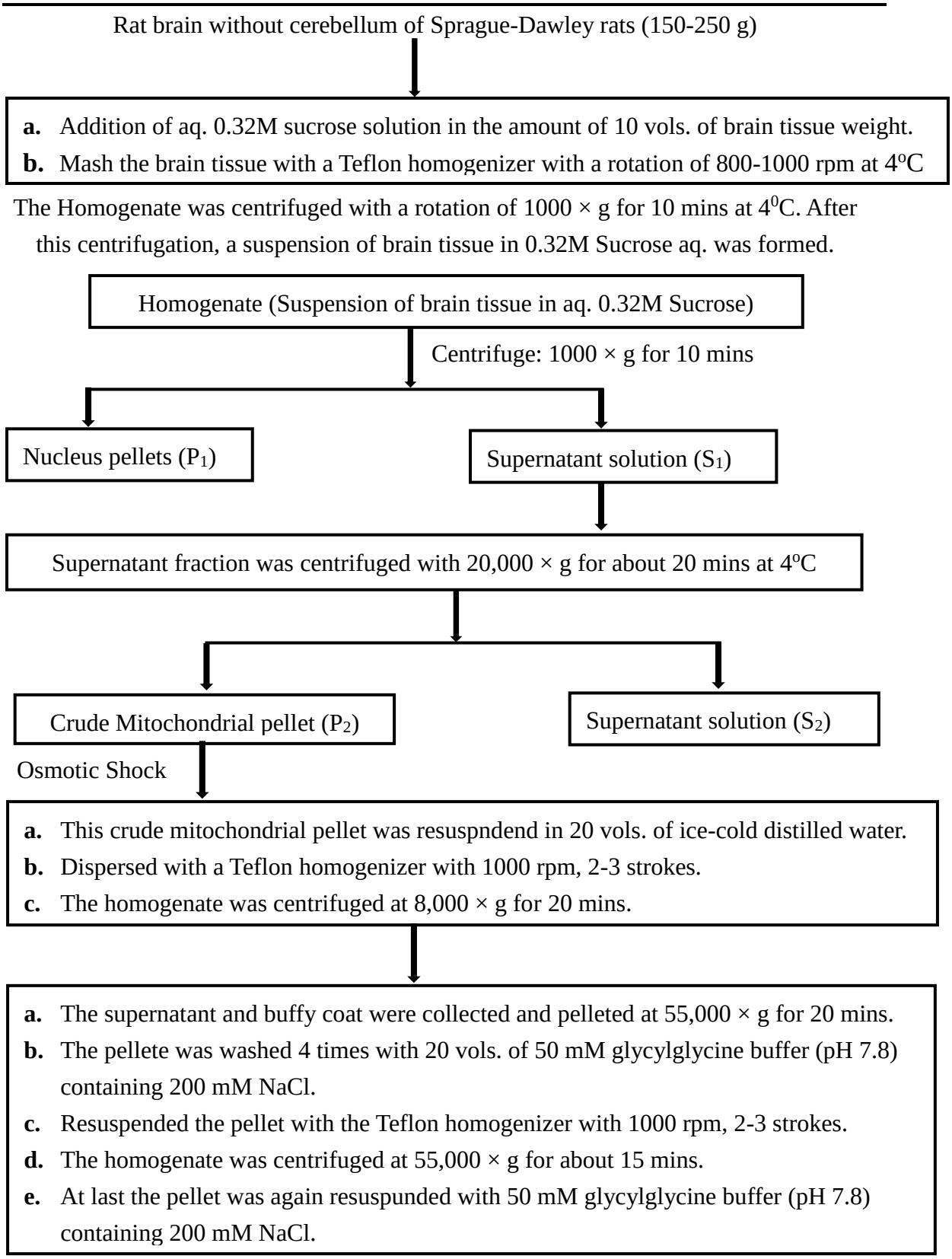

Figure 20: Flow chart for the homogenate reparation of rat cerebral tissues.

5.3.3 *In vitro* HAChT [^{3}H]Hemicholinium-3 binding assay:

[^{3}H]Hemicholinium-3 (K_d = 19.1 nM) (Quirion R 1987) was used as a specific radioligand for the HAChT receptor. Rat cerebral membranes were added to each ice-cold assay tube containing [^{3}H]HC-3 and the displacing ligands at various concentrations ($1.0 \times 10^{-9} – 10^{-4}$) in 50 mM Glycylglycine buffer (pH 7.8) containing 200 mM NaCl in quadruplicate. After the addition of tissues in an ice bath, each reaction mixture in the tube was incubated at 25ºC for 30 min. The incubation was terminated by pitting tubes into ice-cold water followed by immediate filtration using a cell harvester through glass-microfiber filters (Whatman, GF/B), which were presoaked in the in 0.5% (v/v) polyethyleneimine for 01 h to reduce non-specific binding. The filters were washed with 50 mM Tris-HCl buffer (pH 7.8), and their radioactivities were counted with the liquid scintillation counter (Aloka, LSC-5100).

Chapter VI:

*E*valuations of radiobromine labeled decalinvesamicol derivative as VAChT imaging probe

6.1 Results

6.1.1 Chemistry: Synthesis of OBDV and OTDV

4-(2-bromophenyl) piperidine (**7**), the key intermediate for the synthesis of OBDV, was derived from *ortho*–bromobenzaldehyde by four-step reactions (Figure 21) (Kozaka T et al., 2012). Coupling reaction of 4-(2-bromophenyl) piperidine with *trans*-decalin-2,3-oxide furnished OBDV (**8**) in 57% yield. The bromo substituent of OBDV was replaced by a trimethylstannyl group with the reaction of $Pd(PPh_3)_4$ and hexamethylditin to obtain the precursor, *o*-trimethylstannyl-*trans*-decalinvesamicol (OTDV) (**9**) , for the radiosynthesis of [^{77}Br]OBDV, with an yield of 65% .

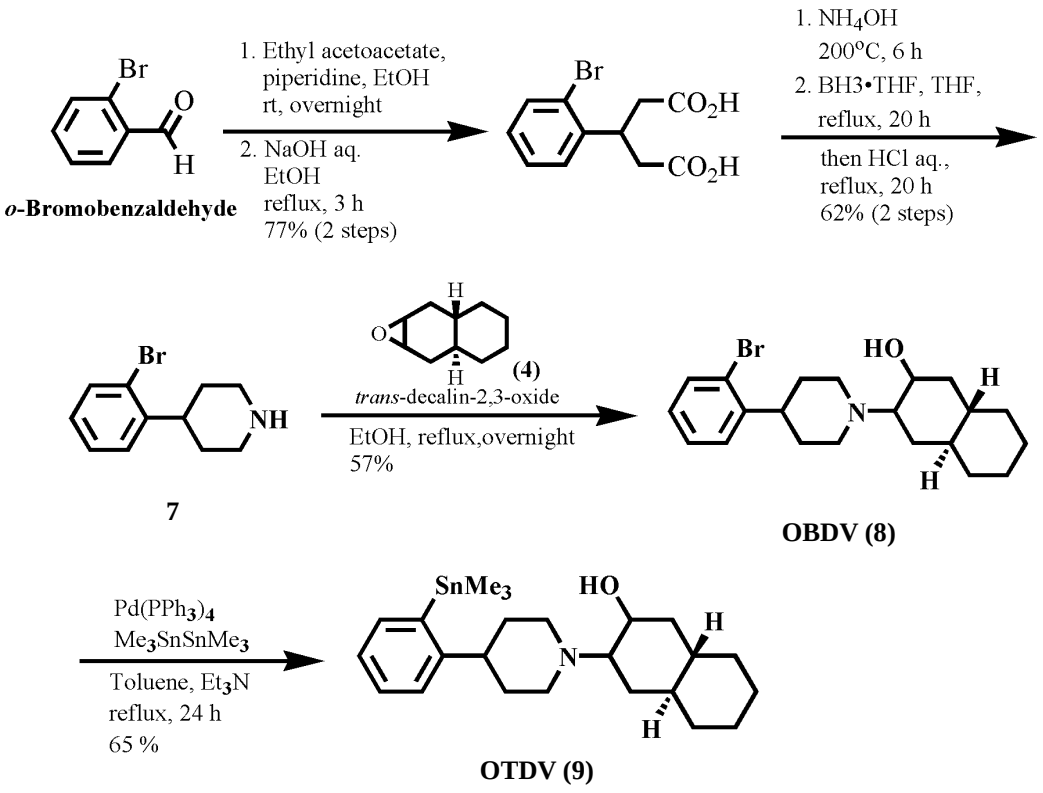

Ref: Kozaka, T. et al. *Bioorg Med Chem.*, 2012, *20*, 4936-4941.

Figure 21: Synthesis scheme of OBDV and OTDV

6.1.2 Radiosynthesis and purification of [^{77}Br]OBDV:

o-trimethylstannyl-*trans*-decalinvesamicol (OTDV) was the main precursor for the synthesis of [^{77}Br]OBDV. [^{77}Br]OBDV was radiosynthesized by the tin-bromine exchange reaction from OTDV with no-carrier added [^{77}Br]Br^{-} (Specific activity: 2.0 TBq/µmol), HCl and chloramine-T (Figure 22). [^{77}Br]OBDV was obtained with a radiochemical yield of 52.3-65.8%. [^{77}Br]OBDV was purified with reversed phase HPLC equipped with a Zorbax-ODS RX-C18 column (9.6 mm × 250 mm) at a flow rate of 4.0 mL/min with a mobile phase of acetonitrile: H_2O: monoethanolamine (90:10:0.2, v/v/v) at 40°C and radiochemical purity was found to be greater than 99%. Ultraviolet (UV) absorption was monitored at 230 nm. The retention time of [^{77}Br]OBDV was found 10 min and the chemical identity of [^{77}Br]OBDV was confirmed by co-injection with reference OBDV (retention time: 10 min) on HPLC under the same condition [Figure 23 (a) and 23 (b)]. The specific activity of [^{77}Br]OBDV was found to be 322 ~ 405.7 GBq/µmol (9.8 ~ 10.9 Ci/µmol).

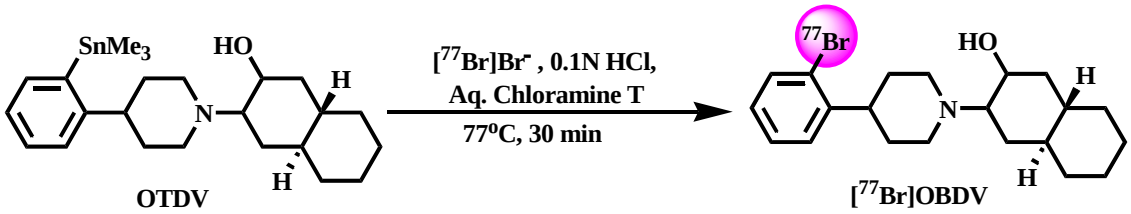

Figure 22: Radiosynthesis of [^{77}Br]OBDV.

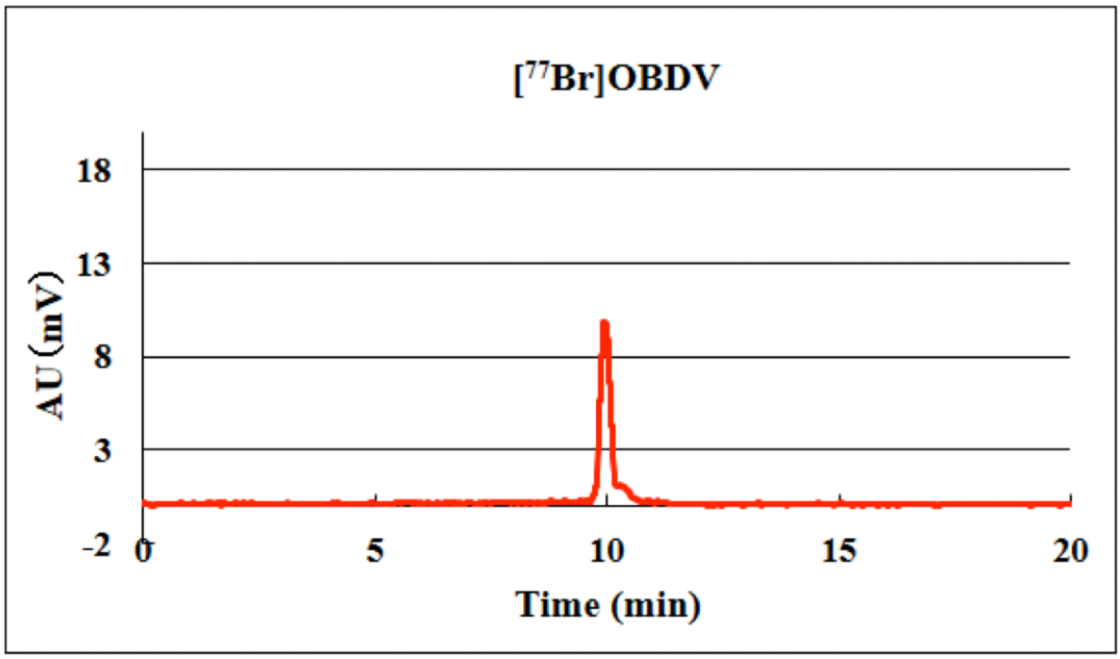

Figure 23 (a): HPLC charts for the retention time of [^{77}Br]OBDV.

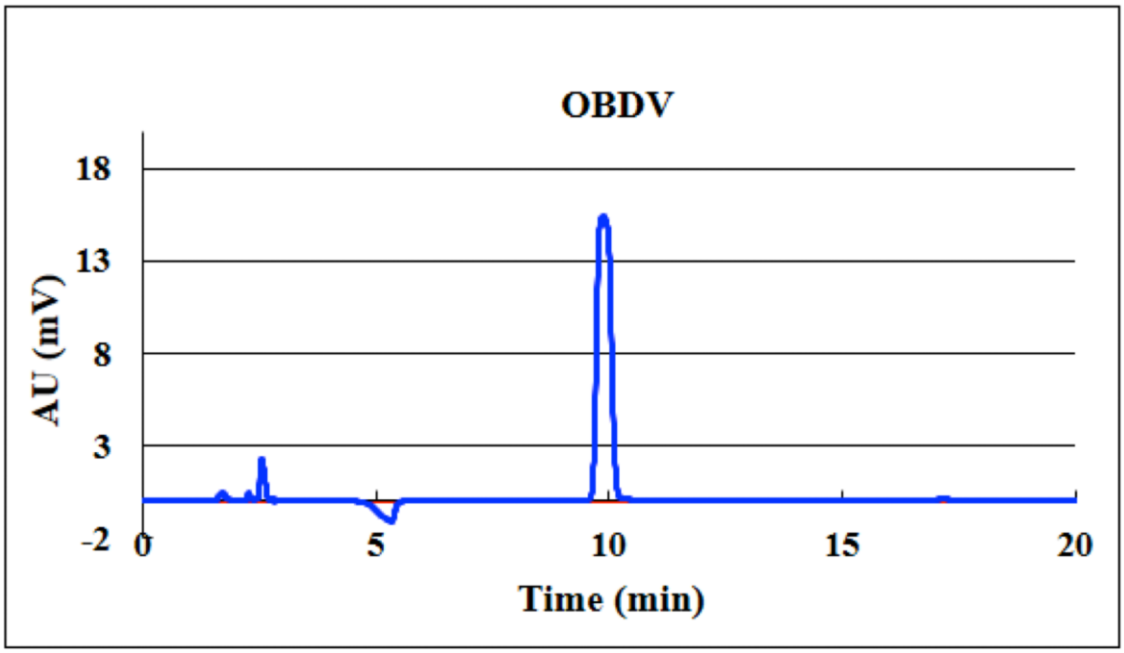

Figure 23 (b): HPLC charts for the retention time of reference OBDV.

6.1.3 *In vivo* biodistribution of [^{77}Br]OBDV:

The distribution of [^{77}Br]OBDV in the rat brain regions, blood, urine and other organs of interest at 2, 30 and 60 minutes post-injection are presented in Table 3. The blood-brain barrier was readily penetrated by [^{77}Br]OBDV. The accumulations of [^{77}Br]OBDV in the cerebral cortex, striatum, cerebellum and the rest of the rat brain regions were 0.64 ± 0.06% ID/g, 0.62 ± 0.08% ID/g, 0.61 ± 0.09% ID/g and 0.61 ± 0.07% ID/g, respectively, at 2 min post injection. The average accumulations of [^{77}Br]OBDV in all brain regions of interest were 0.56 ± 0.06% ID/g and 0.50 ± 0.05% ID/g, respectively, at 30 and 60 min post-injection. The clearance of [^{77}Br]OBDV from blood was also very rapid and the radioactivity in blood was found to be 0.14 ± 0.01% ID/g at 2 min post-injection. At 60 min post-injection, maximum accumulation of [^{77}Br]OBDV was observed in the pancreas (2.98 ± 0.33% ID/g) and small intestine (1.69 ± 0.26% ID/g). The accumulation of [^{77}Br]OBDV in the lung was also found very high (5.57 ± 0.72% ID/g) at 2 min post-injection, but at 60 min post-injection, the accumulation was decreased to 1.23 ± 0.14% ID/g. The accumulations of [^{77}Br]OBDV in bladder at 2, 30 and 60 min post-injection were found 0.15 ± 0.04 % ID/g, 0.19 ± 0.04 % ID/g and 0.20 ± 0.03 % ID/g respectively. At 2, 30 and 60 min post-injection, the accumulations of [^{77}Br]OBDV in urine were found 0.04 ± 0.04 % ID/g, 0.25 ± 0.02 ID/g and 0.32 ± 0.24 ID/g respectively. At both the 30 & 60 min post-injection, the accumulations of [^{77}Br]OBDV in bladder and urine were found very low, compared to the accumulation of [^{77}Br]OBDV in kidney.

Table 4: Biodistribution of [^{77}Br]OBDV in rats after intravenous injection of the tracer[a]

Tissue	Post injection time		
	2 min	30 min	60 min
Blood	0.14 ± 0.01	0.11 ± 0.12	0.04 ± 0.01
Heart	2.19 ± 0.52	0.39 ± 0.03	0.27 ± 0.03
Lung	5.57 ± 0.72	1.54 ± 0.24	1.23 ± 0.14
Pancrease	2.10 ± 0.55	2.52 ± 0.98	2.98 ± 0.33
Spleen	0.89 ± 0.34	1.35 ± 0.25	1.02 ± 0.23
Kidney	2.90 ± 0.36	2.18 ± 0.27	1.68 ± 0.52
Bladder	0.15 ± 0.04	0.19 ± 0.04	0.20 ± 0.03
Urine	0.04 ± 0.04	0.25 ± 0.02	0.32 ± 0.24
Small intestine	0.93 ± 0.14	1.24 ± 0.44	1.69 ± 0.26
Stomach	0.26 ± 0.19	0.32 ± 0.28	0.22 ± 0.14
Liver	1.04 ± 0.12	1.79 ± 0.05	1.62 ± 0.04
Cerebral cortex	0.64 ± 0.06	0.52 ± 0.11	0.50 ± 0.05
Striatum	0.62 ± 0.08	0.59 ± 0.05	0.53 ± 0.09
Cerebellum	0.61 ± 0.09	0.56 ± 0.04	0.45 ± 0.05
Others	0.61 ± 0.07	0.58 ± 0.05	0.50 ± 0.05

[a]Radioactivities are expressed as % injected dose per gram tissue (% ID/g). The values are the mean ± standard deviation (SD) of four rats (n = 4) at each time point.

6.1.4 *In vivo* blocking studies

The ratio of mean radioactivity in cerebral cortex, striatum, cerebellum, and the rest of the brain for [^{77}Br]OBDV (Control only) and for the co-injection of (+/-)-vesamicol (0.250 µmol) or (+)-pentazocine (0.250 µmol) or (+)-3-PPP (0.250 µmol) with the [^{77}Br]OBDV was presented in Figure 24. The uptakes of [^{77}Br]OBDV in the cerebral cortex, striatum, cerebellum, and the rest of the brain were inhibited with the co-administration of 0.250 µmol (+/-)-vesamicol by an amount of 42%, 43%, 42%, and 45%, respectively, relative to [^{77}Br]OBDV (Control only). The inhibition effect of (+/-)-vesamicol on the uptake of [^{77}Br]OBDV in all the brain regions was also found very significant ($P < 0.001$ to $P < 0.01$) with the Tukey's multiple comparison test in

conjunction with an ANOVA. However, with the co-administration of 0.250 µmol (+)-pentazocine or 0.250 µmol (+)-3-PPP, no significant difference in the accumulation of [^{77}Br]OBDV from the control ([^{77}Br]OBDV only) values were observed in all the four brain regions (cerebral cortex, striatum, cerebellum, and the rest).

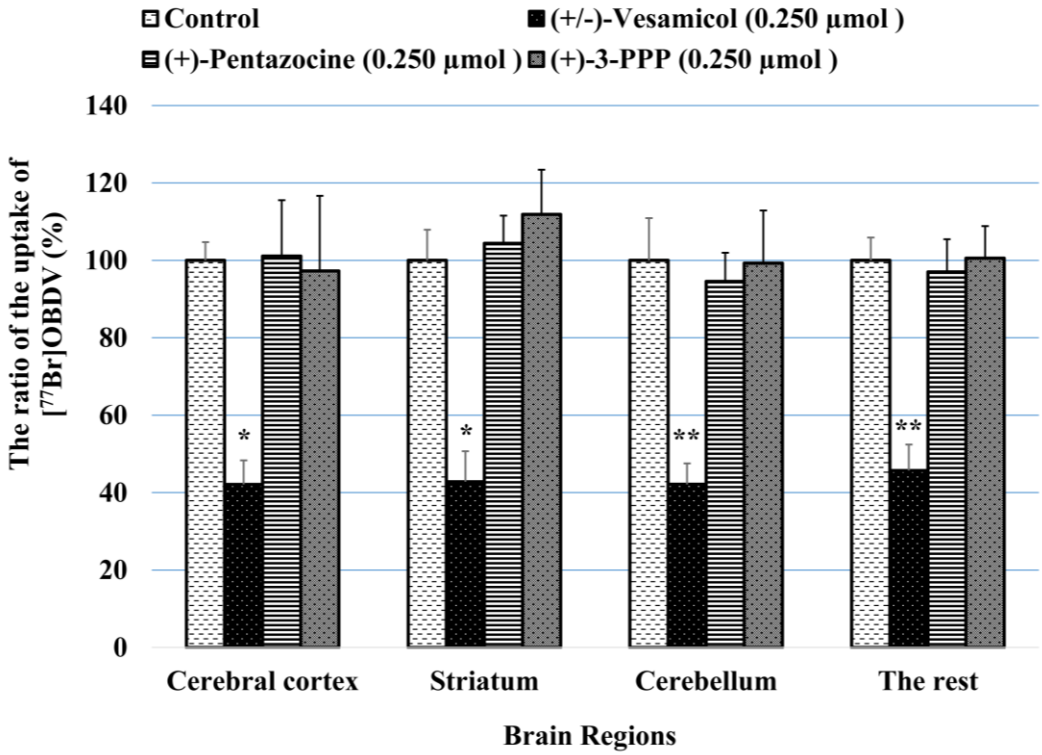

Figure 24: The effect of inhibitors on the uptake of [^{77}Br]OBDV. The vertical axis shows the mean radioactivity rate in the brain regions (cerebral cortex, striatum, cerebellum, and the rest) of each group co-injected with (±)-vesamicol (0.250 µmol) or (+)-pentazocine (0.250 µmol) or (+)-3-PPP (0.250 µmol), estimating the control ([^{77}Br]OBDV only) as 100%. The stars (*) in the figure indicate the significant difference between the uptake of [^{77}Br]OBDV co-injected with (+/-)-vesamicol (0.250 µmol) and none as control in all the brain regions. A one-way ANOVA followed by a Tukey's multiple comparison test was performed by GraphPad Prism Version 4 software, compared with the control. Here, *P <0.01 and **P <0.001.

6.1.5 *In vivo* metabolite analysis

The standard R_f value of [^{77}Br]OBDV was found to be 0.26 (Figure 25) on TLC, where, hexane: ethyl acetate: triethylamine (3:1:0.1, v/v/v) was used as mobile phase. A very weak trace spot around the starting point and a strong spot of R_f value 0.26 ± 0.02 were observed on the TLC plate in case of the brain samples. In case of the plasma samples, only an intense spot of highly polar radioactive metabolite around the starting point was seen on the TLC plate (Figure 25).

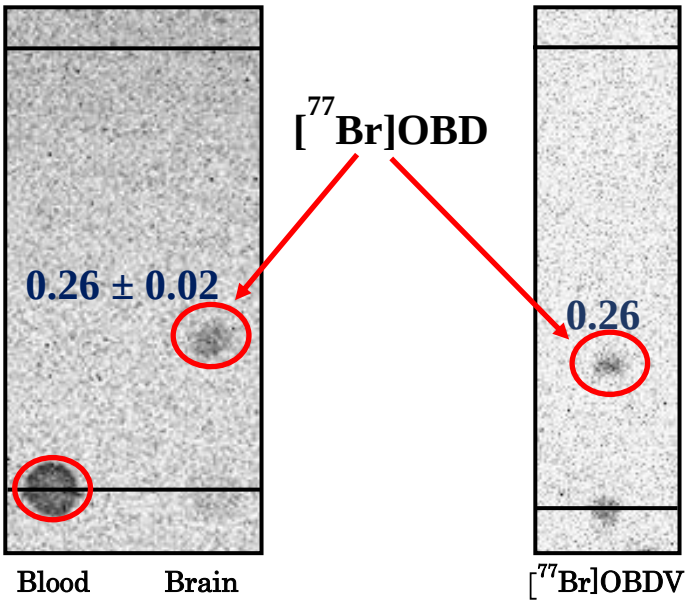

Figure 25: In vivo metabolite analysis of [^{77}Br]OBDV in the rat brain 60 minutes after intravenous injection. Here, (A) & (B) indicate TLC analysis of plasma and brain samples, respectively, and (C) indicates TLC analysis with the control ([^{77}Br]OBDV).

6.1.6 Partition coefficient:

The partition coefficient (log $P_{o/w}$) of [^{77}Br]OBDV was found to be 2.93 ± 0.03, which indicates that [^{77}Br]OBDV has a reasonable degree of lipophilicity to penetrate the blood–brain barrier (BBB).

6.1.7 *Ex vivo* autoradiography:

VAChT-rich regions of the rat brain was prominently visualized by the *ex vivo* autoradiography because [^{77}Br]OBDV was successfully accumulated in the VAChT rich

regions of rat's brain [Figure 25 (a)]. The high accumulation of [^{77}Br]OBDV was observed in the cerebral cortex, striatum, diagonal band, hippocampus, thalamus and amygdaloidal nucleus. The localization of [^{77}Br]OBDV binding was also visualized in the molecular and granular cell layers, facial nucleus and trigeminal nucleus in the cerebellum. No specific accumulation of the radiotracer was observed in any brain regions of rats with the co-injection of 0.250 μmol (+/-)-vesamicol with control ([^{77}Br]OBDV only) [Figure 25 (b)].

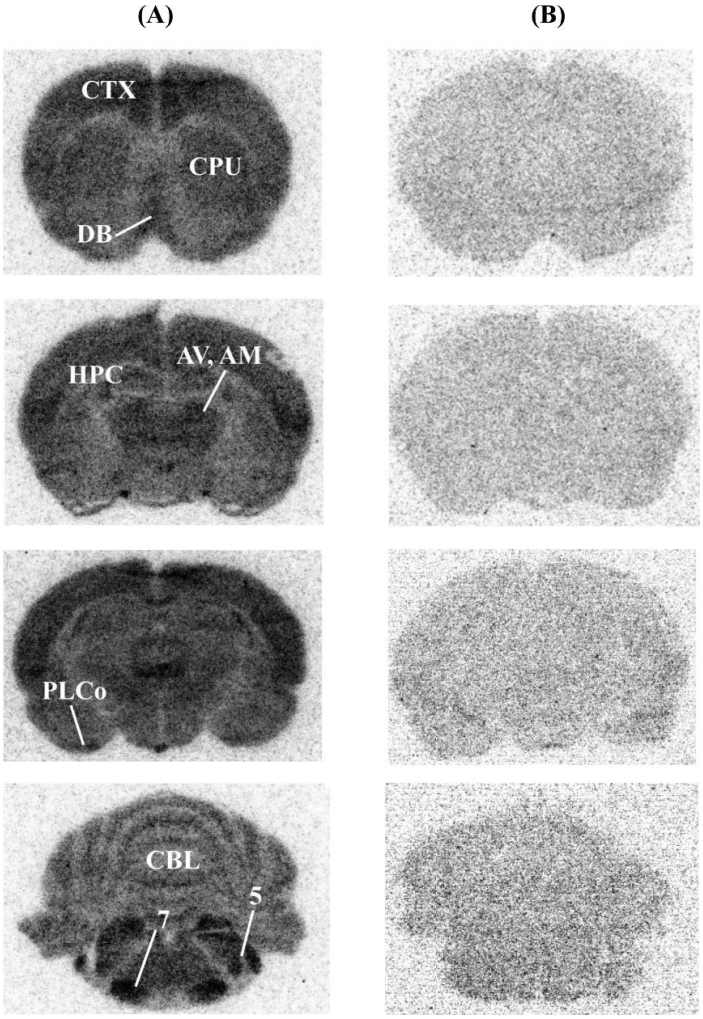

Figure 26: *Ex vivo* autoradiographic distribution of [^{77}Br]OBDV in the rat brain at 30 min post-injection (A) with the control ([^{77}Br]OBDV only); (B) co-injection of 0.250 μmol (+/-)-vesamicol with [^{77}Br]OBDV in the rat brain as an inhibitor. Abbreviations: AM, anteromedial thalamus; AV, anteroventral thalamus; CBL, cerebellum; CPU, striatum; CTX, cerebral cortex; DB, diagonal band; HPC, hippocampus; PLCo, posterolateral cortical amygdaloidal nucleus; 5, trigeminal nucleus; 7, facial nucleus.

6.2 Discussions:

In vitro evaluation of OBDV revealed its high affinity and selectivity for VAChT (Kozaka T et al., 2012). Hence, it was expected that OBDV, radiolabeled with a suitable positron emitter, possesses the strong potentiality to be used as VAChT PET ligand. Bromine and iodine is very similar to each other in chemistry and the chemical reactivity of bromine is milder than that of fluorine but greater than that of iodine. The binding strength of C-Br bond is 59 kcal/mol, while those of C-I and C-F are 45 and 114 kcal/mol, respectively. So, radiobromine labeled compounds are less vulnerable to *in vivo* dehalogenation than iodinated derivatives. Moreover, the obtainability of various radioisotopes of bromine is also an extra benefit of using radiobromine labeled neuroimaging probe over radioflourine labeled neuroimaging probe (Maziere B et al., 1986). On the basis of the features of high affinity for VAChT and selectivity over sigma receptors, radiobromine-labeled OBDV was evaluated through *in vivo* evaluations and *ex vivo* autoradiography as a potential VAChT PET ligand. Among the various radioisotopes of bromine, ^{76}Br is the mostly used for clinical investigations. It is a relatively long-lived ($t_{1/2}$ = 16.2 h) positron emitter that decays with both the positron emission (54%) and electron capture (IAEA, technical series no. 468). To make the best use of the advantage of longer half-life for the present radiosynthesis and *in vivo evaluation* experiments, we have radiolabeled OBDV with ^{77}Br instead of ^{76}Br. ^{77}Br has a half-life of 56 h and decays nearly completely (99.3%) by electron capture, with promising gamma rays at 0.239 and 0.520 MeV (IAEA, technical series no. 468). [^{77}Br]OBDV was radiosynthesized by the oxidative radiobromination of the precursor, OTDV (Figure 20), with no-carrier added conditions with the radiochemical yield of 52.3-65.8% and the specific activity of 322 ~ 406 GBq/μmol.

Maximum accumulation of [^{77}Br]OBDV (>0.6% ID/g) in the cerebral cortex, striatum, cerebellum and the rest of the brain was found at 2 min post-injection from the

intracerebral biodistribution pattern of [^{77}Br]OBDV (Table 4). This confirmed the rapid penetration of [^{77}Br]OBDV into the brain by crossing the blood–brain barrier (BBB). Rapid diffusion through the BBB is also a confirmatory indication of the suitable lipid solubility of [^{77}Br]OBDV, so that it can easily be extracted in the brain.

At 2-min post-injection, the initial brain uptakes of [^{77}Br]OBDV in striatum, cerebral cortex, cerebellum, and the rest of brain were (0.62 ± 0.08% ID/g), (0.64 ± 0.09% ID/g), (0.61 ± 0.06% ID/g), and (0.61 ± 0.07% ID/g) respectively. This relatively homogenous biodistribution in the brain regions is assumed to express the nonspecific binding of [^{77}Br]OBDV reflected by cerebral blood flow in the brain. However, at 30 min post-injection, the specific brain regional accumulation of [^{77}Br]OBDV was observed. The highest accumulation of [^{77}Br]OBDV was found in the striatum, which matched with the known distribution of VAChT density as the highest level of VAChT was found in the striatum (Efange SM et al., 1995; Frey KA et al., 1998; Efange SM et al., 2000). Moderate to high accumulation of [^{77}Br]OBDV was also observed in the cortex, cerebellum and the other regions of the brain. This findings conclude that [^{77}Br]OBDV was accumulated in the VAChT rich regions distributed throughout the whole brain, which is in accordance with the regional brain accumulation of [^{125}I]OIDV (Kozaka et al., 2014).

At 2-min post-injection, the initial blood uptake of [^{77}Br]OBDV was found very low (0.14 ± 0.01 & ID/g). The clearance of radioactivity from the blood was also very fast and the radioactivity in blood was 0.04 ± 0.01% ID/g at 60 min post-injection. The low blood uptake and the fast blood wash out are advantageous for brain imaging. *In vivo* biodistribution study of [^{77}Br]OBDV, the average radioactivity in blood at 2, 30 and 60 min post-injection was found 0.10 ± 0.05 %ID/g. In case of *in vivo* [^{77}Br]OBDV blocking experiments, the radioactivity in blood at 30 min post-injection were found

0.05 %ID/g. The radioactivity in blood in both the *in vivo* biodistribution and *in vivo* [^{77}Br]OBDV blocking experiments was so low that the possibility of confounded experimental results due to the residual level of [^{77}Br]OBDV in blood within intracerebral blood vessels and/or nonspecifically bound to vascular endothelial cells, was considered very minor or negligible.

Depending on the specific activity of [^{77}Br]OBDV, the injected radioactivity of [^{77}Br]OBDV (1.0-1.58 MBq (2.46-3.89 pmol)/ rat) in autoradiographic study was 9-13 times higher than that (0.111 MBq (270.7 fmol) / rat) in *in vivo* blocking study. However, the regional brain distribution in autoradiogram image accorded with that in *in vivo* distribution study. Thus, the confounding effects of intra-vascular versus intra-parenchymal [^{77}Br]OBDV depending on the chemical amount of [^{77}Br]OBDV do not have to be considered.

Significant blocking effects on the regional brain distribution of [^{77}Br]OBDV by (+/-)-vesamicol (0.250 μmol) was revealed in the *in vivo* blocking studies. This validates that [^{77}Br]OBDV binds to vesamicol binding site on VAChT with high affinity (Figure 24). In contrast, with both the (+)-pentazocine (selective σ-1 receptor agonist) or (+)-3-PPP (σ-1 and σ-2 receptor agonist), separately co-injected with [^{77}Br]OBDV into the rats, no significant inhibition of the uptake of [^{77}Br]OBDV in any brain region was observed. This negligible changes in *in vivo* brain regional uptake of [^{77}Br]OBDV, co-injected with 250 μmol of (+)-pentazocine or (+)-3-PPP, revealed that [^{77}Br]OBDV does not significantly bind to σ-1 and σ-2 receptors like most vesamicol analogues do, presumably because of the *o*-Br group of [^{77}Br]OBDV, which prevents binding to σ-1 and σ-2 receptors but not VAChT. In *in vivo* blocking studies, the molar quantities (0.250 μmol) of both the (+)-3-PPP and (+)-pentazocine are almost 9×10^5 times higher than that of injected [^{77}Br]OBDV (273.4 fmol) in each rat and are

maximum enough to block the accumulation of [^{77}Br]OBDV in all brain regions. But no inhibition of the accumulation of [^{77}Br]OBDV was observed, which also confirm the selectivity of [^{77}Br]OBDV binding to VAChT over σ_1 and σ_2 receptors. In our previous paper, from the findings of *in vitro* binding assays, we suggested that OBDV would show comparably higher binding affinity to VAChT than to σ-1 and σ-2 receptors (Kozaka T et al., 2012). The current *in vivo* blocking evaluations also confirmed the affinity and selectivity of [^{77}Br]OBDV binding for VAChT.

The existence of highly polar radiolabeled metabolites in the brain can have a negative influence on VAChT imaging. Therefore, *in vivo* metabolism of [^{77}Br]OBDV in the blood and brain of SD rats was examined at 60 min post-injection using TLC, where hexane: ethyl acetate: triethylamine (3:1:0.1, v/v/v) was used as mobile phase (Figure 24). In case of brain tissue, no indication of the presence of polar metabolite was observed on TLC. Most of the radioactivity in the brain tissue was unchanged with [^{77}Br]OBDV, but only a polar metabolite of [^{77}Br]OBDV was observed in the blood. This result specifies that the distribution of radioactivity in the rat brain at 60 min post-injection is only due to the radioactivity of [^{77}Br]OBDV. The increased uptake of radioactivity in the pancreas or small intestine, even at 60 min post-injection, was assumed to be due to polar metabolites of [^{77}Br]OBDV. Thus, this compound has suitable characteristics for the molecular imaging of VAChT in the brain.

In the *ex vivo* autoradiograms [Figure 25(A)], it was observed that, at 30 min post-injection, [^{77}Br]OBDV was accumulated in VAChT-rich regions of the rat brain, including the cerebral cortex, striatum, diagonal band, hippocampus, thalamus, amygdaloidal nucleus, cerebellum, and nuclei of cranial nerves. With a reference brain atlas, regions of interest (ROIs) were drawn over several brain regions to quantify of brain regional accumulation of [^{77}Br]OBDV. Relative radioactivity concentration

(RRC) on the brain regions were measured by using image analysis software (Multi Gauge version 3, Fujifilm) and expressed as photostimulated luminescence (PSL)/area (mm^2) (Table 5). A heterogeneous distribution pattern of the radioactivity was obtained with the highest level of radioactivity distribution in striatum. The regions including cerebral cortex, diagonal band, hippocampus, and posterolateral cortical amygdaloidal nucleus possess moderate radioactivity distribution and a low level of radioactivity accumulation was found in cerebellum. The brain regional biodistribution of [^{77}Br]OBDV (table 4) almost accord with the RRC of the brain regions (table 5).

Table 5: RRC of [^{77}Br]OBDV on the brain regions.

Brain Regions	Cerebral Cortex	Striatum		Diagonal band	Hippocampus	Cerebellum	Posterolateral cortical Amygdaloidal nucleus
		Lateral	Internal				
RRC (PSL/mm²)	56.6±1.5	61.8±1.4	59.8±1.2	60.5±1.7	53.5±1.5	50.4±0.8	51.5±1.2

The pattern of regional distribution of [^{77}Br]OBDV, revealed from the *ex vivo* autoradiograms were in agreement with the distribution of VAChT-rich brain regions such as pre-synaptic cholinergic nerve terminals, as shown in the *in situ* hybridization histochemistry (ISHC) and immunohistochemistry (IHC) studies (Gilmor ML et al., 1996; Ichikawa T et al., 1997; Schafer MK et al., 1995; Weihe E et al., 1996) as well as the brain regional accumulation of [^{125}I]OIDV (Kozaka t et al., 2014). VAChT exists in the pre-synapse of cholinergic nerve systems (Clarke PB et al., 1984; Hulme EC et al., 1990; Quirion R et al., 1993; Vilaro MT et al., 1993) and mediates the transportation of acetylcholine (ACh) to the cholinergic synaptic vesicles. ACh releases from presynaptic terminals into the synaptic cleft and binds with the acetylcholine receptors in postsynaptic terminals: muscarinic (M_1-M_5) and nicotinic receptors, and lead to a cholinergic responds. There are similarities in between the regional distribution of pre-synaptic cholinergic nerve terminals and acetyl choline receptors, situated at the

post-synapses of cholinergic nerve terminals. Muscarinic acetylcholine M_1 receptors are found in high density in forebrain areas including the cerebral cortex, hippocampus and amygdala (David A., 1989). The muscarinic acetylcholine M_2 receptor was present at high levels in the anterior and intralaminar nuclei of the thalamus, all motor nuclei of the cranial nerves (Allan IL et al., 1991) and granule and purkinjie cell layers of the cerebellum (Kozaka T et al., 2014). The M_1, M_2 and M_4 muscarinic acetylcholine receptors are differentially localized in the striatum (Allan IL et al., 1991) and the diagonal band is a muscarinic acetylcholine M_2–M_5 receptor-abundant area (Kozaka T et al., 2014). The nicotinic receptor is widely distributed in the anteroventral nucleus of the thalamus (Rotter A et al., 1981). ISHC and IHC studies detect widely distributed VAChT-rich presynaptic cholinergic nerve terminals in various brain regions, including the cerebral cortex, striatum, diagonal band, hippocampus, thalamus, amygdaloidal nucleus, cerebellum, and nuclei of cranial nerves, which was also revealed in the autoradiographic study of [^{77}Br]OBDV. So [^{77}Br]OBDV can successfully visualize the VAChT rich regions, widely distributed throughout the whole rat's brain .

The distribution of [^{77}Br]OBDV was completely blocked by the co-injection of [^{77}Br]OBDV with (+/-)-vesamicol, as an inhibitor, and no specific accumulation of the [^{77}Br]OBDV was witnessed in brain sections [Figure 5(B)]. The uptake of [^{77}Br]OBDV in cerebellum was observed in the autoradiogram. Both the in situ hybridization histochemistry (ISHC) and immunohistochemistry (IHC) have detected VAChT-positive neurons in the cerebellar cortex and cranial nerve nuclei (facial nucleus, trigeminal motor nucleus (Ichikawa T et al., 1997). The presence of VAChT-immunoreactive (VAChT-IR) axon terminals in cerebellar nuclei was also confirmed by IHC (Ichikawa T et al., 1997). Moreover, in the cerebellum, purkinje cell bodies contained VAChT mRNA and VAChT protein (Ichikawa T et al., 1997, Gilmor

ML et al., 1996). The accumulation of [^{77}Br]OBDV was also observed in thalamus. In the thalamus, no VAChT- immunoreactive (IR) cell bodies were detected; however, VAChT-positive fibers were seen in most thalamic nuclei. Particularly high densities of VAChT-IR fibres were demonstrated in the anteroventral thalamic nucleus, whereas the other thalamic nuclei contained lower densities of VAChT-positive fibres (Arvidsson U et al., 1997).

The cyclohexane ring in the decalin moiety of OBDV in comparison with vesamicol might affect binding to neuronal receptors by the increasing steric bulk (Kozaka T et al., 2014).

Hence, because of the characteristic features of high lipophilicity, low affinity for σ-1 and σ-2 receptors and high selectivity for VAChT, in comparison with (+/-)-vesamicol and/or other vesamicol derivatives, Br-76 labeled OBDV, with a framework of DV and a halogen atom (-Br) at the ortho-position of the 4-phenylpiperidine moiety, has the potentiality to be used as a promising PET VAChT imaging probe.

6.3 Experimental

6.3.1 Syntheses: 4-(2-Bromophenyl)piperidine (**7**), OBDV (**8**) and OTDV (**9**) were synthesized by following the already published (Kozaka, T. et al. *Bioorg Med Chem.*, 2012, *20*, 4936-4941) synthetic route for compounds (**7**), (**8**), and (**9**). So same synthetic procedures and data of compounds (**7**), (**8**), and (**9**) of that published article were used in the dissertation.

6.3.1.1 Synthesis of 4-(2-Bromophenyl)piperidine (7):

A solution of *o*-bromobenzaldehyde (20.0 g, 108 mmol), ethyl acetoacetate (27.3 mL, 216 mmol), and piperidine (2.14 mL, 21.6 mmol) in EtOH (77.2 mL) was stirred for 15 h at room temperature. To the reaction solution was added 12 M NaOH

(360 mL) and EtOH (350 mL). The reaction mixture was refluxed for 4 h, cooled to room temperature, and the organic solvents removed. The residue was acidified with conc. HCl (450 mL) in an ice bath, extracted with AcOEt, washed with water and brine, and concentrated to dryness. The residue was transferred to a glass filter and washed with cold Et_2O to obtain dicarboxylic acid 2 (23.9 g) as a white solid without further purification.

The above 2 (23.9 g, 83.2 mmol) was dissolved in 28% ammonia solution (280 mL) by heating, and then water was evaporated off under reduced pressure. The resulting residue was heated to 200 ^oC to melt for 6 h, cooled to room temperature, extracted with CH_2Cl_2, washed with Na_2CO_3 aq. and brine, concentrated to dryness, and washed with cold Et_2O. BH_3-THF (1.0 M THF solution; 208 mL, 208 mmol) was added drop wise to a solution of the crude cyclic imide in THF (166 mL) at 0^oC under Ar. The reaction mixture was allowed to gradually reach room temperature and refluxed for 20 h. conc. HCl aq (300 mL) was carefully added to the reaction mixture at 0^oC. The reaction mixture was refluxed for an additional 20 h, neutralized with NaOH aq., extracted with AcOEt, washed with water and brine, and concentrated to dryness. Solvents were evaporated off. Et_2O (1 L) was added to the residue at 0^oC. The resulting white precipitate was isolated by filtration and washed with cold Et_2O to obtain 3 (12.4 g, 48% from 1) as a white solid without further purification: ^1H NMR δ 7.54–7.51 (m, 1H), 7.28–7.26 (m, 2H), 7.07–7.00 (m, 1H), 3.21–3.17 (m, 2H), 3.10 (tt, 1H, J = 3.7, 11.9 Hz), 3.10 (dt, 2H, J = 2.3, 11.9 Hz), 2.21– 2.19 (m, 1H), 1.87–1.83 (m, 2H), 1.65–1.53 (m, 2H); EI MS m/z 240 (M^+ +1, 85.3), 241 (M^+, 73.6). (Kozaka et al., 2012)

6.3.1.2 *o*-Bromo-trans-decalinvesamicol (OBDV) (8):

A mixture of 3 (2.25 g, 9.36 mmol) and trans-decalin-2,3- oxide (2.14 g, 14.0 mmol) in EtOH (9.4 mL) was refluxed for 20 h. The solvent was evaporated off. The

residue was chromatographed on silica gel with hexane-AcOEt (5:1) to give 5 (2.10 g, 57%) as a white solid: ^{1}H NMR δ 7.54–7.52 (m, 1H), 7.30–7.25 (m, 2H), 7.06–7.02 (m, 1H), 4.10–4.07 (m, 1H), 3.14–3.11 (m, 2H), 3.10 (tt, 1H, J = 3.4, 12.0 Hz), 2.33–2.30 (m, 1H), 2.21–2.16 (m, 1H), 2.12–2.07 (m, 1H), 1.92–1.19 (m, 17H), 1.03–0.91 (m, 2H); ^{13}C NMR δ 144.9, 132.8, 127.6, 127.5, 127.3, 124.5, 67.0, 64.7, 52.9, 49.4, 41.8, 36.7, 36.5, 35.9, 33.8, 33.7, 32.6, 32.5, 29.4, 26.6, 26.5; DART MS m/z 392 (M^+ +1, 50.8), 394 (M^+ +1, 47.3). (Kozaka et al., 2012)

6.3.1.3 *o*-Trimethylstannyl-trans-decalinvesamicol (OTDV) (9):

A mixture of 5 (42.1 mg, 0.107 mmol), $Pd(PPh_3)_4$ (7.5 mg, 6.44×10^{-3} mmol) and hexamethylditin (87.9 mg, 0.268 mmol) in anhydrous toluene (1.1 mL) was refluxed for 15 h under Ar. The solvent was evaporated off. The residue was chromatographed on silica gel with hexane-AcOEt (10:1) to give 6 (33.4 mg, 65%) as a white solid: ^{1}H NMR δ 7.18–7.15 (m, 1H), 7.09–7.04 (m, 2H), 6.95– 6.90 (m, 1H), 3.86–3.81 (m, 1H), 2.94–2.86 (m, 2H), 2.15–0.65 (m, 23H), 0.06 (m, 9H); ^{13}C NMR δ 153.02, 141.65, 135.95, 128.80, 125.79, 125.65, 66.94, 64.65, 53.11, 49.85, 47.21, 36.62, 36.49, 35.85, 34.57, 34.54, 33.75, 33.62, 29.46, 26.55, 26.48, - 8.22; DART MS m/z 478 (M^+ +1, 1). (Kozaka et al., 2012)

6.3.2 Preparation of rat cerebral and liver membranes:

All the performed animal experiments meet the criteria of the guidelines for the care and use of Laboratory Animals at the Takara-machi Campus of Kanazawa University. The cerebrum or livers of Sprague-Dawley rat (8 weeks, male, 250–300 g) were homogenized with a Teflon-glass homogenizer in ice-cold 0.32 M sucrose buffer (pH 7.8). The homogenate was centrifuged at 1000 × g at 4^{o}C for 10 min. The resulting precipitate from the centrifugation was removed and the collected supernatant was centrifuged at 55000 × g at 4^{o}C for 1 h. The resulting precipitate from the centrifugation

was resuspended in ice-cold water with a Teflon-glass homogenizer and again centrifuged at 55000 × g at 4ºC for 1 h. The resulting pellets of rat cerebrum or liver were resuspended in an ice-cold buffer (50 mM Tris–HCl/0.32 M sucrose, pH 7.8) with a Teflon-glass homogenizer (Kozaka, T. et al. *Bioorg Med Chem.*, 2012, *20*, 4936-4941).

6.3.3 In vitro binding assay:

6.3.3.1 VAChT

For VAChT *in vitro* binding assay, (-)-[^{3}H]Vesamicol (K_d = 7.40 nM) was used as a radioligand. Rat cerebral membranes was added to each ice-cold assay tube arranged in quadruplicate. Each of the assay tube contains (-)-[^{3}H]vesamicol, DTG (0.2l M) to mask the σ receptors and the displacing ligands at various concentrations (1.0×10^{-10} – 10^{-5} M) in 50 mM Tris–HCl buffer (pH 7.8). The rat's cerebral tissue was added to each assay tube on an ice bath, followed by the incubation of each reaction mixture in tubes at 37ºC for 60 min, and then the reaction mixtures were quenched by cooling in an ice bath. Each sample of the assay tubes was treated with cell harvester and passed through glass-microfiber filters (Whatman, GF/F). The glass-microfiber filters were presoaked in 0.3% polyethyleneimine to reduce the non-specific binding. 50 mM Tris–HCl (pH 7.8) was used as the washing buffer for the filters and the radioactivities of the filters were counted with a liquid scintillation counter (Aloka, LSC-5100). Three independent *in vitro* VAChT binding assays were carried out (Kozaka, T. et al. *Bioorg Med Chem.*, 2012, *20*, 4936-4941).

6.3.3.2 σ-1 Receptor

For the σ-1 receptor *in vitro* binding assay, (+)-[^{3}H]Pentazocine (K_d = 19.9 nM) was used as a specific radioligand. Rat cerebral membranes was added to each ice-cold assay tube arranged in quadruplicate. Each of the assay tubes contains

(+)-[^{3}H]Pentazocine and the displacing ligands at various concentrations (1.0×10^{-10} – 10^{-5} M) in 50 mM Tris–HCl buffer (pH 7.8). The rat's cerebral tissue was added to each assay tube on an ice bath, followed by the incubation of each reaction mixture in tubes at 37^{o}C for 90 min, and then the reaction mixtures were quenched by cooling in an ice bath. Each sample of the assay tubes was treated with cell harvester and passed through glass-microfiber filters (Whatman, GF/B). The glass-microfiber filters were presoaked in 0.3% polyethyleneimine to reduce the non-specific binding. 50 mM Tris–HCl (pH 7.8) was used as the washing buffer for the filters and the radioactivities of the filters were counted with a liquid scintillation counter (Aloka, LSC-5100). Three independent σ-1 receptor *in vitro* binding assay were carried out (Kozaka, T. et al. *Bioorg Med Chem.*, 2012, *20*, 4936-4941).

6.3.3.3 σ-2 Receptor

For the σ-2 receptor *in vitro* binding assay, [^{3}H]DTG (K_d = 22.3 nM) was used as a radioligand with (+)-[^{3}H]Pentazocine to mask the σ-1 receptor. Rat cerebral membranes was added to each ice-cold assay tube arranged in quadruplicate. Each of the assay tubes contains [^{3}H]DTG, pentazocine (1.0 μM), and the displacing ligands at various concentrations (1.0×10^{-10} – 10^{-5} M) in 50 mM Tris–HCl buffer (pH 7.8). The rat's cerebral tissue was added to each assay tube on an ice bath, followed by the incubation of each reaction mixture in tubes at 37^{o}C for 90 min, and then the reaction mixtures were quenched by cooling in an ice bath. Each sample of the assay tubes was treated with cell harvester and passed through glass-microfiber filters (Whatman, GF/B). The glass-microfiber filters were presoaked in 0.3% polyethyleneimine and washed with 50 mM Tris–HCl (pH 7.8). Radioactivities of the filters were counted with a liquid scintillation counter (Aloka, LSC-5100). Three independent σ-2 receptor *in vitro* binding assay were carried out (Kozaka, T. et al. *Bioorg Med Chem.*, 2012).

6.3.4 Radiosynthesis and purification of [^{77}Br]OBDV:

o-trimethylstannyl-*trans*-decalinvesamicol (OTDV) was the main precursor for the synthesis of [^{77}Br]OBDV. [^{77}Br]OBDV was radiosynthesized by the tin-bromine exchange reaction from OTDV with no-carrier added [^{77}Br]Br^- (Specific activity: 2.0 TBq/μmol), HCl and chloramine-T (Figure 22). The cyclotron facility of the biomedical imaging research center of Fukui University supplied no carrier added [^{77}Br]Br^-. Briefly, [^{77}Br]Br^-, (18.5 MBq/5~10 μL in EtOH) was added to a reaction vial containing OTDV (21.2 mM in EtOH, 50 μL), followed by the addition of 0.1 M HCl (50 μL) and aq. chloramine T (23.7 mM in H_2O, 40 μL). The reaction mixture was shaken for 5 min at room temperature, followed by the incubation at 77^oC for 30 min. With the addition of $Na_2S_2O_5$ (15.8 mM in H_2O, 20 μL) and 6M NH_3 (100 μL, the reaction mixture was quenched. The unreacted water-soluble by products from the resultant mixture were removed by passing the reaction mixture through a Sep-Pack C-18 light column. The SEP-Pack C-18 light column was washed with an additional 15 mL H_2O. The trapped [^{77}Br]OBDV in the SEP-Pack C-18 light column was then eluted with 5 mL EtOH and the collected eluent was concentrated by heating under N_2. [^{77}Br]OBDV was purified with reversed phase HPLC at a flow rate of 4.0 mL/min with a mobile phase of acetonitrile: H_2O: monoethanolamine (90:10:0.2, v/v/v) at 40°C. The reversed phase HPLC was equipped with a Zorbax-ODS RX-C18 column (9.6 mm × 250 mm). Ultraviolet (UV) absorption was monitored at 230 nm. The chemical identity of [^{77}Br]OBDV was confirmed by co-injection with the reference OBDV on HPLC under same conditions.

During the purification of [^{77}Br]OBDV with HPLC, the chemical amount of [^{77}Br]OBDV in the injected volume of [^{77}Br]OBDV is lower than the minimum detectable limit of UV detector at 230 nm, with which reference OBDV was detected.

So, 300 μL of each of the different concentrations (10^{3} μM ~ 10^{-5} μM) of reference OBDV were injected in the HPLC under the same conditions to determine the minimum detectable concentration of reference OBDV. 0^{-1} μM of OBDV was found to be the minimum detectable concentration of reference OBDV with the HPLC at 230 nm and mass of the reference OBDV was calculated. Then the radioactivity of 300 μL of pure [^{77}Br]OBDV was also recorded and the specific activity (SA) of [^{77}Br]OBDV was measured.

6.3.5 *In vivo* biodistribution

All the animal experiments were carried out in accordance with the *Guidelines for the Care and Use of Laboratory Animals* at the Takara-machi Campus of Kanazawa University. To perform the *in vivo* biodistribution studies, Sprague-Dawley (SD) rats (8 weeks, male, 250-300 g, n = 4 in each group) were intravenously injected 0.129 MBq (317.7 fmol) of [^{77}Br]OBDV in 400 μL of 5% ethanol/saline solution (v/v) via the tail vein. At 2, 30 and 60 min post-injection, the rats were sacrificed by decapitation under anesthesia with diethyl ether and blood samples were collected. The removed brain was immediately placed on ice and dissected into four segments: cerebral cortex, striatum, cerebellum, and the rest of the brain. The brain regions, blood, urine, and the organs of interest (heart, lung, liver, spleen, pancreas, stomach, small intestine, kidney and bladder) were collected and weighed. The radioactivities of all the harvested organs, brain regions, blood, and urea were measured with an auto well gamma system (AccuFLEX γ7010; Aloka). Data were calculated as the percent of injected dose per gram of tissue (% ID/g).

6.3.6 *In vivo* blocking studies

To evaluate the specific uptake of [^{77}Br]OBDV, receptor blocking experiments were performed. Randomly divided four groups of SD rats (8 weeks, male, 250-300 g,

n = 4 in each group) were injected with 0.111 MBq (273.4 fmol) of [^{77}Br]OBDV in 400 μL of 5% ethanol/saline solution (v/v) intravenously via the tail vein with 0.250 μmol (+/-)-vesamicol, 0.250 μmol [(+)-3-PPP], 0.250 μmol (+)-pentazocine, and none as a control. The rats were sacrificed at 30 min post-injection by decapitation under anesthesia with diethyl ether and blood samples were collected. The brain was removed and immediately placed on ice and dissected into segments consisting of 4 parts (cerebral cortex, striatum, cerebellum, and the rest). The four dissected brain parts were collected and weighed. The radioactivity of each part was measured with an auto well gamma system (AccuFLEX γ7010; Aloka). Analysis of the data of the data from the blocking studies were performed using a one-way ANOVA followed by a Tukey's multiple comparison test (GraphPad Prism Version 4 software). Differences were considered significant when $P < 0.05$.

6.3.7 *In vivo* metabolite analysis

In vivo metabolite analysis with [77Br]OBDV was performed by the autoradiographic analysis of thin layer chromatography (TLC). The SD rats 8 weeks, male, 250-300 g, n = 3) received intravenous injection of of 0.400 MBq (985.2 fmol) of [^{77}Br]OBDV in 400 μL of 5% ethanol/saline solution (v/v) via the tail vein. The rats were sacrificed at 60 min post-injection by decapitation under anesthesia with diethyl ether and blood samples were collected in a heparin-coated tube. The brain was removed, immediately place on ice and the brain segments were harvested without the cerebellum. The blood corpuscle are separated by centrifugation at 15000 rpm for 15 min at 4^{o}C. The resulting plasma (300 μL) was separated from the involved macromolecules (>10000 molecular weight) by ultrafiltration. The resulting filtrates was analyzed by TLC using mobile phase of hexane: ethyl acetate: triethylamine (3:1:0.1, v/v/v). The brain tissue was homogenized for 1 min with an ultrasonic

homogenizer for 1 min with an ultrasonic homogenizer in acetonitrile and H_2O (2:1). The brain homogenate suspensions were centrifuged 20000 × g for 20 min at 4 ºC. The supernatant was collected and separated from the involved macromolecules (>10000 molecular weight) by ultrafiltration. The resulting filtrate was analyzed by TLC using mobile phase of hexane: ethyl acetate: triethylamine (3:1:0.1, v/v/v). The TLC plates were then exposed to an imaging plate (BAS-IP SR 2025; Fujifilm) for 5 days (120 hrs), after which the plates were scanned by a BAS-5000 phosphoimager (Fujifilm).

6.3.8 Determination of partition coefficient:

The partition coefficient (log $P_{o/w}$) of [^{77}Br]OBDV was determined by the standard method using *n*-octanol and 0.1 M phosphate buffer (pH = 7.4). Briefly, [^{77}Br]OBDV was mixed with *n*-octanol (15 mL) and 0.1 M phosphate buffer (15 mL), in each 50 mL centrifuge tube (where, n = 4). Then the mixture was vortexed for 5 min, followed by centrifugation of the mixture at 1000 × g for 10 min. After centrifugation, 1mL *n*-octanol and 1 mL phosphate buffer were separately transferred to the polyethylene tube from each centrifuge tube in quadruplicate. The radioactivity of the each tube was measured with an auto well gamma system (AccuFLEX γ7010; Aloka). The partition coefficient was calculated with the formula: log $P_{o/w}$ = $\log_{10}$ C_o/C_w (radioactivity in *n*-octanol layer/radioactivity in aqueous layer).

6.3.9 *Ex vivo* autoradiography

In *ex vivo* autoradiography, 1.00-1.58 MBq (2.46-3.89 pmol) of [^{77}Br]OBDV in 400 μL of 5% ethanol/saline solution (v/v) was intravenously injected (8 weeks, male, 250-300 g, n = 3) via the tail vein with 0.250 μmol (+/-)-vesamicol, and none as a control. The rats were sacrificed by decapitation under anesthesia with diethyl ether at 30 min post-injection and blood samples were collected. The whole brain was harvested and immediately frozen in Tissue-Tek O.C.T. Compound (Sakura Finetek) at −78 ºC.

The frozen brain was cut into 20-μm-thick horizontal slices at −20 °C using a cryostat microtome (HM 525 Cryostat; Thermo Scientific) and mounted on glass slides. The slices were then exposed to an imaging plate (BAS-IP SR 2025; Fujifilm) for 2 days, after which the plates were scanned with a BAS-5000 phosphoimager (Fujifilm).

Chapter VII:
Concluding Remarks

PART A: Evaluation of Tacirine derivatives as HAChT imaging probes

In an effort for the development of tacirine and its 2-oxo-1-pyrilidineacetyl derivatives as HAChT imaging probe, tacirine, DMTA (2,3-dimethylfuran derivative of tacirine) and their corresponding 2-oxo-1-pyrrolidineacetyl derivatives, namely PTAA and MKC-231, was synthesized and the binding affinities of these derivatives for HAChT were evaluated through *in vitro* HAChT [^{3}H]HC-3 competitive binding assay. No affinity towards HAChT of the synthesized compounds was revealed from the *In vitro* binding assay.

Hemicholinium-3 is a competitive inhibitor of the HACU system and it is worthy to do further research works for the development of radiolabelled HC-3 derivatives with high affinity for HAChT, which can diffuse the BBB, to enable the *in vivo* investigation of HACU system. It is also worthy to do more extensive review to develop an effective *in vitro* HAChT [^{3}H]HC-3 competitive binding assay protocol and the protocol for the preparation of brain homogenate, used in the *in vitro* HAChT [^{3}H]HC-3 competitive binding assay.

PART B: *In vivo* evaluation of radiobromine labelled decalinvesamicol analogue as VAChT imaging probe.

Radiosynthesis of [^{77}Br]OBDV was performed with moderate radiochemical yield and the radiochemical purity of [^{77}Br]OBDV was > 99%. The specific activity of [^{77}Br]OBDV was found to be 322 ~ 406 GBq/μmol. After the intravenous injection in the rat's tail vein, [^{77}Br]OBDV readily crossed the BBB and accumulated throughout the whole brain with the highest accumulation in the striatum in the rat brain followed by the cerebral cortex and cerebellum. Rapid penetration through BBB of [^{77}Br]OBDV

is also an indication of the lipophilicity of the tracer which is very important for neuroimaging radioligand. Significant inhibition of the *in vivo* accumulation of [^{77}Br]OBDV in rat brain with the co-injection of [^{77}Br]OBDV and 0.250 μmol of (+/-)-vesamicol revealed the affinity of [^{77}Br]OBDV for the binding sites of VACT. On the other hand, no significant inhibition of the accumulation of [^{77}Br]OBDV with the con-injection of [^{77}Br]OBDV and 0.250 μmol of (+)-pentazocine or (+)-3PPP revealed the selectivity of [^{77}Br]OBDV over sigma receptors, which is in accordance with the previously reported *in vitro* binding assay of OBDV. *Ex vivo* autoradiography revealed that [^{77}Br]OBDV accumulated in the corresponding VAChT-rich regions in the rat brain including the cerebral cortex, striatum, diagonal band, hippocampus, thalamus, amygdaloidal nucleus, cerebellum, and nuclei of cranial nerves. The distribution pattern of relative radioactivity concentration (RRC) of [^{77}Br]OBDV in rat's brain regions was found heterogeneous, with the highest level in the striatum. On the other hand, no specific brain regional accumulation was observed, when [^{77}Br]OBDV was co-injected with (+/-)-vesamicol. Hence, on the basis of the findings of *in vivo* evaluations of [^{77}Br]OBDV, it can be concluded that [^{76}Br]OBDV has the potential to be a prospective VAChT PET ligand for the early diagnosis of Alzheimer's disease.

References

Akaike A, Maeda T, Tamura Y. 1998. Protective effect of MKC-231, a novel high affinity choline uptake enhancer, or glutamate cytotoxicity in cultured cortical neurons. Jpn J Pharmacol 76: 219.

Allan IL, Cheryl AK, Willium FS, Donald LP, Mark RB. 1991. Identification and localization of Muscarinic Acetylcholine Receptor Proteins in Brain with Subtype-specific Antibodies. The Journal of Neuroscience 11 (*10*): 3218-3226.

Altar CA, Marien MR. 1988. [^{3}H]vesamicol binding in brain: autoradiographic distribution, pharmacology, and effects of cholinergic lesions. Synapse 2(*5*):486-493.

Arockia BM., Lakshmi M., Vasanthanathan P., Kaskhedikar S.G. 2005. Recent Therapeutic Approaches for Management of Alzheimer's disease. Indian J Pharm Sci 67: 1-10.

Arvidsson U, Riedl M, Elde R, Meister B. 1997. Vesicular acetylcholine transporter (VAChT) protein: a novel and unique marker for cholinergic neurons in the central and peripheral nervous systems. J. Comp. Neurol 378, 454–467.

Barret O, Mazere J, Seibyl J, Allard M. 2008. Comparison of noninvasive quantification methods of in vivo vesicular acetylcholine transporter using [I-123]-IBVM SPECT imaging. J. Cereb. Blood Flow Metab 28, 1624−1634.

Bartus RT, Dean RL, Beer B, Lippa AS. 1982. The cholinergic hypothesis of geriatric memory dysfunction. Science 217: 408–17.

Bessho T, Takashina K, Tabata R, Ohshima C, Chaki H, Yamabe H, Egawa M, Tobe A, Saito K.1996.Effect of the novel high affinity choline uptake enhancer 2-(2-oxopyrrolidin-1-yl)-*N*-(2,3-dimethyl-5,6,7,8-tetrahydrofuro[2,3-b]quinolin -4-yl)acetoamide on deficits of water maze learning in rats. Arzneim.-Forsch

/Drug Res 46(*1*), 4, 369-373.

Blennow K, de Leon MJ, Zetterberg H. 2006.Alzheimer's disease. Lancet 368, 387-403.

Blusztajn J. K. 1998. Choline, a vital amine. Science 281, 794–795.

Bowen DM, Smith CB, White P, Davison AN. 1976. Neurotransmitter related enzymes and indices of hypoxia in senile dementia and other abiotrophies. Brain 99:459–96.

Bravo D. T, Kolmakova N. G, Parsons SM. 2004. Choline is transported by vesicular acetylcholine transporter. J. Neurochem 91, 766–768.

Brayson HM, Benfield P. 1997. Donepzil. Drugs Aging 10: 234.

Brookmeyer R, Johnson E, Ziegler-Graham K, Arrighi HM. 2007. Forecasting the global burden of Alzheimer's disease. Alzheimers Dement 3:186-191.

Brookmeyer R, Gray S, Kawas C. 1998. Pro*j*ections of Alzheimer's disease in the United States and the public health impact of delaying disease onset. Am J Public Health 88 (*9*), 1337– 1342.

Chaki H, Yamabe H, Sugano M, Morita S, Bessho T, Tabata R, Saito KI, Egawa M, Tobe A, Morinaka Y. 1995. Design and synthesis of 4-acylaminopyridine derivatives: Novel high affinity choline uptake enhancer I[1)]. Bioorganic and Medicinal Chemistry Letters 5 (*14)*: 1489-1494.

Chaki H, Yamabe H, Sugano M, Morita S, Bessho T, Tabata R, Saito KI, Egawa M, Tobe A, Morinaka Y. 1995. Design and synthesis of 4-acylaminopyridine derivatives: Novel high affinity choline uptake enhancer II[1)]. Bioorganic and Medicinal Chemistry Letters 5 (*14)*: 1495-1500.

Chandra V, Pandav R, Dodge HH, Johnston JM, Belle SH, DeKosky ST, Ganguli M. 2001. Incidence of Alzheimer's disease in a rural community in India: the Indo-US study. Neurology 57:985-989.

Chen YL, Nielsen J, Hedberg K, Dunaiskis A, Jones S, Russo L, Johnson J, Ives J, Liston D. 1992. Synthesis, resolution, and structure-activity relationships of potent acetylcholinesterase inhibitors: 8-carbaphysostigmine analogues. J Med Chem 35: 1429.

Clarke PB, Pert CB, Pert A. 1984. Autoradiographic distribution of nicotine receptors in rat brain. Brain research 323(*2*):390-395.

Cleusa PF, Martin P, Carol B, Henry B, Laura F, Mary G, Kathleen H, Kazuo H, Hugh H, Yueqin H, Anthony J, Colin M, Paulo RM, Elizabeth R, Marcia S. 2005. Global prevalence of dementia: a Delphi consensus study. Lancet 366:2112-2117.

Corrada MM, Brookmeyer R, Berlau D, Paganini-Hill A, Kawas CH. 2008. Prevalence of dementia after age 90: results from the 90+ study. Neurology 71:337-343.

Costa JS da, Pisoni DS, Silva CB da, Petzhold CL, Russowsky D, Ceschi MA. 2009. Lewis Acid Protonated Friedlander Condensation Reactions between Anthranilonitrile and Ketones for the Synthesis of Tacirine and its Analogues. J. Braz. Chem. Soc. 20 (9): 1448-1454.

Cvetkovic-Dozic D, Skender-Gazibara M, Dozic S. 2001. Neuropathological hallmarks of Alzheimer's diseases. Archive of Oncology 9(*3*): 195-199.

David A. McCormick. 1989. Acetylcholine: distribution, receptors, and actions. Section of Neuroanatomy, Yale Univrersity of School of Medicine. 333 Cedar Street, New Haven, CT 06510, USA.

Davies P, Maloney AJF. 1976. Selective loss of central cholinergic neurones in Alzheimer's disease. Lancet ii: 1403.

DeGrado TR, Mulholland GK, Wieland DM, Schwaiger M. 1994. Evaluation of (-) [^{18}F] Fluoroethoxybenzovesamicol as new PET tracer of cholinergic neurons of

the heart. Nucl. Med. Biol 21, 189–195.

Drachman DA, Leavitt J. Human memory and the cholinergic system. 1974. Arch Neurol 30:113–21.

Efange SM, Khare AB, von Hohenberg K, Mach RH, Parsons SM, Zhude Tu. 2010. Synthesis and *in vitro* biological evaluation of carbonyl group-containing inhibitors of vesicular acetylcholine transporter. J Med Chem 53: 2825-2835.

Efange SM. 2000. *In vivo* imaging of the vesicular acetylcholine transporter and the vesicular monoamine transporter. FASEB J 14: 2401–2413.

Efange SM, Mach RH, Smith CR, Khare AB, Foulon C, Akella SK, Childers SR, Parsons SM. 1995. Vesamicol analogues as sigma ligands: Molecular determinants of selectivity at the vesamicol receptor. Biochem Pharmacol 49:791-797.

Efange SM, Mach RH, Smith CR, Khare AB, Foulon C, Akella SK, Childers SR, Parsons SM. 1994. Vesamicol analogues as sigma ligands: Molecular determinants of selectivity at the vesamicol receptor. Biochem. Pharmacol. 49, 791-797.

Efange SM, Mach RH, Khare A, Michelson RH, Nowak PA, Evora PH. 1994. [^{18}F] Fluorobenzyltrozamicol ([^{18}F]FBT): Molecular decomposition-reconstitution approach to vesamicol receptor radioligands for positron emission tomography. Appl. Radiat. Isot 45, 465–472.

Efange SM, Michelson RH, Khare AB, Thomas JR. 1993. Synthesis and tissue distribution of (m-[^{125}I]iodobenzyl)trozamicol ([^{125}I]MIBT): Potential radioligand for mapping central cholinergic innervation. J. Med. Chem 36, 1754–1760.

Francis PT, Palmer AM, Snape M, Wilcock GK. 1999. The cholinergic hypothesis of

Alzheimer's disease: a review. J Neurol Neurosurg Psychiatry 66:137–147

Francis PT, Sims NR, Procter AW, Bowen DM. 1993. Cortical pyramidal neurone loss may cause glutamatergic hypoactivity and cognitive impairment in Alzheimer's disease: investigative and therapeutic perspectives. *J Neurochemical* 60:1589–604.

Fratiglioni L, Launer LJ, Andersen K, Breteler MM, Copeland JR, Dartigues JF, Lobo A, Martinez-Lage J, Soininen H, Hofman A. 2000. Incidence of dementia and major subtypes in Europe: a collaborative study of population-based cohorts. Neurology 54:S10-S15.

Frey KA, Wieland DM, Kilbourn MR. 1998. Imaging of monoaminergic and cholinergic vesicular transporters in the brain. Adv Pharmacol 42: 269–272.

Fulton B, Benfield P. 1996. Galanthamine. Drugs Aging, 9: 60.

Gao M, Miller MA, DeGrado TR, Mock BH, Lopshire JC, Rosenberger JG, Dusa C, Das MK, Groh WJ, Zipes DP, Hutchins GD, Zheng QH. 2007. Evaluation of [^{11}C]hemicholinium-15 and [^{18}F]hemicholinium-15 as new potential PET tracers for the high-affinity choline uptake system in the heart. Bioorg. Med. Chem 15(*3*), 1289-1297.

Gage HD, Voytko ML, Ehrenkaufer RL, Tobin JR, Efange SM, Mach RH. 2000. Reproducibility of Repeated Measures of Cholinergic Terminal Density Using [^{18}F](1)-4-Fluorobenzyltrozamicol and PET in the Rhesus Monkey Brain J. Nucl. Med 41, 2069–2076.

Giboureau N, Emond P, Fulton RR, Henderson DJ, Chalon S, Garreau L, Roselt P, Eberl S, Mavel S, Bodard S, Fulham MJ, Guilloteau D, Kassiou M. 2007. Ex vivo and in vivo evaluation of (2R,3R)-5-[(18)F]-fluoroethoxy- and fluoropropoxy-benzovesamicol, as PET radioligands for the vesicular

acetylcholine transporter. Synapse 61(12):962-970.

Gilissen C, de Groot T, Bronfman F, van Leuven F, Verbruggen A. M, Bormans G. M. 2003. Evaluation of ^{18}F–FA-4 and ^{11}C–pipzA-4 as Radioligands for the In Vivo Evaluation of the High-Affinity Choline Uptake System. J Nucl. Med 269-275.

Gilmor ML, Nash NR, Roghani A, Edwards RH, Yi H, Hersch SM, Levey A.I. 1996. Expression of the putative vesicular acetylcholine transporter in rat brain and localization in cholinergic synaptic vesicles. J Neurosci 16:2179–2190.

Goedert M, Hasegawa M, Jakes R., Lawler S, Cuenda A, Cohen P. 1997. Phosphorylation of microtubule-associated protein tau by stress-activated protein kinases. FEBS Lett 409, 57-62.

Goedert M, Spillantini MG, Cairns NJ, Crowther RA. 1992. Tau proteins of Alzheimer paired helical filaments: abnormal phosphorylation of all six brain isoforms. Neuron *8*, 159-68.

Goedert M, Wischik C. M., Crowther R. A., Walker J. E., Klug A. 1988. Cloning and sequencing of the cDNA encoding a core protein of the paired helical filament of Alzheimer disease: identification as the microtubule-associated protein tau. Proc. Natl. Acad. Sci. U. S. A. *85*, 4051-5.

Haga T, Noda H. 1973. Choline uptake systems of rat brain synaptosomes. Biochim. Biophys. Acta 291**,** 564–575.

Haga, T. 1971. Synthesis and release of [^{14}C] acetylcholine in synaptosomes. J. Neurochem 18**,** 781–798.

Happe HK, Murrin LC. 1993. High-affinity choline transport sites: use of [^{3}H] hemicholinium-3 as a quantitative marker. J. Neurochem 60**,** 1191–1201.

Hara T, Bansal A, DeGrado TR. 2006. Choline transporter as a novel target for molecular imaging of cancer. Molecular Imaging 5, 498-509.

Hardy J, Selkoe DJ. 2002. The Amyloid Hypothesis of Alzheimer's disease: Progress and Problems on the Road to Therapeutics. Science 297, 353-356.

Haruyuki Chaki, Haruko Yamabe, Mamoru Sugano, Shuji Morita, Tomoko Bessho, Reiko Tabata, Ken-Ichi Saito, Mitsuo Egawa, Akihiro Tobe and Yasuhiro Morinaka. 1995. Design and syntheses of 4-acylaminopyridine derivatives: Novel high affinity choline uptake enhancers. Bioorganic & Medicinal Chemistry Letters 14(*5*), 1489-1494.

Helzner EP, Scarmeas N, Cosentino S, Tang MX, Schupf N, Stern Y. 2008. Survival in Alzheimer disease: a multiethnic, population-based study of incident cases. Neurology 71:1489-1495.

Hoover DB, Ganote CE, Ferguson SM, Blakely RD, Parsons R. 2004. Localization of cholinergic innervation in guinea pig heart by immunohistochemistry for high-affinity choline transporters. Cardiovasc. Res 62, 112-21.

Hulme EC, Birdsall NJ, Buckley NJ. 1990. Muscarinic receptor subtypes. Annual review of pharmacology and toxicology 30:633-673.

Ichikawa T, Ajiki K, Matsuura J, Misawa H. 1997. Localization of two cholinergic markers, choline acetyltransferase and vesicular acetylcholine transporter in the central nervous system of the rat: In situ hybridization histochemistry and immunohistochemistry. J Chem Neuroanatomy 13:23–39.

International Atomic Energy Agency. Cyclotron Produced Radionuclides: Physical Characteristics and Production Methods. Technical Reports Series no. 468:53-62.

Jansen FP, Vanderheyden JL. 2007. The future of SPECT in a time of PET. Nucl. Med. Biol 34, 733−735.

John V, Liberburg I, Thorsett ED. 1993. Imina 1.2.3.4-tetrahydrocyclopent[b]indole

carbamates as dual inhibitors of acetylcholinesterase and monoamine oxidase. Ann Rep Chem 29: 197.

Jorm AF, Jolley D. 1998. The incidence of dementia: a meta-analysis. Neurology 51:728-733.

Junfeng Li, Xiang Zhang, Zhanbin Zhang, Prashanth K. Padakanti, Hongjun Jin, Jinquan Cui, Aixiao Li, Dexing Zeng, Nigam P. Rath, Hubert Flores, Joel S. Perlmutter, Stanley M. Parsons, Zhude Tu. 2013. Heteroaromatic and aniline derivatives of piperidines as potent ligands for vesicular acetylcholine transporter. J. Med. Chem 2013, 56, 6216−6233.

Jung YW, Van Dort ME, Gildersleeve DL, Wieland DM. 1990. A radiotracer for mapping cholinergic neurons of the brain. J. Med. Chem 33, 2065–2068.

Kalaria RN, Maestre GE, Arizaga R, Friedland RP, Galasko D, Hall K, Luchsinger JA, Ogunniyi A, Perry EK, Potocnik F, Prince M, Stewart R, Wimo A, Zhang ZX, Antuono P; World Federation of Neurology Dementia Research Group. 2008. Alzheimer's disease and vascular dementia in developing countries: prevalence, management, and risk factors. Lancet Neurol 7:812-826.

Kawamura K, Shiba K, Tsukada H, Nishiyama S, Mori H, Ishiwata K. 2006. Synthesis and evaluation of vesamicol analog (−)-*o*-[^{11}C]methylvesamicol as a PET ligand for vesicular acetylcholine transporter. Annals of Nuclear Medicine 20 (6), 417–424.

Kawas C, Gray S, Brookmeyer R, Fozard J, Zonderman A. 2000. Age-specific incidence rates of Alzheimer's disease: the Baltimore Longitudinal Study of Aging. Neurology 54:2072-2077.

Kozaka T, Uno I, Kitamura Y, Miwa D, Ogawa K, Shiba K. 2012. Syntheses and in vitro evaluation of decalinvesamicol analogues as potential imaging probes for

vesicular acetylcholine transporter (VAChT). Bioorganic & medicinal chemistry 20(16):4936-4941.

Kozaka T, Uno I, Kitamura Y, Miwa D, Azim MA, Ogawa K, Shiba K.2014. Regional brain imaging of vesicular acetylcholine transporter (VAChT) using *o*-[^{125}I]iodo-*trans*-decalinvesamicol as a new potential imaging probe. Synapse 68(3): 107-113.

Kuhar MJ, Murrin LC. 1978. Sodium-dependent, high-affinity choline uptake. J. Neurochem 30, 15–21.

Kuhar MJ, Sethy VH, Roth RH, Aghajanian GK. 1973. Choline: selective accumulation by central cholinergic neurons. J. Neurochem 20**,** 581–593.

Kuhl DE, Koeppe RA, Fessler JA, Minoshima S, Ackermann RJ, Carey JE, Gildersleeve DL, Frey KA, Wieland DM. 1994. *In Vivo* Mapping of cholinergic neurons in the human Brain using SPECT and IBVM. J. Nucl. Med 35, 405–410.

Kukull WA, Higdon R, Bowen JD, McCormick WC, Teri L, Schellenberg GD, Van Belle G, Jolley L, Larson EB. 2002. Dementia and Alzheimer disease incidence: a prospective cohort study. Arch Neurol 59:1737- 1746.

Laruelle M. Slifstein M, Huang Y. 2003. Relationships between radiotracer properties and image quality in molecular imaging of the brain with positron emission tomography. Mol. Imaging Biol. 5, 363–375.

Lobo A, Launer LJ, Fratiglioni L, Andersen K, Di Carlo A, Breteler MM, Copeland JR, Dartigues JF, Jagger C, Martinez-Lage J, Soininen H, Hofman A. 2000. Prevalence of dementia and major subtypes in Europe: A collaborative study of population-based cohorts. Neurology 54: S4-S9.

Mach RH, Voytko ML, Ehrenkaufer RL, Nader MA, Tobin JR, Efange SM, Parsons

SM, Gage HD, Smith CR, Morton TE. 1997. Imaging of cholinergic terminals using the radiotracer [^{18}F](1)-4-Fluorobenzyltrozamicol: In vitro binding studies and positron emission tomography studies in nonhuman primates. Synapse 25, 368–380.

Mathers C, Leonardi M .2000. Global burden of dementia in the year 2000: Summary of methods and data sources. Global Burden of Disease 2000. (http://www.who.int/healthinfo/statistics/bod_dementia.pdf)

Maziere B, Loc'h C. 1986. Bromine radiopharmaceuticals. Radiopharmaceuticals labelled with bromine isotopes. Appl Radiat Isot 37:703-713.

Mehta KM, Yaffe K, Pérez-Stable EJ, Stewart A, Barnes D, Kurland BF, Miller BL. 2008. Race/ethnic differences in AD survival in US Alzheimer's Disease Centers. Neurology 70:1163- 1170.

Miyazaki S, Onodera K, Imaizumi M, Timmerman H. 1997. Effects of clobenpropit (VUF-9153), a histamine H3- receptor antagonist, on learning and memory, and on cholinergic and monoaminergic systems in mice. Life Sci 61: 335.

Mulholland GK, Wieland DM, Kilbourn MR, Frey KA, Sherman PS, Carey JE, Kuhl DE, 1998. [^{18}F]fluoroethoxy-benzovesamicol, a PET radiotracer for the vesicular acetylcholine transporter and cholinergic synapses. Synapse 30, 263-274.

Murrin LC, Kuhar MJ. 1976. Activation of high-affinity choline uptake *in vitro* by depolarizing agents. Mol. Pharmacol 12**,** 1082–1090.

Näslund J, Haroutunian V, Mohs R, Davis KL. Davies P, Greengard P, Buxbaum JD. 2000. Correlation between elevated levels of amyloid beta-peptide in the brain and cognitive decline. J. Am. Med. Assoc 283, 1571-7.

National Institute on Aging. October 26, 2007. Understanding stages and symptoms of

Alzheimer's disease. (http://www.nia.nih.gov/Alzheimers/Publications/stages.htm).

Nilsson L, Nordberg A, Hardy J, Wester P, Winblad B. 1986. Physostigmine restores [^{3}H]-acetylcholine efflux from Alzheimer brain slices to normal level. J Neural Transm 67:275–85.

Nitsch RM. 1996. From acetylcholine to amyloid: neurotransmitters and the pathology of Alzheimer's disease. Neurodegeneration 5: 477–82.

Ohno M, Sametsky EA, Younkin LH, Oakley H, Younkin SG, Citron M, Vassar R, Disterhoft JF. 2004. BACE1 deficiency rescues memory deficits and cholinergic dysfunction in a mouse model of Alzheimer's disease. Neuron *41*, 27-33.

Oda Y. 1999. Choline acetyltransferase: The structure, distribution and pathologic changes in the central nervous system. Pathology International 49: 921–937.

Palmer AM, Gershon S. 1990. Is the neurochemical basis of Alzheimer's disease cholinergic or glutamatergic? FASEB 4:2745–52.

Parent M, Bedard MA, Aliaga A, Soucy JP, Landry St-Pierre E, Cyr M, Kostikov A, Schirrmacher E, Massarweh G, Rosa-Neto P. 2012. PET imaging of cholinergic deficits in rats using [^{18}F]fluoroethoxybenzovesamicol ([^{18}F]FEOBV). NeuroImage 62(1):555-561.

Parsons SM, Prior C, Marshall IG. 1993. Acetylcholine transport, storage and release. Int. Rev. Neurobiol 35, 279-390.

Pascual J, Fontán A, Zarranz JJ, Berciano J, Flórez J, Pazos A. 1991. High-affinity choline uptake carrier in Alzheimer's disease: implications for the cholinergic hypothesis of dementia. Brain Res 552**,** 170–174.

Perry EK, Gibson PH, Blessed G, Perry RH, Tomlinson BE. 1977. Neurotransmitter enzyme abnormalities in senile dementia. Choline acetyltransferase and

glutamic acid decarboxlyase activities in necropsy brain tissue. J Neurol Sci 34:247–65.

Plassman BL, Langa KM, Fisher GG, Heeringa SG, Weir DR, Ofstedal MB, Burke JR, Hurd MD, Potter GG, Rodgers WL, Steffens DC, Willis RJ, Wallace RB. 2007. Prevalence of dementia in the United States: the aging, demographics, and memory study. Neuroepidemiology 29:125-132.

Prado VF, Martins-Silva C, de Castro BM, Lima RF, Barros DM, Amaral E, Ramsey AJ, Sotnikova TD, Ramirez MR, Kim HG, Rossato JI, Koenen J, Quan H, Cota VR, Moraes MF, Gomez MV, Guatimosim C, Wetsel WC, Kushmerick C, Pereira GS, Gainetdinov RR, Izquierdo I, Caron MG, Prado MA. 2006. Mice deficient for the vesicular acetylcholine transporter are myasthenic and have deficits in object and social recognition. Neuron 51(5):601-612.

Prior C, Marshall IG, Parsons SM. 1992**.** The pharmacology of vesamicol: an inhibitor of the vesicular acetylcholine transporter. Gen. Pharmacol 23, 1017-1022.

Quirion R, Aubert I, Araujo DM, Hersi A, Gaudreau P. 1993. Autoradiographic distribution of putative muscarinic receptor sub-types in mammalian brain. Progress in brain research 98:85-93.

Quirion R. 1987. Characterization and autoradiographic distribution of Hemicholinium-3 high affinity choline uptake sites in mammalian brain. Synapse 1: 293-303.

Rahmim A, Zaidi H. 2008. PET versus SPECT: strengths, limitations and challenges. Nucl. Med. Commun. 29, 193−207.

Rizzo S. 2009. Design and Synthesis of Multi Target Compounds for the Treatment of Alzheimer's disease. Alma Mater Studiorum Università di Bologna. Dottorato di ricerca in Scienze farmaceutiche, 21. Ciclo.

(http://amsdottorato.cib.unibo.it/1751/)

Rogers GA, Stone-Elander S, Ingvar M, Eriksson L, Parsons SM, Widen L. 1994. ^{18}F-labelled vesamicol derivatives: Syntheses and preliminary *in Vivo* small animal positron emission tomography evaluation. Nucl. Med. Biol 21, 219–230.

Rogers GA, Parsons SM, Anderson DC, Nilsson LM, Bahr BA, Kornreich WD, Kaufman R, Jacobs RS, Kirtman B. 1989. Synthesis, in Vitro Acetylcholine-Storage- Blocking Activities, and Biological Properties of Derivatives and analogues of *trans*-2-(4-Phenylpiperidineo)cyclohexanol (Vesamicol). J. Med. Chem 32, 1217-1230.

Rotter A, Jacobwitz DM. 1981. Neurochemical identification of cholinergic forebrain projection sites of the nucleus tegmentalis dorsalis lateralis. Brain Res Bull 6:525-529.

Rylett RJ, Ball MJ, Colhuon EH. 1983. Evidence for high affinity choline transport in synaptosomes prepared from hippocampus and neocortex of patients with Alzheimer's disease. Brain Res 289:169–75.

Sandberg K, Coyle JT. 1985. Characterization of [^{3}H]Hemicholinium-3 binding associated with Neuronal choline uptake sites in rat membranes. Brain research 348: 321-330.

Schafer M. K.-H., Weihe E., Varoqui H., Eiden L. E. and Erickson J. D. 1994. Distribution of the vesicular acetylcholine transporter (VAChT) in the central and peripheral nervous systems of the rat. J. Mol. Neurosci 5**,** 1–26.

Sarter M, Parikh V. 2005. Choline transporters, cholinergic transmission and cognition. Nature Reviews Neuroscience (www.nature.com/reviews/neuro). 6: 48-56.

Schafer MK, Weihe E, Erickson JD, Eiden LE. 1995. Human and monkey cholinergic neurons visualized in paraffin-embedded tissues by immunoreactivity for

VAChT, the vesicular acetylcholine transporter. J Mol Neurosci 6:225–235.

Schafer MK, Weihe E, Varoqui H, Eiden LE, Erickson JD. 1994. Distribution of the vesicular acetylcholine transporter (VAChT) in the central and peripheral nervous systems of the rat. J. Mol. Neurosci 5, 1–26.

Schnee ME, Brown BS. 1998. Selectivity of Linopirdine (DuP 996), a Neurotransmitter Release Enhancer, in Blocking Voltage Dependant and calcium-Activated Potassium Currents in Hippocampal Neurons. J Pharmacol Exp Ther 286, 709.

Shiba K, Yano T, Sato W, Mori H, Tonami N. 2002. Characterization of radioiodinated (-)-ortho-iodovesamicol binding in rat brain preparations. Life Sciences 71, 1591–1598.

Shiba K, Mori H, Tonami N. 2003. Evaluation of radioiodinated (-)-o-iodovesamicol as a radiotracer for mapping the vesicular acetylcholine transporter. Annals of Nuclear Medicine 17 (6), 451-456.

Shiba K, Ogawa K, Ishiwata K, Yajima k, Mori H. 2006. Synthesis and binding affinities of methylvesamicol analogs for the acetylcholine transporter and sigma receptor Bioorg. Med. Chem 14, 2620-2626.

Simon JR, Kuhar MJ. 1975. Impulse-flow regulation of high affinity choline uptake in brain cholinergic nerve terminals. Nature 255**,** 162–163.

Smart LA. 1983. Synthesis and biological activity of a 2-bromoethylamine (mustard) derivative of hemicholinium-3 and hemicholinium-15. J Med. Chem 26, 104-107.

Staley JK, Mash DC, Parsons SM, Khare AB, Efange SM. 1997. Pharmacological characterization of the vesamicol analogue (+)-[^{125}I]MIBT in primate brain. Eur. J. Pharmacol 338, 159–169.

Stark H, Purand K, Ligneau X, Rouleau A, Arrang JM, Garbarg M, Schwartz

JC, Schunack W. 1996. Novel Carbamates as Potent Histamine H_3 Receptor Antagonists with High in Vitro and Oral *in Vivo* Activity. J Med Chem 39: 1157.

Stephen S. Flitman. Update on Alzheimer's disease. February 2011, 21st Century Neurology, 2601 North Third Street Suite 125, Phoenix, Arizona, (602) 265-6500. (www.neurozone.org).

Sorger D, Schliebs R, Kampfer I, Rossner S, Heinicke J, Dannenberg C, Georgi P. 2000. *In Vivo* [^{125}I]-Iodobenzovesamicol binding reflects cortical cholinergic deficiency induced by specific immunolesion of rat basal forebrain cholinergic system. Nucl. Med. Biol 27, 23–31.

Takashina K, Bessho T, Mori R, Eguchi J, Saito K. 2008. MKC-231, a choline uptake enhancer: (2) Effect on synthesis and release of acetylcholine in AF64A-treated rats. J Neural Transm 115: 1-27-1035.

Terry AV Jr, Buccafusco JJ. 2003. The cholinergic hypothesis of age and Alzheimer's disease related cognitive deficits: Recent challenges and their implications for novel drug development. J Pharmacol Exp Ther 306: 821-827

The Canadian Study of Health and Aging Working Group. 2000. The incidence of dementia in Canada. Neurology 55:66-73.

Tucek R. 1985. Regulation of acetylcholine synthesis in the brain. J. Neurochem 44, 11-24.

Usdin TB, Eiden LE, Bonner TI, Erickson JD. 1995. Molecular biology of the vesicular ACh transporter. Trends Neurosci 18, 218–224.

Vilaro MT, Mengod G, Palacios JM. 1993. Advances and limitations of the molecular neuroanatomy of cholinergic receptors: the example of multiple muscarinic receptors. Progress in brain research 98:95-101.

Von Strauss E, Viitanen M, De Ronchi D, Winblad B, Fratiglioni L. 1999. Aging and the occurrence of dementia: findings from a population-based cohort with a large sample of nonagenarians. Arch Neurol 56:587-592.

Voytko ML, Mach RH, Gage HD, Ehrenkaufer RL, Efange SM, Tobin JR, 2001. Cholinergic activity of aged rhesus monkeys revealed by positron emission tomography. Synapse 39. 95–100.

Weihe E, Tao-Cheng JH, Schafer MKH, Erickson JD, Eiden LE. 1996. Visualization of the vesicular acetylcholine transporter in cholinergic nerve terminals and its targeting to a specific population of small synaptic vesicles. Proc. Natl. Acad. Sci. USA 93**,** 3547–3552.

Whitehouse PJ, Price DL, Struble RG, Clark AW, Coyle JT, Delon MR. 1982. Alzheimer's disease and senile dementia: loss of neurones in basal forebrain. Science 215:1237–9.

Widen L, Eriksson L, Ingvar M, Parsons SM, Rogers GA, Stone-Elander S. 1993. PET studies of central cholinergic nerve terminals in animals and man. J. Cereb. Blood Flow Metab 13(Suppl. 1), S300.

Wimo A, Winblad B, Jönsson L. 2007. An estimate of total worldwide societal costs of dementia in 2005. Alzheimers Dement 3:81-91.

Wimo A, Winblad B, Agüero-Torres H, von Strauss E. 2003. The magnitude of dementia occurrence in the world. Alzheimer Dis Assoc Disord 17:63-67.

Yamamura HI, Snyder SH. 1972. Choline: high-affinity uptake by rat brain synaptosomes. Science 178, 626–628.

Zheng QH, Gao M, Mock BH, Wang S, Hara T, Nazih R, Miller MA, Receveur TJ, Lopshire JC, Groh WJ, Zipes DP, Hutchins GD, DeGrado TR. 2007. Synthesis and biodistribution of new radiolabeled high affinity choline

transporter inhibitors [^{11}C]hemicholinium-3 and [^{18}F]hemicholinium-3; Bioorganic & Medicinal Chemistry Letters 17, 2220-2224.

Tu Z, Wang W, Cui J, Zhang X, Lu X, Xu J, Parsons SM. 2012. Synthesis and evaluation of *in vitro* bioactivity for vesicular acetylcholine transporter inhibitors containing two carbonyl groups. Bioorganic & Medicinal Chemistry 20 (14): 4422–4429.

Zhude Tu, Efange SM, Xu J, Li S, Jones LA, Parsons SM, Mach RH. 2009. Synthesis and *in vitro* and *in vivo* evaluation of ^{18}F-labeled positron emission tomography (PET) ligands for imaging the vesicular acetylcholine transporter. J Med Chem 52: 1358-1369

Appendices

Appendix I:

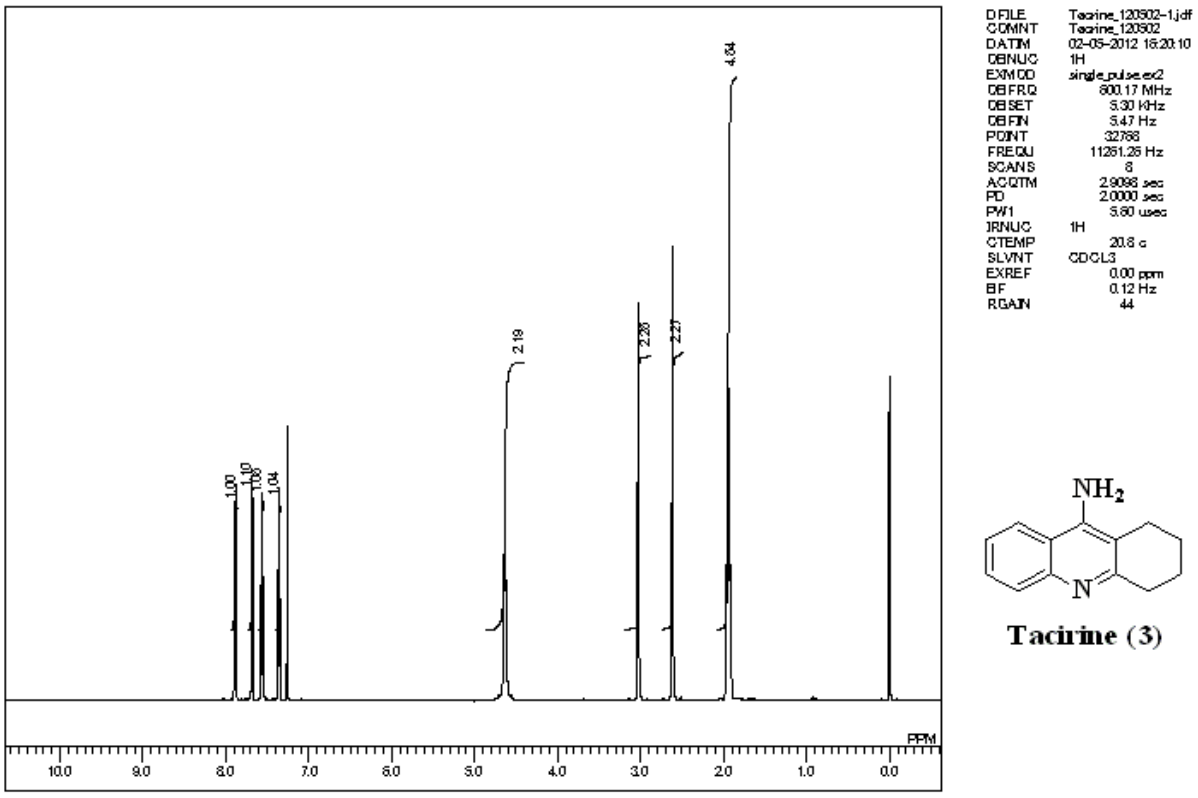

Figure 27 (a): ^{1}H NMR Spectra of Tacirine.

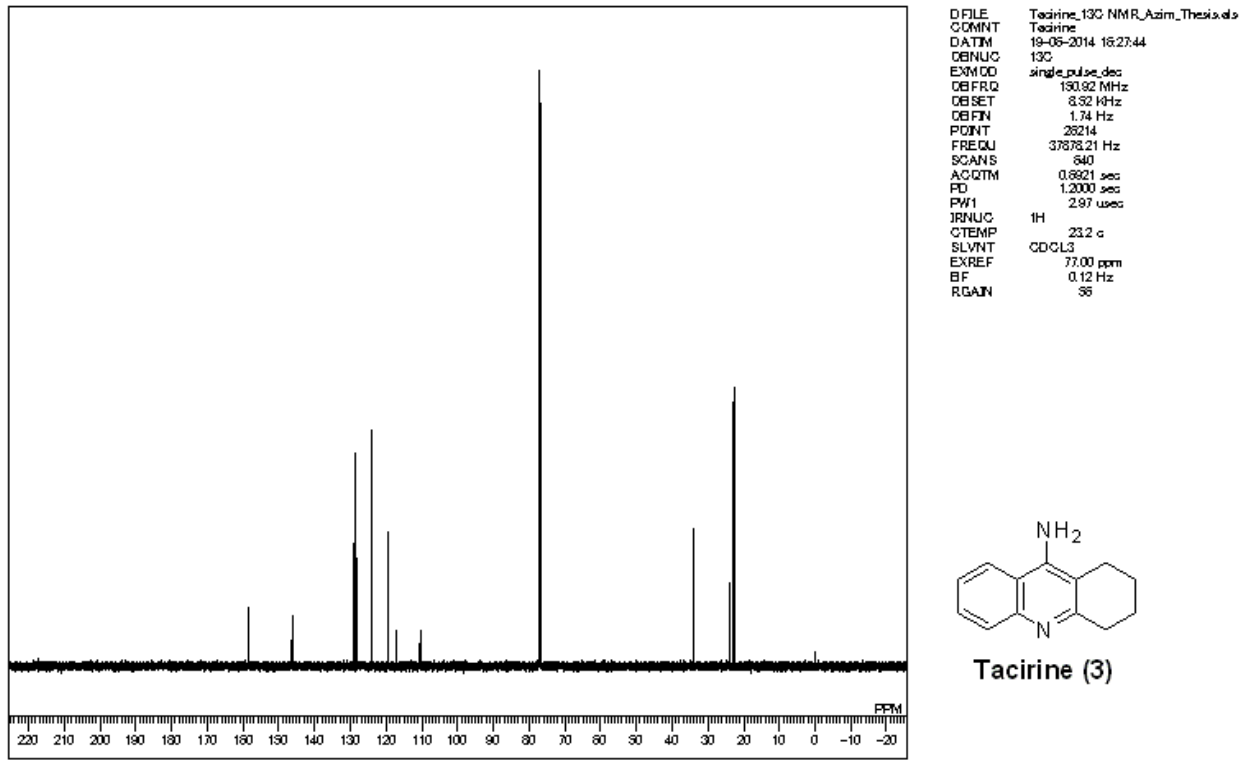

Figure 27 (b): ^{13}C NMR Spectra of Tacirine.

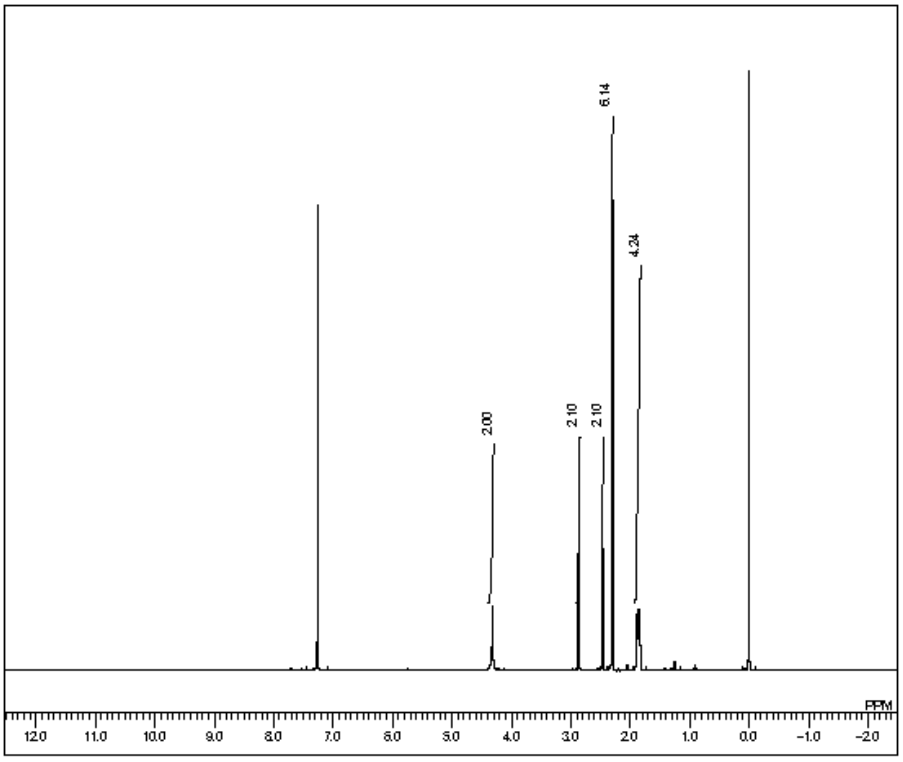

DFILE	DMTA_1H NMR_Azim_2_Thesis.els
COMNT	Reaction 1-1_Azim
DATIM	21-11-2011 16:30:14
OBNUC	1H
EXMOD	single_pulse.ex2
OBFRQ	600.17 MHz
OBSET	3.30 KHz
OBFIN	3.47 Hz
POINT	26214
FREQU	9008.67 Hz
SCANS	8
ACQTM	2.9098 sec
PD	2.0000 sec
PW1	8.60 usec
IRNUC	1H
CTEMP	19.2 c
SLVNT	CDCL3
EXREF	0.00 ppm
BF	0.12 Hz
RGAIN	80

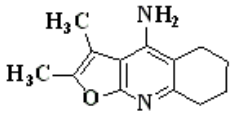

DMTA (4)

Figure 28 (a): ^{1}H NMR Spectra of DMTA.

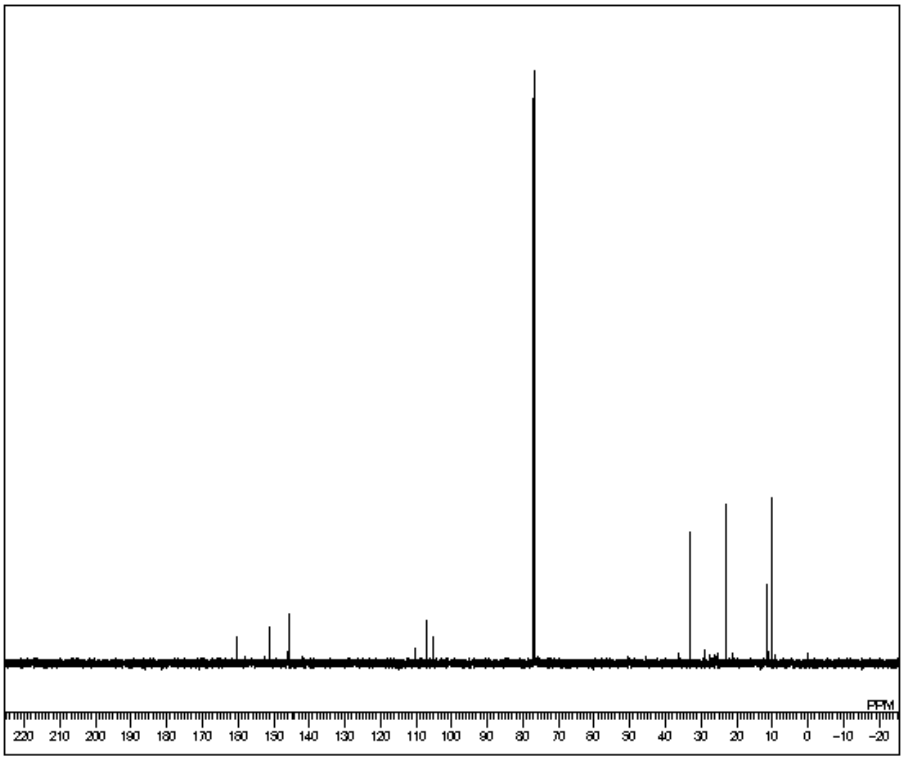

DFILE	DMTA_13C NMR_Azim_Thesis.els
COMNT	DMTA
DATIM	19-05-2014 16:54:49
OBNUC	13C
EXMOD	single_pulse_dec
OBFRQ	150.92 MHz
OBSET	8.32 KHz
OBFIN	1.74 Hz
POINT	26214
FREQU	37878.21 Hz
SCANS	840
ACQTM	0.6921 sec
PD	1.2000 sec
PW1	2.97 usec
IRNUC	1H
CTEMP	23.1 c
SLVNT	CDCL3
EXREF	77.00 ppm
BF	0.12 Hz
RGAIN	56

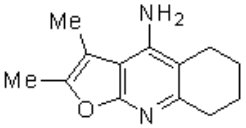

DMTA (4)

Figure 28 (b): ^{13}C NMR Spectra of DMTA.

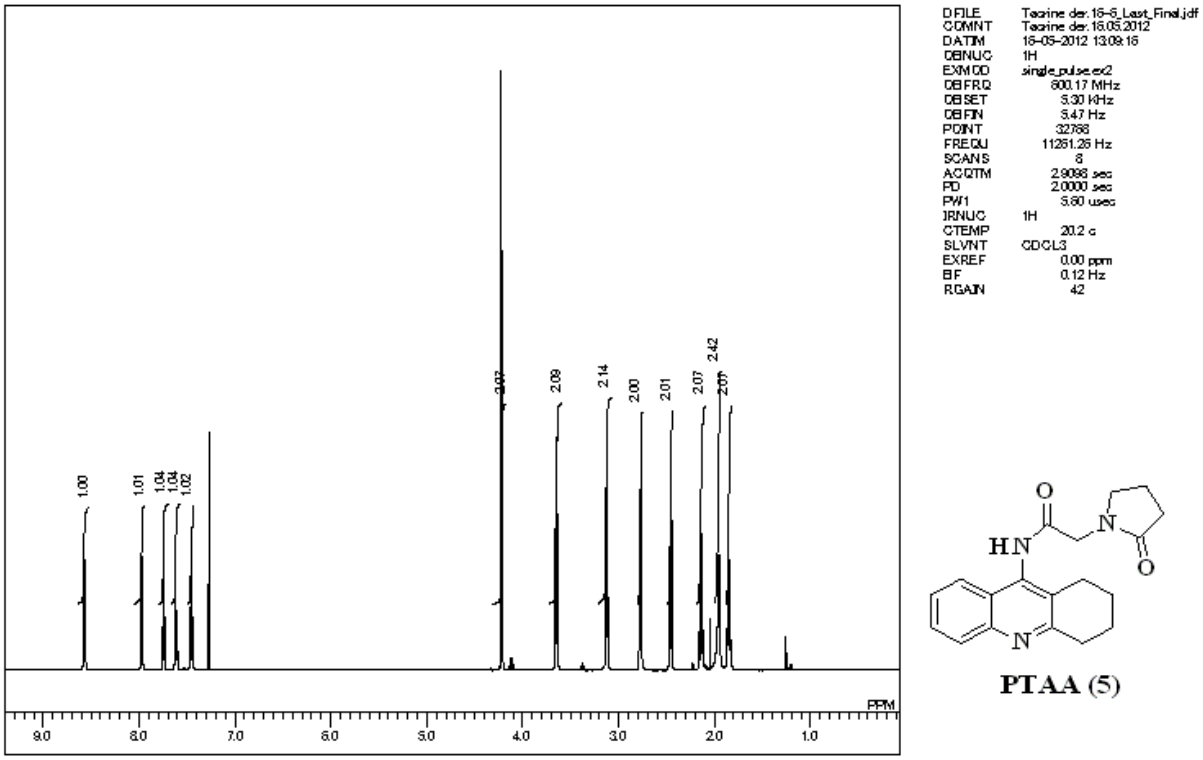

Figure 29 (a): ^{1}H NMR Spectra of PTAA.

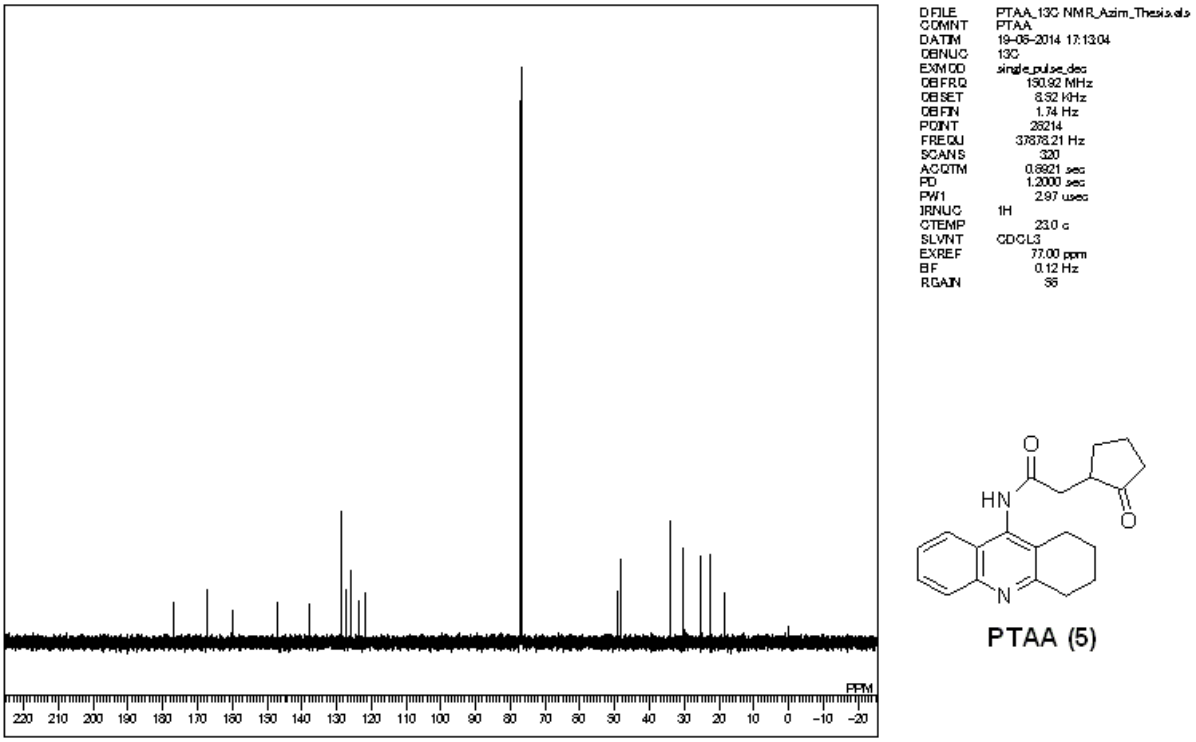

Figure 29 (b): ^{13}C NMR Spectra of PTAA.

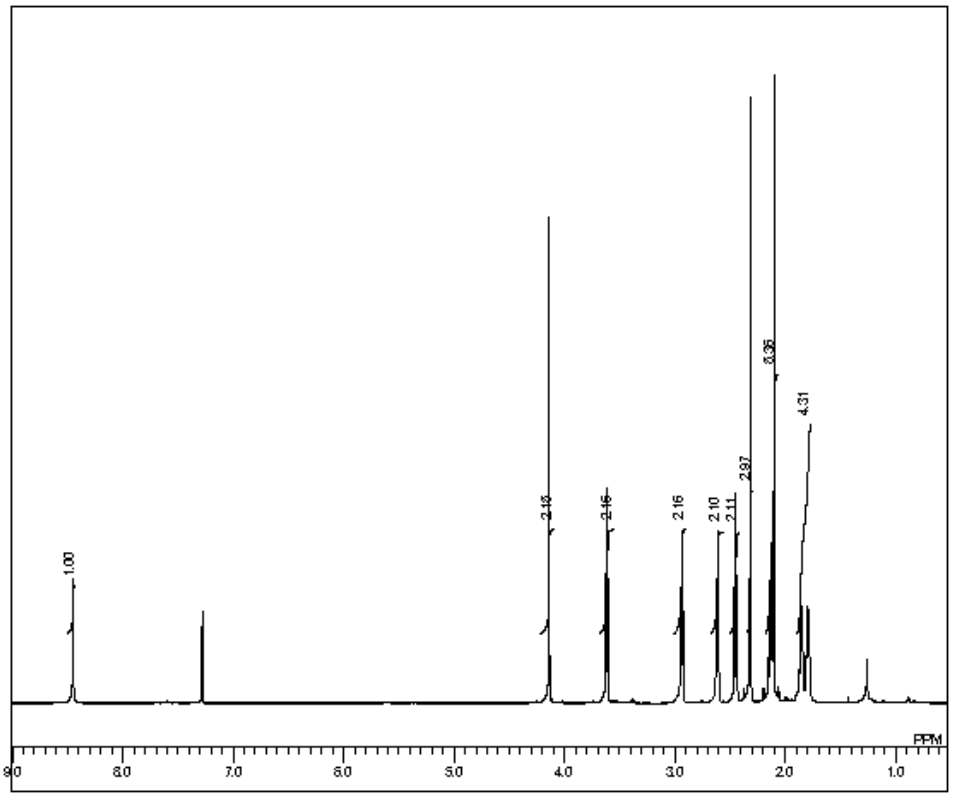

DFILE	MKC_NaH~1.jdf
COMNT	MKC
DATIM	06-02-2012 15:28:37
OBNUC	1H
EXMOD	single_pulse.ex2
OBFRQ	600.17 MHz
OBSET	3.30 kHz
OBFIN	5.47 Hz
POINT	32768
FREQU	11261.26 Hz
SCANS	8
ACQTM	2.9098 sec
PD	2.0000 sec
PW1	9.80 usec
IRNUC	1H
CTEMP	19.3 c
SLVNT	CDCL3
EXREF	0.00 ppm
BF	0.12 Hz
RGAIN	34

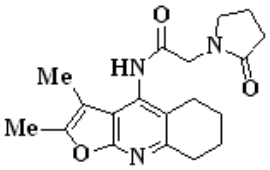

MKC-231 (6)

Figure 30 (a): ^{1}H NMR Spectra of MKC-231.

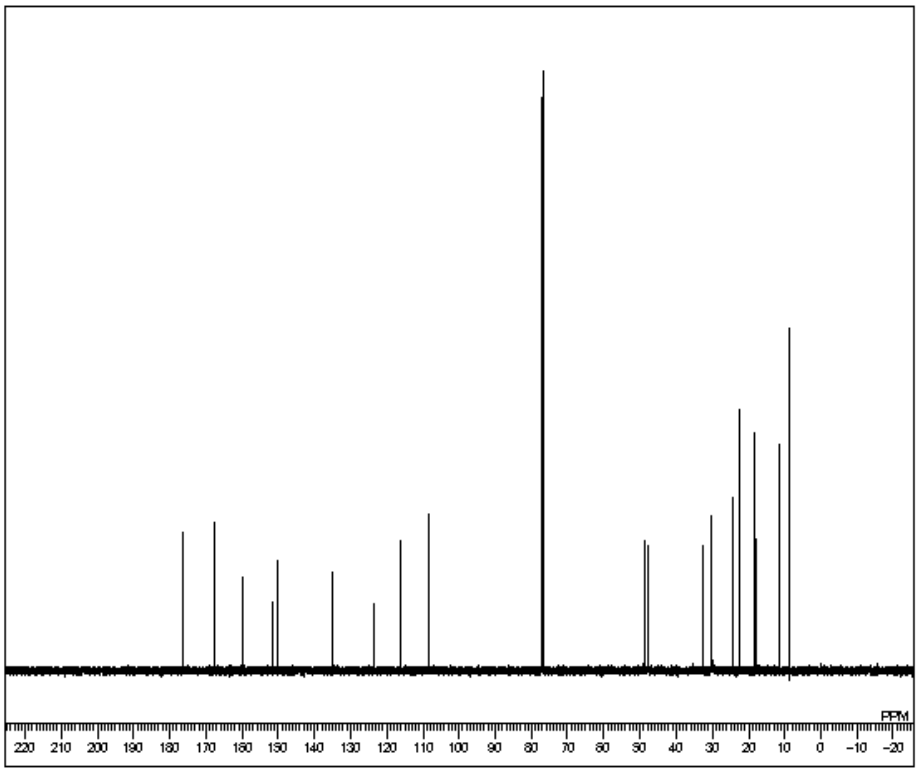

DFILE	MKC_13C NMR_Azim_Thesis.als
COMNT	MKC
DATIM	06-02-2012 15:55:05
OBNUC	13C
EXMOD	single_pulse_dec
OBFRQ	150.92 MHz
OBSET	8.52 kHz
OBFIN	1.74 Hz
POINT	28214
FREQU	37878.21 Hz
SCANS	640
ACQTM	0.8921 sec
PD	1.2000 sec
PW1	2.77 usec
IRNUC	1H
CTEMP	19.6 c
SLVNT	CDCL3
EXREF	77.00 ppm
BF	0.12 Hz
RGAIN	52

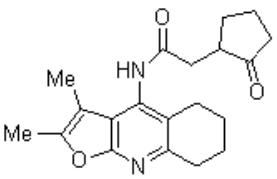

MKC-231(6)

Figure 30 (b): ^{13}C NMR Spectra of MKC-231.

Appendix II

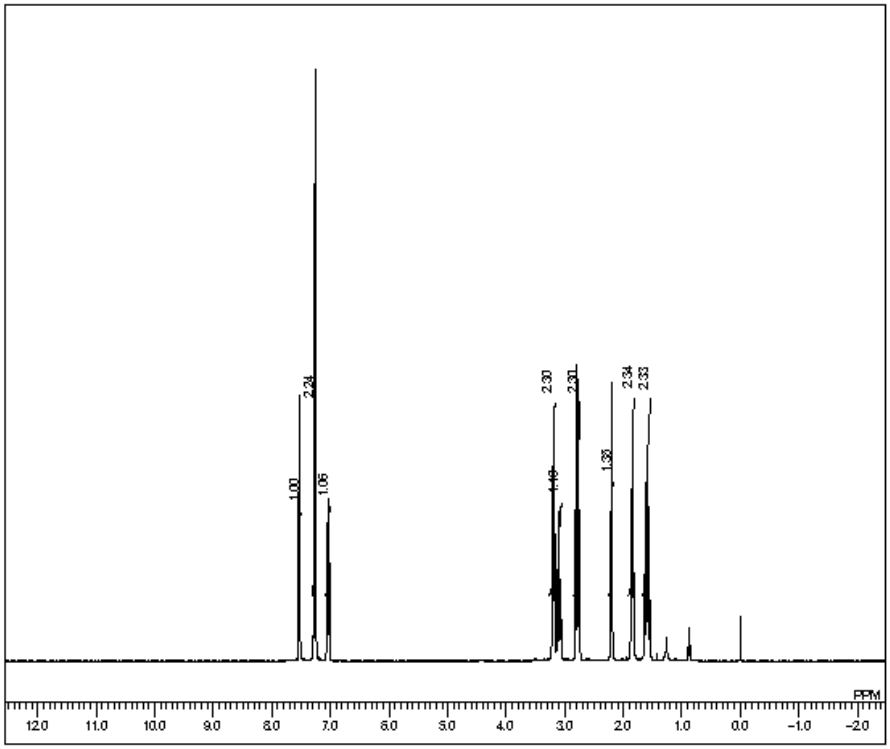

DFILE After Reduction – 4–1.als
COMNT After Reduction – 4
DATIM 05–07–2010 18:50:53
OBNUC 1H
EXMOD single_pulse.ex2
OBFRQ 399.78 MHz
OBSET 4.19 kHz
OBFIN 7.29 Hz
POINT 13107
FREQU 6002.31 Hz
SCANS 16
ACQTM 2.1837 sec
PD 2.0000 sec
PW1 4.75 usec
IRNUC 1H
CTEMP 23.1 c
SLVNT CDCL3
EXREF 0.00 ppm
BF 0.12 Hz
RGAIN 24

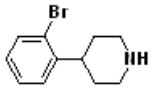

4-(2-Bromophenyl)piperidine, (7)

Figure 31: ^{1}H NMR Spectra of 4-(2-Bromophenylpiperidine)

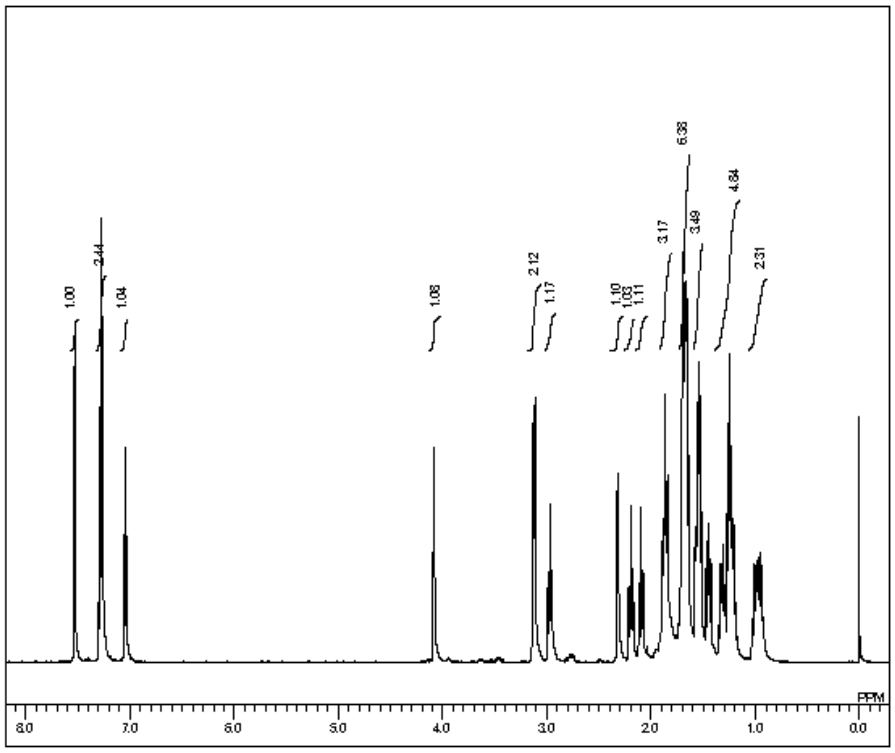

DFILE TK–OBDV–1H–3.als
COMNT OBDV_1H
DATIM 28–07–2010 19:52:22
OBNUC 1H
EXMOD single_pulse.ex2
OBFRQ 600.17 MHz
OBSET 5.30 kHz
OBFIN 5.47 Hz
POINT 26214
FREQU 9008.67 Hz
SCANS 8
ACQTM 2.9098 sec
PD 2.0000 sec
PW1 6.00 usec
IRNUC 1H
CTEMP 25.2 c
SLVNT CDCL3
EXREF 0.00 ppm
BF 0.12 Hz
RGAIN 38

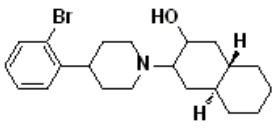

OBDV (8)

Figure 32 (a): ^{1}H NMR Spectra of OBDV.

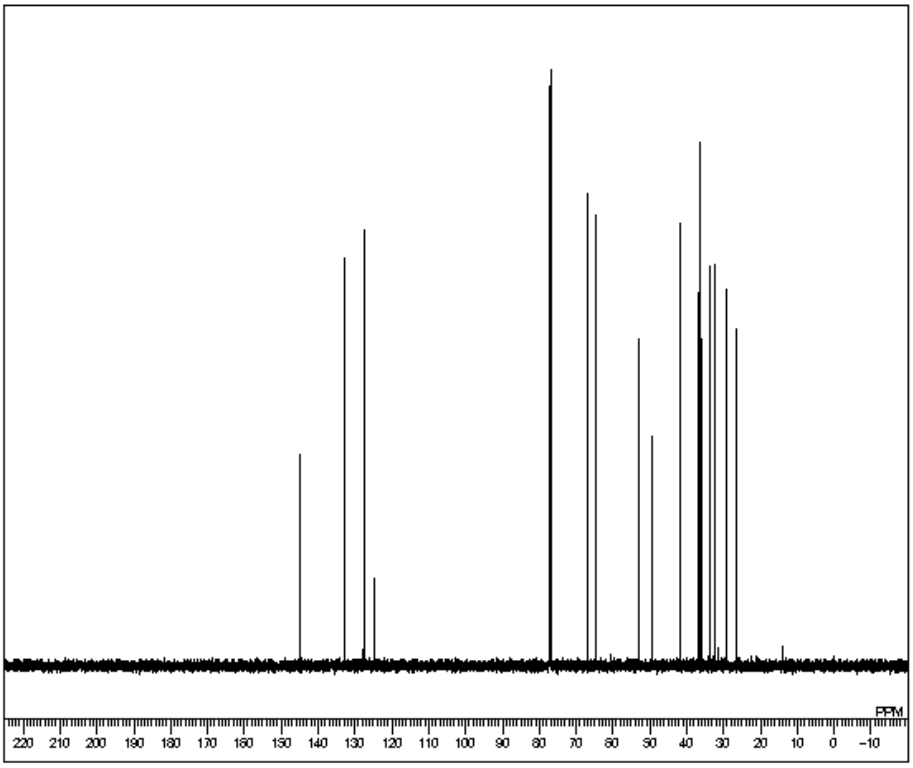

DFILE OBDV-4-13C.als
COMNT Coupling-4-13C
DATIM 07-07-2010 18:15:17
OBNUC 13C
EXMOD single_pulse_dec
OBFRQ 150.92 MHz
OBSET 8.92 kHz
OBFIN 1.74 Hz
POINT 26214
FREQU 37878.21 Hz
SCANS 435
ACQTM 0.6921 sec
PD 1.2000 sec
PW1 2.83 usec
IRNUC 1H
CTEMP 24.3 c
SLVNT CDCL3
EXREF 77.00 ppm
BF 0.12 Hz
RGAIN 54

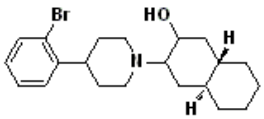

OBDV (8)

Figure 32 (b): ^{13}C NMR Spectra of OBDV.

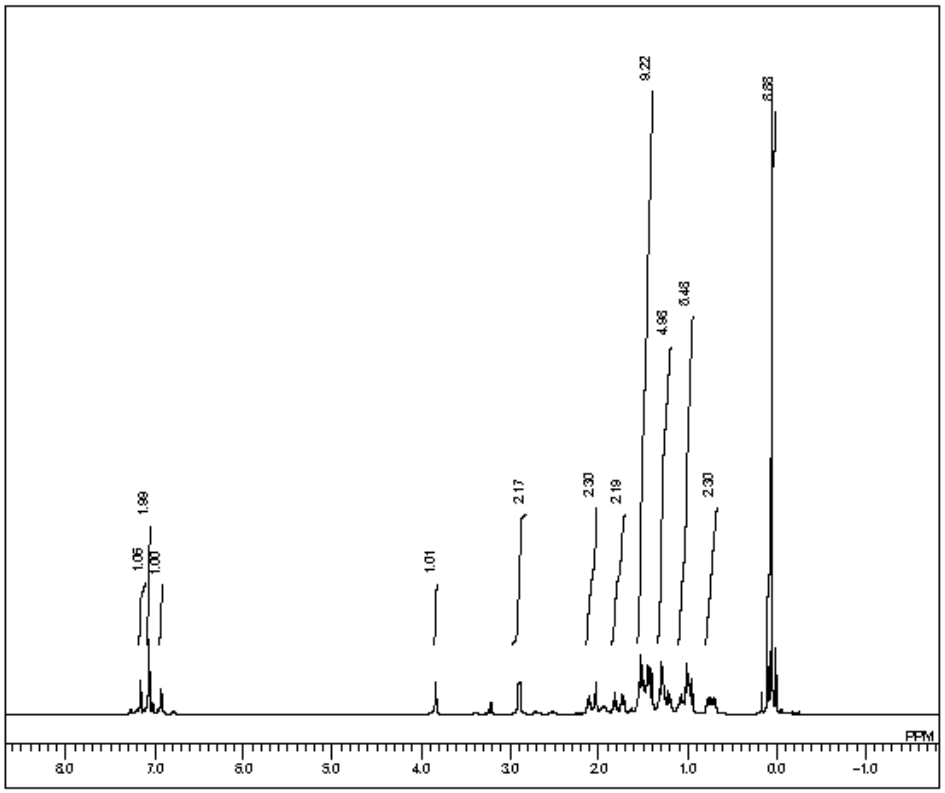

DFILE OTDV-1H-1.als
COMNT OTDV-1H
DATIM 16-04-2012 13:27:54
OBNUC 1H
EXMOD single_pulse.exc2
OBFRQ 600.17 MHz
OBSET 3.30 kHz
OBFIN 3.47 Hz
POINT 26214
FREQU 9008.67 Hz
SCANS 32
ACQTM 2.9098 sec
PD 2.0000 sec
PW1 8.60 usec
IRNUC 1H
CTEMP 19.9 c
SLVNT CDCL3
EXREF 0.00 ppm
BF 0.12 Hz
RGAIN 16

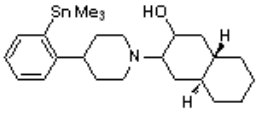

OTDV (9)

Figure 33 (a): ^{1}H NMR Spectra of OTDV.

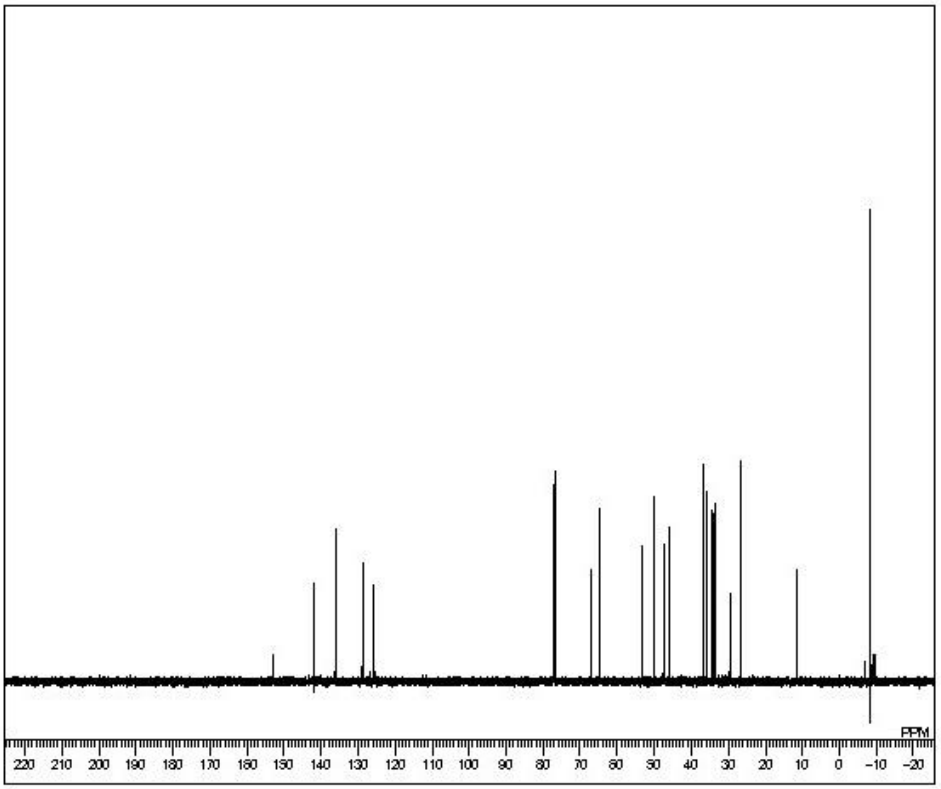

Figure 33 (b): ^{13}C NMR Spectra of OTDV.